

University of Alberta

Rime Ice Adhesion To Heated Surfaces

By

Timothy M. Weis



A thesis submitted to the Faculty of Graduate Studies and Research in partial fulfillment
of the requirements for the degree of Master of Science.

Department of Mechanical Engineering

Edmonton, Alberta

Fall 2002



**National Library
of Canada**

**Acquisitions and
Bibliographic Services**

**395 Wellington Street
Ottawa ON K1A 0N4
Canada**

**Bibliothèque nationale
du Canada**

**Acquisitions et
services bibliographiques**

**395, rue Wellington
Ottawa ON K1A 0N4
Canada**

Your file Votre référence

Our file Notre référence

The author has granted a non-exclusive licence allowing the National Library of Canada to reproduce, loan, distribute or sell copies of this thesis in microform, paper or electronic formats.

The author retains ownership of the copyright in this thesis. Neither the thesis nor substantial extracts from it may be printed or otherwise reproduced without the author's permission.

L'auteur a accordé une licence non exclusive permettant à la Bibliothèque nationale du Canada de reproduire, prêter, distribuer ou vendre des copies de cette thèse sous la forme de microfiche/film, de reproduction sur papier ou sur format électronique.

L'auteur conserve la propriété du droit d'auteur qui protège cette thèse. Ni la thèse ni des extraits substantiels de celle-ci ne doivent être imprimés ou autrement reproduits sans son autorisation.

0-612-81496-3

University of Alberta

Library Release Form

Name of Author: Timothy M. Weis

Title of Thesis: Rime Ice Adhesion to Heated Surfaces

Degree: Master of Science

Year this Degree Granted: 2002

Permission is hereby granted to the University of Alberta Library to reproduce single copies of this thesis and to lend or sell such copies for private, scholarly or scientific purpose only.

The author reserves all other publication and other rights in association with the copyright in the thesis, and except as herein before provided, neither the thesis nor any substantial portion thereof may be printed or otherwise reproduced in any material form whatever without the author's prior written permission.




#1004 8708-106 Street
Edmonton, AB
T6E 4J5

Date: Aug 9 / 2002


University of Alberta

Faculty of Graduate Studies and Research

The undersigned certify that they have read, and recommend to the Faculty of Graduate Studies and Research for acceptance, a thesis entitled Rime Ice Adhesion to Heated Surfaces submitted by Timothy M. Weis in partial fulfillment of the requirements for the degree of Master of Science.


Dr. J.D. Dale


Dr. T.W. Forest


Dr. E. Lozowski

Date: August 9, 2002

ABSTRACT

A centrifuge technique was developed in order to investigate the adhesion strength of rime ice to various polymer surfaces. The centrifuge induced a steady tensile or shear centripetal body force on rime ice samples. Similar forces are exerted on rime ice that may accrete on wind turbine blades and can cause the ice to self-shed. The surface on which the ice sample was adhered was heated until the ice adhesion bond failed. The results indicated that the normal and shear adhesion strength of rime ice was very similar. Tests were performed at ambient temperatures of -15°C and -8°C . The results indicated a linear relationship between the adhesion strength of rime ice to the temperature of the surface, regardless of whether the ice was created at -15°C and -8°C . For ice to self-shed from a wind turbine blade, temperatures close to -3°C would need to be obtained for the surfaces tested.

A society grows great when old men plant trees whose shade they know they shall never sit in.
- Greek Proverb

*If you assume that there's no hope, you guarantee that there will be no hope.
If you assume that there is an instinct for freedom,
that there are opportunities to change things,
there's a chance you may contribute to making a better world.
That's your choice.
- Noam Chomsky*

ACKNOWLEDGEMENTS

I wish to thank the following people, whose support helped me achieve this goal:

Dr. Doug Dale, for the flexibility and trust to allow me to pursue this topic, and for his guidance and advice;

Mr. Bernie Faulkner to whom every experimental graduate student is indebted to for his timely advice, support and optimism when it seems least warranted;

Mr. Don Fuhr and Mr. Albert Yuen for their hard work, input and cheerful conversation;

Mr. Terry Nord for his help as the project (and the wires) twisted and turned;

Dr. Tom Forest and Dr. Edward Lozowski for their guidance early on in the project, Mr. Mark Ackerman for his technical help with data collection, and Dr. Daniel Kwok for his help with contact angle measurements;

The entire combustion lab for the enlightening conversations inside and outside the office, and particularly Pascal Poudenx, Glen Thomas, Dr. Matthew Johnson and Ryan Chladny who had to listen to my political side;

The MSA, CEPPal and ISPHR who helped me grow outside the lab in pursuit of a more peaceful planet;

The NSERC for its support of my graduate research;

My father, Art, my brother, Tony and my sister, Joanna, for their support and inspiration, despite being thousands of miles away;

And finally, a special acknowledgement to my loving wife Howaida, who has stood by me during this pursuit and our dreams for the future.

TABLE OF CONTENTS

CHAPTER 1	INTRODUCTION	1
1.1	Wind Energy in Canada's North	1
1.2	Rime Ice and Wind Energy	4
1.3	Ice Accretion and Removal	5
1.3.1	Types of Ice	5
1.3.2	Ice Protection Techniques	6
1.4	Motivation for Current Research	7
1.5	Goals of Thesis Work	8
CHAPTER 2	REVIEW OF RELEVANT LITERATURE	10
2.1	Icing of Wind Turbine Blades	10
2.1.1	Meteorological Conditions for Rime Icing Events	11
2.1.2	Rime Ice and Altered Blade Geometry	12
2.2	Ice Protection Power Consumption	15
2.3	Contact Angles and Ice Adhesion	16
2.4	Ice Adhesion Testing Techniques	19
2.5	Ice Adhesion Strength	21
2.6	Summary	23
CHAPTER 3	EXPERIMENTAL EQUIPMENT AND METHODOLOGY	24
3.1	University of Alberta Cold Room Facilities	24
3.2	Surface Characteristics of Samples	25
3.3	Cloud Simulation	28
3.4	Adhesion Strength Centrifuge	32
3.4.1	Forces on a Wind Turbine Blade	32
3.4.2	Adhesion Centrifuge Design	36
3.5	Experimental Methodology and Data Collection	40

3.5.1	Rime Ice Creation Procedure	40
3.5.2	Adhesion Test Procedure	43
3.6	Temperature Measurement Error	45
3.6.1	Thermal Contact	45
3.6.2	Slip Ring Errors	47
CHAPTER 4	EXPERIMENTAL RESULTS AND ANALYSIS	50
4.1	Results	50
4.1.1	Numerical Determination of Surface Temperature	50
4.1.2	Adhesion Strength Results	59
4.1.2.1	Normal Strength Results	62
4.1.2.2	Shear Strength Results	68
4.2	Discussion of Results	74
4.2.1	System Performance	74
4.2.2	Analysis of Results	76
4.2.3	Limitations of the Results	80
CHAPTER 5	CONCLUSIONS AND RECOMMENDATIONS	83
5.1	Adhesion Strength of Rime Ice	83
5.2	Applicability to Wind Turbines	84
5.3	Future Work	84
REFERENCES		85
APPENDIX A: SURFACE CONTACT ANGLES		89
A.1 Advancing Contact Angles With Distilled Water		89
APPENDIX B: DATA SHEETS FOR EXPERIMENTAL SURFACES		92
B.1 21st Century Coatings Data Sheets		92
B.2 Ameron PSX 1 Data Sheet		97
APPENDIX C: DROPLET SUPERCOOLING ESTIMATE		99
APPENDIX D: DATA COLLECTION AND SYSTEM CONTROL CODE		101
D.1 Quick Basic Code for Temperature Control and Data Acquisition		101

APPENDIX E: ERROR ESTIMATES	121
E.1 Surface Temperature Measurement Error Estimates	121
E.2 Interface Stress Measurement Errors Estimates	123

LIST OF TABLES

Table 1-1: Comparison of Various Nations' Installed Wind Power	2
Table 3-1: Test Surface Characteristics	27
Table 3-2: Peak Stresses at the Ice Interface with an Airfoil	34
Table 4-1: Test Results Summary	76
Table 4-2: Work of Adhesion and Failure Strengths	77
Table 4-3: Adhesion Strength Along Wind Turbine Blade	80

LIST OF FIGURES

Figure 1-1: Global Growth in Installed Wind Energy	2
Figure 2-1: Droplet Trajectories	13
Figure 2-2: Typical Rime Ice Accretion Geometry on a Horizontal Axis Wind Turbine Blade	15
Figure 2-3: The destruction of one interface and the creation of two new ones.	17
Figure 2-4: Contact Angle of a Liquid on a Surface	18
Figure 2-5: Glaze Ice Tensile Test Technique	19
Figure 2-6: Torsion Technique for Inducing a Shear Stress	20
Figure 2-7: Centrifugal Shear Stress Test Apparatus	21
Figure 3-1: Cold Room Setup (Plan View)	25
Figure 3-2: Surface Sample Base Plate Design	26
Figure 3-3: Cloud Simulation Spray System Schematic and Thermocouple Locations	29
Figure 3-4: Spray Nozzle Setup	30
Figure 3-5: Rime Ice Accretion on Test Surface	32
Figure 3-6: Body Forces Induced on Accreted Rime Ice	33
Figure 3-7: Stresses at Ice-Airfoil Interface	36
Figure 3-8: Adhesion Strength Centrifuge System Schematic	37
Figure 3-9: Centrifuge Hub Setup For Normal Stress Tests	39
Figure 3-10: Shear Stress Centrifuge Setup	40
Figure 3-11: System Temperatures During Rime Ice Creation	42
Figure 3-12: Uniform Rime Ice Sample Above Test Surface	43
Figure 3-13: Adhesion Strength Test Process	44
Figure 3-14: Experimental and Theoretical Surface Temperature Rise in Heated Aluminum Base Plate	46
Figure 3-15: Thermocouple Slip Ring Circuit Diagram	47
Figure 3-16: Rotor Speed Influence on Indicated and Corrected Surface Temperature	49
Figure 4-1: Numerical Simulation of Temperature Distribution in Aluminum Plate During Heating	53
Figure 4-2: Heat Transfer Across Surface Coating	55
Figure 4-3: Experimental Temperature Rise Compared with Numerical Simulation to Determine Overall Boundary Condition	57
Figure 4-4: Equivalent Thermal Circuit of Ice Sample	58
Figure 4-5: Predicted Plate Temperature Distribution During Heating	59
Figure 4-6: Rime Ice Structure Showing Voids	61
Figure 4-7: Main Adhesion Failure With Cohesive Failure Around Edges of the Sample	62
Figure 4-8: Tensile Adhesion Strength of Rime Ice to PC 100 Surface Coating	63
Figure 4-9: Tensile Adhesion Strength of Rime Ice to PC 200 Surface Coating	64
Figure 4-10: Tensile Adhesion Strength of Rime Ice to PSX 700 Surface Coating	65
Figure 4-11: Tensile Adhesion Strength of Rime Ice to 20-4969FX Surface Coating	66
Figure 4-12: Tensile Stress Failures For All Surfaces	67
Figure 4-13: Shear Stress Adhesion Strength of Rime Ice to PC 100 Surface Coating	69
Figure 4-14: Shear Stress Adhesion Strength of Rime Ice to PC 200 Surface Coating	70
Figure 4-15: Shear Stress Adhesion Strength of Rime Ice to PSX 700 Surface Coating	71
Figure 4-16: Shear Stress Adhesion Strength of Rime Ice to 20-4969FX Surface Coating	72
Figure 4-17: Shear Stress Failures For All Surfaces	73
Figure 4-18: System Calibration Results	75
Figure 4-19: Work of Adhesion and Failure Stress at -4°C	78
Figure 4-20: Correlation Between Work of Adhesion and Failure Stresses -7°C	78

Figure A-1: Contact Angle of Water on Fluorinated Polyurethane & Silicone PC100 Coating	89
Figure A-2: Contact Angle of Water on Fluorinated Polyurethane PC200 Coating	90
Figure A-3: Contact Angle of Water on Siloxane PSX700 Coating	90
Figure A-4: Contact Angle of Water on Isophthalic Polyester 20-4969FX Coating	91
Figure A-5: Contact Angle of Water on Polished Aluminum 2024	91

NOMENCLATURE

c_p	Specific Heat (J/kg·K)
T	Temperature (°C)
λ	Latent Heat of Freezing (J/kg)
u_∞	Free Stream Fluid Velocity (m/s)
β_{CL}	Impinging Droplet Collision Limit (°)
Ste	Stefan Number
$u_{relative}$	Relative Wind Speed (m/s)
W_{adh}	Work of Adhesion per Unit Surface Area (mJ/m ²)
γ	Interfacial Energy per Unit Surface Area (mJ/m ²)
ϕ	Liquid Contact Angle on a Solid Surface (°)
F_c	Centripetal Force (N)
y	Thickness of Accreted Ice on an Airfoil (m)
m	Mass (kg)
ω	Rotational Speed (rad/s)
r	Radial Distance from Axis of Rotation (m)
ρ	Density (kg/m ³)
A	Surface Area (m ²)
τ	Shear Stress (Pa)
P	Surface Pressure (Pa)
C_p	Coefficient of Pressure
σ_b	Stress at Failure due to Centripetal Body Force (Pa)
q_h	Energy Input into Heater (W)

$x(1)...x(11)$	Numerical Grid Points
α	Thermal Diffusivity (m^2/s)
x	Distance From Heater Within Test Sample (m)
t	Time From Beginning of Power Supplied to Heater (s)
L_o	Thickness of Aluminum Base Plate (m)
Fo	Fourier Number
x^*	Non-Dimensional Distance From Heater
T_o	Initial Uniform Temperature ($^{\circ}\text{C}$)
θ	Non-Dimensional Temperature
q''	Heater Energy per Unit Area (W/m^2)
U	Overall Heat Transfer Coefficient ($\text{W}/\text{m}^2\cdot\text{K}$)
R	Thermal Resistance ($\text{m}^2\cdot\text{K}/\text{W}$)
k	Thermal Conductivity ($\text{W}/\text{m}\cdot\text{K}$)
h_{∞}	Convective Heat Transfer Coefficient ($\text{W}/\text{m}^2\cdot\text{K}$)
Nu	Nusselt Number
V	Volume (m^3)
CT	Surface Temperature Correction Term ($^{\circ}\text{C}$)
εX	Absolute Error Estimate (units depend on variable X)

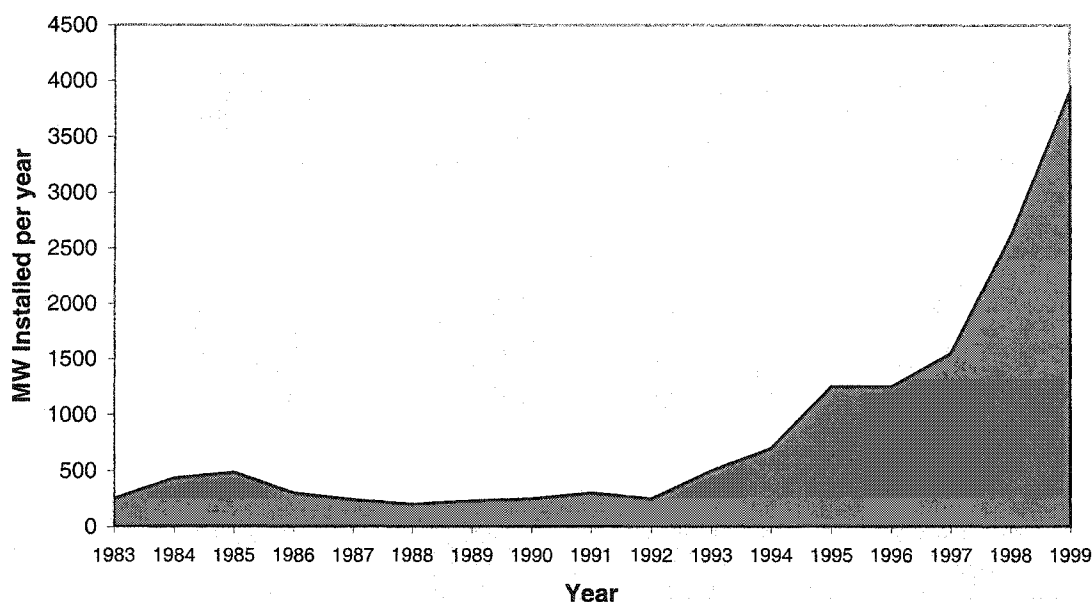
Chapter 1

INTRODUCTION

1.1 Wind Energy in Canada's North

Wind energy is the transformation of kinetic energy in the wind into mechanical or electrical power in a completely renewable and sustainable fashion. Humanity has been harnessing the power of wind for mechanical systems for thousands of years, from grinding grain in 1st century Persia to pumping seawater in 19th century Holland. It was not until the “energy crisis” of the early 1970s, when oil prices skyrocketed, that anybody seriously considered the wind as a source of electrical energy for the future. Modern wind turbines, designed to generate electricity, were erected for the first time en masse in the late 1970's in California. Despite many early disappointments and failures, by the year 2002, wind energy has become the fastest growing energy source in the world. Wind energy's rapid growth, can be attributed not only to the inherent environmental benefits of a low impact renewable energy source, but also to the gradual technological advances since the 1980's that have made wind energy an economically competitive option in many parts of the world. As countries attempt to ratify the 1997 Kyoto protocol for reductions in greenhouse gas emissions, wind energy development is likely to continue to increase for the foreseeable future.

BTM Consult ApS (2000) reported that between 1992 and 2000, there has been an average annual growth of over 25% in installed wind energy capacity globally (see Figure 1-1).



source: BTM Consult ApS, March 2000

Figure 1-1: Global Growth in Installed Wind Energy

Most of this development has been in Europe and the United States, although many less industrialized countries including India, Egypt, Argentina, Brazil and Morocco have also begun large-scale wind energy programs. Despite having a vast wind energy resource, it can be seen from Table 1-1 that Canada lags behind many nations in wind energy installation (Wind Power Monthly, 2000).

Table 1-1: Comparison of Various Nations' Installed Wind Power

Country	Installed Wind Power Capacity (MW) as of November 2000
Germany	6,113
Denmark	2,297
USA	2,555
Spain	2,402
India	1,220
Canada	140

source: Wind Power Monthly, November 2000

Large scale wind energy development in Europe and the United States has been successful as a result of many factors that include technological improvements, cost reductions through local manufacturing, as well as significant government incentives or

credits to develop sustainable energy sources. The latter two factors are both currently absent in the Canadian market.

Electricity markets in Alberta and Ontario have recently been deregulated, opening a window for 'green power' alternatives such as wind energy, to individuals or organizations that wish to purchase it, although usually at a premium. Consumer prices for wind energy in Canada will be competitive with traditional hydro, nuclear or fossil fuel plants only when capital costs can be reduced as a result of domestic manufacturing. Recent large-scale developments such as the 1999 Nordais project in Quebec (100 MW wind farm), the 2000 developments in Pincher Creek, Alberta (16.4 MW installed in 2000) and the 2002 development in Saskatchewan (11 MW installed in 2002) have begun a move towards wind energy growth in Canada. The Canadian Wind Energy Association (2001) stated that the federal and provincial levels of Canadian Government must implement legislation that will help foster a sustained market for wind energy so that the industry can establish manufacturing in Canada. Some form of legislation is probable in the future as Canada moves to meet its Kyoto protocol commitments, as wind energy can play a large role in reducing greenhouse gases emissions. Environment Canada (2000) estimates that 18% of Canada's greenhouse gas emissions result from electricity generation. Using data from Reynolds and Pape (2000), every megawatt of wind energy installed in Canada in place of coal power displaces 2,500-3,000 tonnes of CO₂ annually (assuming a 0.3 wind capacity factor).

Despite the current barriers, wind energy is already a cost effective alternative in many locations where a wind turbine would offset methods of electricity generation that have high fuel costs, such as diesel systems.

Canada has over 200,000 citizens in over 300 remote communities that are not connected to provincial or national power grids, (Ah-You and Leng 1999) so they often rely heavily on diesel generators, a very expensive and relatively inefficient method of generating electricity. Although consumers receive subsidies, Ross et al. (1998) reported that diesel power generation could cost as much as \$0.25-\$1.00/kWh,

compared to roughly \$0.05/kWh-\$0.08/kWh most Canadians consumers pay who receive power from the provincial grids. The electricity costs are therefore subsidized by governments, so although the development of environmentally benign energy is a goal of the Yukon Development Corporation (1999), the Yukon Energy Corporation began investigating commercial wind power systems, not for their environmental benefits, but as a cost-saving alternative to diesel power generation (Maisson 2001).

In the Yukon, remote communities represent an annual requirement of 50 GWh, up to 20% of the territory's power consumption (Maisson 2001). Many of Canada's remote northern communities are located near the coast with wind regimes adequate for wind turbines (Lodge 1996). The high cost of energy in these isolated communities along with a desire to become more self-sufficient has led to an interest in renewable energy systems. Short daylight hours and frozen bodies of water make renewables such as solar or micro-hydro incompatible with the arctic winters. Wind energy is particularly suitable for northern climates as cold winter temperatures increase the air density, and therefore increase the power available in the wind when it is needed most. However, in extremely cold climates such as Canada's northern territories, rotor blade icing poses a potential obstacle for wind turbine operation. This problem must be overcome, to facilitate wind energy development as a cost effective as well as an environmentally benign alternative for many of Canada's northern communities.

1.2 Rime Ice and Wind Energy

Structural ice loading is always a concern when engineering machinery for cold climates. Wind energy is no exception, especially with respect to the dynamics of the large rotors that are directly exposed to the environment. The success of wind turbines has depended greatly on gradual refinement of blade design and pitch control, so that even small losses in the ability to control a turbine are major problems. Changes to the aerodynamics of the wind turbine blades due to rotor blade icing can seriously affect a turbine's performance (Kimura et al. 1994 and 1997). Beyond the loss of control, blade icing can lead to a decrease in power output, an increase in fatigue loading, unbalanced rotor loads, or long periods without production as an iced turbine is very unlikely to self

start if it stopped due to erratic behaviour caused by ice accretion. Small amounts of clear ice on the leading edge of a blade increase the blade's chord length and can actually increase the blade's lift. This coupled with increased air density at cold temperatures, can lead to turbine overproduction. Ice throw is also a potential safety hazard.

The European Non Nuclear Energy Programme funded Tammelin et al. (2000) to investigate wind energy development in cold climates. They found that rotor blade icing is a potential problem not only for wind turbines operating in northern climate, but also at high altitudes, particularly near large bodies of water. Of the new wind farms that are to be erected in Europe in order to meet the EU goal of 40,000 MW by the year 2010, Tammelin et al. (2000) estimate that 10-20% will be in regions where icing will be a significant factor in the design of the wind turbines and the wind farm.

Icing of rotor blades or weather monitoring equipment can be very costly and potentially dangerous. Anemometer icing interferes with wind turbine control and often causes power output losses, particularly with pitch-controlled machines. Heated anemometers or sonic anemometers are now used successfully where icing is common. Unlike heated anemometers, blade heaters have often proven to be expensive. The large surface area of a wind turbine blade, as well as the high relative wind speeds they are exposed to result in high rates of convection. Thus large amounts of energy must be used to heat the blades for effective de-icing.

1.3 Ice Accretion and Removal

1.3.1 Types of Ice

Ice accretes on wind turbines when water droplets present in the air, either in the form of rain or clouds, collide with the blades. Frost and the freezing of condensed water vapour on turbine blades pose negligible impacts for the operation of a turbine (Makkonen 1991). There are two main categories of atmospheric icing known as wet or glaze ice, and dry or rime ice. As the name would indicate, wet icing occurs when the impinging water droplet does not freeze completely on contact, and part of the

impacting mass can either be partially lost or freeze in a different location from the point of impact due to run-back. Dry icing occurs when there is no liquid or run-off, rather the droplets freeze on contact with the surface, as would be the case in a supercooled fog or cloud at temperatures well below freezing.

For wind turbines, glaze ice tends to be the result of freezing rain. Although unavoidable, freezing rain is infrequent and is usually predictable and detectable at meteorological stations and can thus be planned for. Glaze ice does not pose a major problem for wind turbines, even in areas such as Atlantic Canada where glaze icing is common (Brothers 2001).

The most severe problem for wind turbines comes from in-cloud icing, which is common for turbines located in hilly or mountainous terrain (Tammelin et al. 2000). When the temperature is below freezing, a cloud consists of supercooled water droplets, which result in ice accretion if they collide with the cold turbine blades. Tammelin et al. (2000) found that in practice, rime ice collects most heavily within 10 to 15 percent of the chord length, from the leading edge of the turbine blade. Near the stagnation point, the greatest number of water droplets depart from the sharp turns that the streamlines make around the airfoil nose and collide with the blade (Finstad et al. 1993). Therefore, rime ice accretion tends to result in an elongation of the turbine blade's chord length. The change in chord length and surface roughness, result in an increased drag and a decrease in lift as the blade will be pitched according to the un-iced profile. This results in a decrease in power and a loss of control, both of which can easily ruin a project that would be economically feasible were icing not present.

1.3.2 Ice Protection Techniques

In order to prevent or reduce the penalties resulting from ice accretion on machinery and to ensure their safe and reliable operation, different types of ice protection techniques are available. Two general categories of protection systems exist:

1. Anti-Icing systems prevent ice from forming, usually thermally or chemically,

2. De-Icing systems allow for some ice to build up to a maximum thickness before the system is engaged to remove the ice; these systems include thermal and mechanical techniques.

Electro-thermal anti-icing systems are the current method of choice for wind turbines operating in climates with icing problems, due to their simplicity and low initial cost. Many other techniques exist for helicopters and aircraft, such as freezing point depressant sprays, leading edge pneumatic boots and electromagnetic impulse systems (Thomas et al. 1996). Although aircraft icing problems are similar to wind turbines, many of the techniques that are useful for aircraft are not appropriate for wind turbines, given the differences in operating conditions. Wind turbines need to operate continuously, unmonitored and often through lengthy heavy icing periods. Turbines that are subjected to severe icing represent a small enough fraction of the market that blade manufacturers are reluctant to incorporate high-cost ice protection systems, such as electro-magnetic pulsing, into their designs. Therefore, a simple, reliable after market technique is necessary to protect turbines that are at risk. Currently, the preferred technique is simply to add resistance heaters to the leading edges of the turbine blades. This has proven effective in mitigating the adverse effects of icing in certain circumstances (Maison 2001). However, if used improperly or unnecessarily this technique can be more costly than the penalty of ice accretion (Brothers 2001).

1.4 Motivation for Current Research

For the past 15 years, wind turbines have operated successfully in harsh arctic environments such as Lapland, Alaska and Antarctica, although, few have been without problems associated with icing. In order to prevent increased stresses and vibrations, wind turbines are typically powered down when icing conditions are present. This is by no means an ideal solution, not only because of the immediate loss of power production from the wind turbine while it is shut down, but ice accreted on the blades may prevent the turbine from re-starting long after the icing conditions have lifted. In areas of frequent and heavy icing, such as mountaintops, a turbine may be off-line for days or weeks at a time if it is shut down at every icing event. Both situations carry potentially

severe economic penalties even if the turbine is undamaged due to the ice. Maisson (2001) estimated that a wind turbine subjected to extended periods of rime icing without any treatment, could lose up to 20% of its annual power output.

It is known that the adhesion strength of ice tends to decrease with increasing temperature (Hobbs 1973). As the surface temperature is increased, the adhesion strength will eventually drop to a point where the ice would self-shed under the centripetal forces of the turbine blades. For most materials this point is close to melting. By selecting a low-energy surface coating it may be possible to decrease this temperature in order to minimize the amount of input heat required. The thrust of the research in this thesis is therefore to develop a technique that can measure the adhesion strength of rime ice to various surfaces as it is heated. For example, if the blades could be kept at a temperature of -5°C instead of 0°C , the author predicts that blade heating costs could be reduced by 33%.

1.5 Goals of Thesis Work

The adhesion of ice to solids is a subject of very practical importance, from aircraft, to marine applications, to wind turbines. Wind turbines, however, present unique obstacles, such as extended exposures to icing conditions, continuous operation requirements and unmanned operation and control. Most importantly, ice protection techniques must be effective and inexpensive to ensure a turbine is economically viable. Consequently, much of the research on ice removal in the past is not fully relevant to wind energy systems. Ice removal techniques previously focused on are mechanical, chemical or single use, high-energy strategies that are simply not available to wind turbines. Furthermore, the work has also not focused on rime ice, and has used investigation methods, such as loading ice frozen between two plates, which are not applicable to rime ice.

To investigate the possibility that a properly selected surface coating combined with the addition of heat below 0°C , will enable rime ice to shed under the body forces subjected to ice adhered to wind turbine blades, a centrifugal system was designed to test normal and shear strengths of rime ice as it is heated. The purpose of this test will

then be to determine if the combination of low-energy surface coatings and heating systems can reduce the overall cost of ice protection systems for wind turbines. The intent is to be able to predict the temperature at which ice-shedding events will occur for a given surface coating, and to determine how much, if any, energy is required. If suitable combinations of heat and surface coatings can be found, it will reduce the energy consumption of an ice protection technique, as well as improving the overall system's predictability and reliability.

Reducing the cost and increasing the reliability of ice protection systems will facilitate the development of wind-energy systems in northern communities, particularly remote and off-grid systems.

Chapter 2

REVIEW OF RELEVANT LITERATURE

2.1 Icing of Wind Turbine Blades

Cold climate wind power is still in its infancy. There does however, exist significant potential for wind energy development in cold climates, particularly along coastal and within mountainous regions, provided problems associated with low temperatures and ice accretion can be overcome.

Ice accreted on wind turbine blades poses a danger of ice throw and inducing excessive stresses on the turbine. As wind energy continues to grow, more and more turbines are being erected on sites where icing may occur and within proximity of roads and other infrastructure (Seifert et al. 1998). Consequently, it is important to understand under which conditions ice throw will be a danger, for safety as well as zoning guidelines, since ice debris up to 1 kg has been found up to 40 m from turbines (Seifert and Tammelin 1996a).

The most significant obstacle that ice accretion poses to wind energy development in cold climates is the aerodynamic degradation of the blades. Freezing rain can result in an increase in surface roughness of a turbine blade, while turbines that operate at high altitudes are frequently subjected to in-cloud operation which leads to rime ice accretion if the temperature drops sufficiently below 0°C. Even small increases in the surface roughness of a turbine's blades can reduce energy output by up to 20% (Yekutieli and Clark 1987), while leading edge rime icing that causes only marginal increases in stress loads, can reduce a turbine's output by up to 25% (Vølund 1998). Although both problems can significantly reduce a turbine's energy output, freezing rain generally poses a much less severe problem than rime ice, as the former events are generally infrequent and short in duration, while the latter may last for months at a time (Seifert and Tammelin 1996a).

Brothers (2001) estimates that only 1-2% of the energy harvested at the Atlantic Wind Test Site that is located at sea level, on Prince Edward Island is lost annually to ice, predominantly glaze. Bose (1992) also found that glaze icing posed the greatest threat to a test wind turbine close to sea level on the Newfoundland coast, which would accumulate ice for approximately 1.5% of the year. Bose (1992) found that climate statistics indicated that icing downtime could amount to 8% of the year, at higher altitudes closer region of St. John's, Newfoundland. Severe rime icing can cause very high power losses, as is the case in the Yukon where icing can cause capacity factors to be reduced by 20% (Maisson 2001). Problems with rime ice accretion are likely for proposed future development in Canada, in Northern British Columbia, the Gaspé region of Quebec and the western mountains of Newfoundland (Edworthy 2002).

To allow for further wind energy development in cold climates, it is necessary to understand more about rime icing and de-icing under typical ambient conditions. Moreover, methods must be developed to effectively and economically protect a turbine from the adverse effects of ice. In order to effectively protect against rime ice, it is important to know under what conditions the ice forms and how it accumulates on the turbine blade.

2.1.1 Meteorological Conditions for Rime Icing Events

Cloud droplets readily supercool at air temperatures between 0°C and -40°C, the latter being the homogeneous nucleation temperature. Larger droplets and those with impurities tend to nucleate at temperatures closer to 0°C, while pure droplets with μm scale diameters are able to supercool to the lower range of temperatures (Hobbs 1974). Clouds in northern climates tend to have water droplets with diameters on the order of 10-60 μm (Pruppacher and Klett 1979). As there are relatively few atmospheric particles to serve as nucleation sites, it is quite common for cloud droplets to supercool, and therefore ice crystals are often not be found in non-precipitating clouds at temperatures as low as -10°C (Rogers and Yau 1989). Although conditions vary from cloud to cloud, it is not uncommon to find supercooled droplets in clouds at temperatures as low as -20°C (Hobbs 1974).

Wind turbines that operate on mountaintops frequently experience in-cloud operation. The temperature range between 0°C and -20°C poses a dangerous condition, as supercooled cloud water droplets readily freeze and adhere to any surface that provides a nucleation site. Maisson (2001) found that the Yukon Energy Corporation wind turbines operating at an altitude of 1430 m, are subjected to the highest rime icing incidents in early winter, while lakes are not yet frozen over, and the ambient temperatures are passing between the dangerous 0°C to -20°C range. Craig and Craig (1996) found that wind turbine icing incidents in Yukon were very rare below -25°C , and did not occur below -30°C .

The rate of rime ice accretion is dependent on many factors such as cloud height, air temperature and wind speed. Tammelin and S  ntti (1994) found that the turbines that are subjected to the most intense rime ice accretion are generally located over 500 m above sea level, with icing intensity continuing to increase with altitude, as the turbine is more likely to experience longer and more frequent in-cloud conditions. Icing events depend greatly on the local weather patterns, which vary in frequency and duration annually. Icing events may be relatively short and frequent, as was observed outside of Whitehorse, Yukon, where single events rarely lasted more than 3 hours, but could occur as frequently as several times a day (Craig and Craig 1996), while other locations in Germany have observed continuous icing periods of up to 60 days (Seifert and Tammelin 1996a). It is therefore essential to monitor the climate well before installing a northern wind turbine, and to be prepared to deal with rime icing if the turbine may be operating in in-cloud conditions to avoid extended downtime.

2.1.2 Rime Ice and Altered Blade Geometry

In-cloud icing is the most common cause of severe rime icing of wind turbines. The inertia of water droplets within a cloud cause them to deviate from the air's streamlines as they flow around the turbine blades. Larger droplets, having a greater mass, will depart further from the air streamlines than smaller droplets. Larger droplets, and those close to the stagnation streamline will have an increased likelihood of colliding with the airfoil (see Figure 2-1). The fractional mass of droplets that collide

with the airfoil, compared to the mass of droplets in the projected cross-sectional area upstream of the body is known as the *collision efficiency*. The collision efficiency and the bounding trajectories are a function of airfoil type, wind speed, droplet size distribution and angle of attack.

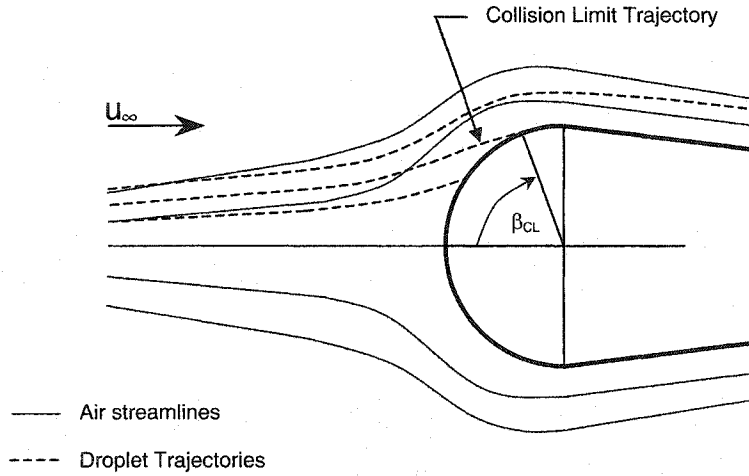


Figure 2-1: Droplet Trajectories

Supercooled droplets that collide with the airfoil will freeze. The rate at which the droplets freeze initially is described by the ratio of sensible to latent heat, also known as the Stefan number described in Equation (2.1):

$$St = \frac{c_p (T_{freeze} - T_i)}{\lambda} \quad (2.1)$$

where St = Stefan Number,

c_p = Specific Heat (J/kg K),

T_{freeze} = Freezing Temperature (K),

T_i = Initial Droplet Temperature (K),

λ = Specific Latent Heat (J/kg).

If $St > 1$, an impinging droplet will instantaneously freeze upon impact. For this to be the case, the impinging water would have to be close to -80°C . In natural conditions instantaneous freezing does not occur, as water does not tend to supercool beyond -40°C . However, if $St \cong O(1)$, the impinging droplets can freeze very quickly as

the additional heat can be lost to the surrounding air. The accreted ice becomes stacks of individual droplets, forming a porous structure giving it an opaque, white colour. This is known as rime ice or dry accretion, and it can have a density between 400-700 kg/m³. If $St \ll 1$, a droplet may freeze only partially on impact, while the remaining unfrozen water is free to run back along the length of the blade. This is known as glaze ice or wet accretion, and is characterized by a clear appearance and a density close to 920 kg/m³.

In-cloud icing typically results in rime ice, as clouds consist of small diameter droplets and have relatively low liquid water contents (usually 0.1-1.0 g/m³), such that the surrounding air is able to carry away the released latent heat. The rotation of the blades of a wind turbine will increase the heat transfer coefficient even further, so it is not surprising that rime ice is the most problematic type of accretion for wind turbines that frequently operate in in-cloud conditions.

The nature of rime ice is such that it collects only between the droplet collision limits on the airfoil. As wind turbine airfoils are typically pitched at an angle of attack into the flow, rime ice generally accretes slightly more on the pressure side than the suction side. The collision limits are typically no more than 10-15% of the chord length (Tammelin et al. 2000) depending on the angle of attack. Makkonen and Finstad (1996) found similar results using TURBICE, a computer modeling code they developed for droplet collision efficiency and rime ice accumulation. This leading edge accumulation results in an elongation of the airfoil, approximately equal to the width of the airfoil itself. In practice, it has been observed that the chord length may be elongated by as much as 44% (Seifert and Richert 1998). Because the relative air velocity increases towards the tip of the blade, ice build-up is the greatest at the blade tip and the thickness decreases approximately linearly towards the hub (Seifert and Tammelin 1996b). The general location of rime ice on turbine blades is illustrated in Figure 2-2. The change in geometry of the turbine blade dramatically affects the ability to control the machine, particularly if it is pitch-regulated. Therefore, even modest amounts of icing can result in significant power production losses.

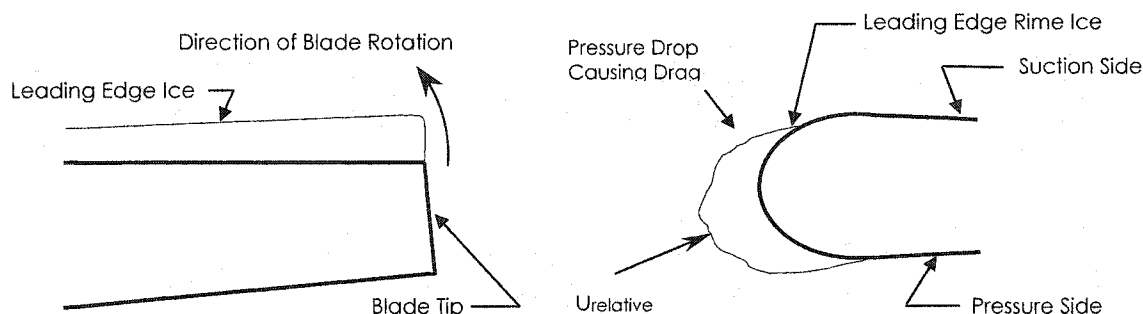


Figure 2-2: Typical Rime Ice Accretion Geometry on a Horizontal Axis Wind Turbine Blade

The effect of ice accretion on airfoil performance has been studied extensively since the early 1950s, as it pertains to aircraft. Seifert and Richert (1998) have done similar wind tunnel testing to measure the degradation in lift and drag using simulated rime ice accretion profiles to predict the power losses for wind turbines. They calculated that the power production could be reduced by 20% as a result of icing depending on the exposure to icing conditions. This figure may well be understated, as it assumes that the turbine continues to operate at a degraded performance, while in practice turbine control systems typically shut down a wind turbine if the power output deviates significantly from the expected power output at a given wind speed. This will exaggerate icing power losses, especially in locations where icing is less frequent. As such, it is important to keep wind turbine blades operating with little or no ice as often as possible. Knowing where the ice accumulates has allowed turbine owners and operators to add leading edge heaters to mitigate ice accretion.

2.2 Ice Protection Power Consumption

Maisson (2001) from the Yukon Energy Corporation found that although anti-icing electric heaters were necessary to enable their 125 kW turbine to operate throughout the winter, they consume up to 1,700 W. The capacity factor of this turbine is roughly 20%, representing an average output of 25 kW. Therefore the anti-icing energy requirement represents almost 7% of the turbine's winter output. This is a major improvement over the 20% annual power loss without ice protection, but it still

represents a significant decrease in output power ,during the winter months, when the turbine's power is most needed.

De-icing would require less energy than anti-icing, as the heaters would not be continuously operating. Makkonen and Autti (1991) predicted that de-icing the blades of a 100 kW wind turbine could require upwards of 350 kW, exceeding the machine's maximum rated output power. This would require an additional power source to de-ice the blades that may not be available in remote locations. An additional complication to anti-icing may be the run-back of any of the melted ice, which may re-freeze at a location on the blade behind the heaters, and thus unprotected. To be able to reduce the amount of power required to protect the blades, while avoiding run-back would result in cost reductions and improved overall system reliability.

To prevent ice from forming on the blades it is necessary to maintain the surface temperature above 0°C. Assuming an average ambient temperature of -15°C, every 1°C below 0°C that the blades can safely be maintained at represents a 6.5% drop in the power required to be supplied to the heaters. If the blades can be maintained at -5°C, this would make a 33% improvement, which in the case of the Yukon turbine, would represent 2.3% of the total winter power consumption. This is a notable improvement considering the length of time that the heaters would be operating. The savings would be amplified if several wind turbines or a wind farm was operational.

2.3 Contact Angles and Ice Adhesion

Ice has the ability to adhere strongly to many different surfaces. The strength of this bond is a property of the ice-solid interface, and depends on the way in which the ice was accreted. Atmospheric ice accretion is a process with many possible variables that relate to adhesion strength; a review of these variables relevant to this work is presented in the following section.

The surface energy of an interface is defined as the work required to create a unit area of that interface. The amount of energy required to destroy the interface between two different materials initially in contact, and to create two new interfaces

between the surrounding fluid (generally air) and the respective materials (see Figure 2-3) is typically referred to as the *work of adhesion*. Thus, the work of adhesion can be described as:

$$W_{adh} = \gamma_{AGas} + \gamma_{BGas} - \gamma_{AB} \quad (2.2)$$

where W_{adh} = work of adhesion per unit surface area (mJ/m^2),

γ = interfacial energy per unit area (mJ/m^2).

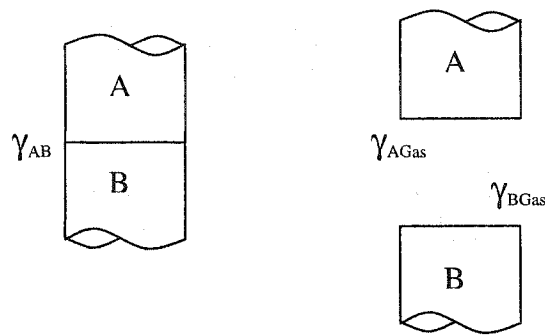


Figure 2-3: The destruction of one interface and the creation of two new ones.

Although the interfacial energy (γ) is a useful concept to mathematically describe adhesion, in practice, there is no direct method of measuring the interfacial energy or tensions of a solid. Therefore, an indirect method, by measuring the angle a liquid drop makes on a solid surface, the contact angle (ϕ), is usually used (see Figure 2-4). This is not always a straightforward property to measure and it is temperature dependent. Because of the complexity and continuing scientific debate concerning surface energy measurements, it is not the intention of this thesis to thoroughly examine this area. However, the surface energy is an important thermodynamic parameter, and therefore should not be ignored entirely.

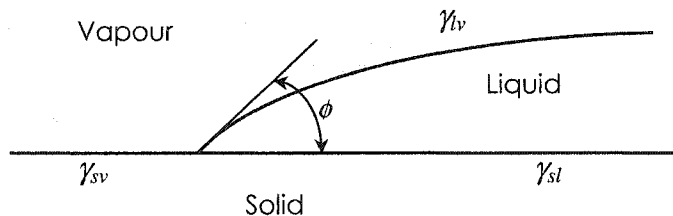


Figure 2-4: Contact Angle of a Liquid on a Surface

Contact angles are typically measured simply by depositing a drop of liquid on a given solid surface, and measuring the tangent to the drop at its base. The contact angle, ϕ , gives an inverse measure of the wettability of the surface, that is if $\phi = 0^\circ$ the liquid completely wets the surface, while if $\phi > 0^\circ$ the liquid cannot spread over the entire surface. Surfaces on which water forms a contact angle of less than 90° are generally considered hydrophilic and contact angles greater than 90° are considered hydrophobic.

Young's equation (Equation 2.3) makes use of the contact angle to determine interfacial energies (γ), also known as surface tensions.

$$\gamma_{sv} - \gamma_{sl} = \gamma_{lv} \cos \phi \quad (2.3)$$

If substance 'A' in Equation 2.2 were to be a liquid, Equation 2.2 could be combined with Equation 2.3 to find a relationship for the work of adhesion based on the contact angle and the liquid-vapour interfacial energy (Equation 2.4).

$$W_{adh} = \gamma_{lv} (1 + \cos \phi) \quad (2.4)$$

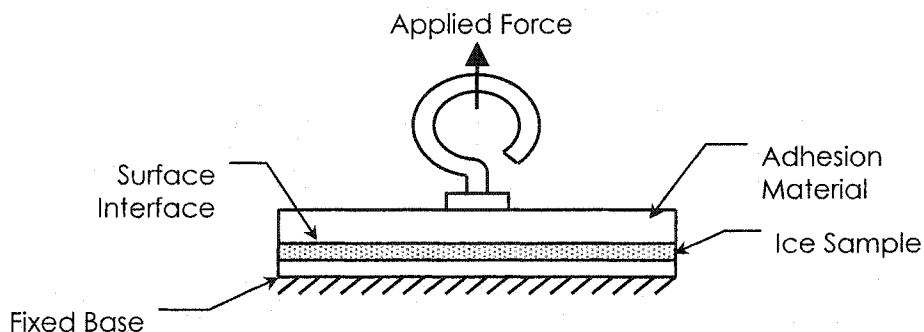
In theory, in the case of water and air, the interfacial energy (γ_{lv}) can be assumed to be a constant at a given temperature, such that the work of adhesion is therefore directly related to the contact angle. In the case of ice, it has been assumed that the contact angle of liquid water would relate to the adhesion strength of ice because of its importance in the work of adhesion in the case of liquid water. In practice, factors such as surface roughness and chemical heterogeneity, as well as the validity and

applicability of Young's equation present difficulties in obtaining the unique relationship stated in Equation 2.4 even for the case of liquid droplets. It is not surprising then that Forest (1980) and Petrenko and Whitworth (1999) have found that although the contact angle may be a useful qualitative tool, the quantitative relationship, if any, between the contact angle and ice adhesion is not a simple one.

2.4 Ice Adhesion Testing Techniques

Ice adhesion tests have been performed by a number of researchers in the past using a variety of techniques for normal and shear tests, some of which are described in this section. Tensile tests have been performed by Jellinek (1959), Eskin et al. (1957) as well as Archer and Gupta (1998). Jellinek and Eskin et al. both used similar tensile test techniques by forming ice between two circular discs and simply pulling them apart shown in figure 2-5.

Figure 2-5: Glaze Ice Tensile Test Technique



Archer and Gupta used a laser spallation technique for tensile strength measurements. The technique involves pulsing a laser onto a substrate on which a layer of ice has been formed. The laser pulse induces a compressive stress into the system that develops into a tensile wave as it reflects off of the free surface of the ice, pulling the ice off of the substrate at sufficiently high amplitudes. Neither of these techniques is appropriate for

testing rime ice. Because rime ice is formed by a deposition of supercooled droplets, a tensile technique that requires forming the ice between two plates would not be appropriate. The non-uniform structure and uneven surface would likely pose problems for the laser spallation technique, which requires a compression wave to reflect off of the free ice surface.

Various techniques have been used to test the adhesion shear stress of ice. Bascom et al. (1969) used a hydraulic ram to induce a shear force on an ice sample. The ram simply pushes a flat surface against one side of a rectangular ice sample. Oksanen (1983), Jellinek (1959) and Eskin et al. (1957) all used similar ideas to directly push on ice samples in order to create shear stresses and measure the magnitude of applied force with load cells. In an attempt to avoid stress concentrations, Rarty and Tabor (1958) developed a method to create a shear stress at the ice interface by loading an ice sample in torsion shown in Figure 2-6.

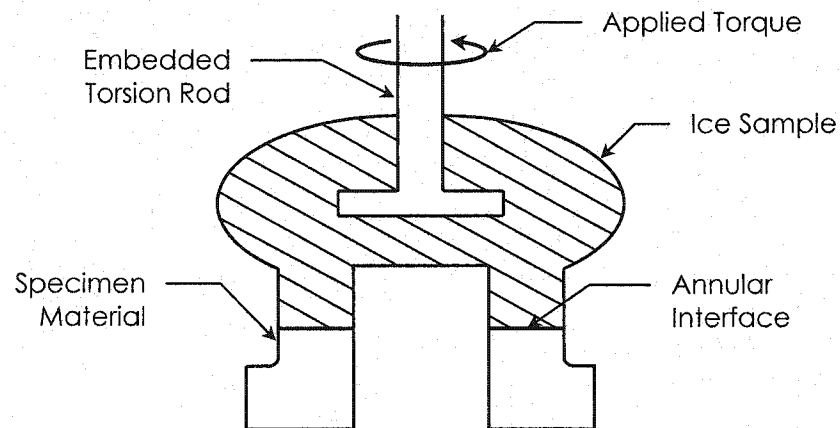


Figure 2-6: Torsion Technique for Inducing a Shear Stress

Again, the aforementioned techniques for shear stress testing are not appropriate for rime ice, as it has a tendency to crush when it is laterally loaded.

Loughborough and Haas (1946) used a centrifugal technique to examine the adhesion strength of ice to rubber for airplane pneumatic de-icing boots. An ice sample was frozen on the edge of a rotor plate and the rotor speed was increased until the ice

released from the plate. A window was added to the apparatus to monitor the rotor speed using a strobe light, as well as monitor for the ice failure. Although Loughborough and Haas did not use rime ice, this technique is more appropriate for rime ice testing as the ice can be created by deposition onto the plate; therefore it was used as a starting point for the design in the current research.

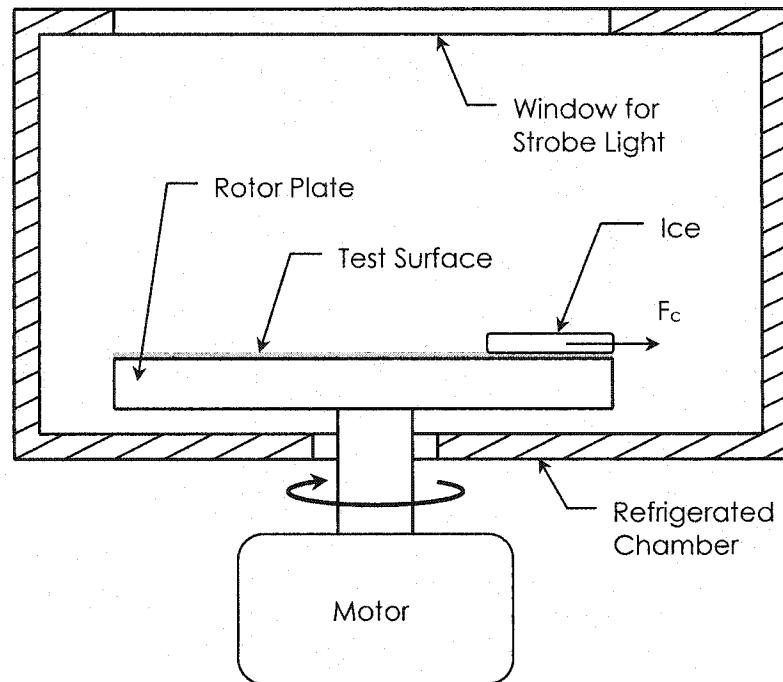


Figure 2-7: Centrifugal Shear Stress Test Apparatus

2.5 Ice Adhesion Strength

There have been numerous studies of ice adhesion looking for various aspects of the adhesion strength and fracture processes under varying conditions. The conditions under which the ice is formed and the forces it is subsequently subjected to are therefore important to understanding the utility of the results. For wind turbines, accreted ice is formed at a constant ambient temperature, is subjected to a steady centripetal load and is usually heated at the surface to remove it. Results that are applicable to these conditions are therefore presented in this section.

Prior to the current study, rime ice adhesion strength has not been a major focus of ice adhesion testing. Thus, most of the available studies have focused on testing ice that is free of as many air pockets as possible, essentially ideal glaze ice. Rime ice and glaze ice form under different atmospheric conditions and can have significantly different adhesion strengths (Lock 1990). The following results are therefore presented as a frame of reference, but are not directly comparable to the current research.

Forest (1980) compiled a summary of seven earlier shear stress studies and compared the adhesion shear strength to the surface free energy of the material to which the ice was bonded. He concluded that the surface energy of the interface does relate to the adhesion strength of the bond, although it is not the only factor involved. Petrenko and Whitworth (1999), found similar results after compiling three separate studies and comparing the shear adhesion strength to the water contact angle. Forest also found using tests performed at -25°C , -12°C and -6°C , that the shear strength of the ice consistently decreased with increasing temperature.

Jellinek (1970), Raraty and Tabor (1958) as well as Loughborough and Haas (1946) all found that the adhesion shear strength of ice increases linearly with decreasing temperature. Jellinek also found that a sharp transition occurs from adhesive to cohesive failures. For steel, at approximately -13°C , the ice no longer fails at the interface, but rather within the ice itself. All of these measurements were done with ice created and maintained at a given temperatures, not created at a one temperature and subsequently heated to another, as was done for the current experiment.

Although the same general trends are observed in different studies, the results vary from one study to another. Petrenko and Whitworth's compilation (1999) shows glaze ice shear strengths on the order of 100-500 kPa for materials with contact angles with liquid water on the order of 110° . Bascom et al. (1969) found that at -6°C , different polymers, all with water contact angles of 111° , had shear strengths ranging from 62 kPa to 151 kPa with glaze ice.

2.6 Summary

Rime icing can be a serious problem for wind turbines that operate at high altitudes, particularly in the polar regions of the planet. Rime ice removal can be an expensive process, which is typically done by electrically heating the turbine blades, thereby reducing the turbine's output in the winter season, often when it is most needed.

Based on previous work, it has been found that the adhesion strength of ice decreases linearly with increasing temperature for a given surface. Furthermore, surfaces that form larger contact angles with water droplets tend to have reduced adhesion strengths with ice. It is therefore plausible that if the proper surface is chosen, it can be heated to a temperature such that any accreted ice will self-shed with melting it. This will reduce the costs of protecting wind turbines against icing as well as ensuring that run-back does not occur.

Chapter 3

EXPERIMENTAL EQUIPMENT AND METHODOLOGY

Rime ice samples were created on various test surfaces that were placed into a centrifuge designed to induce a steady normal or shear force at the ice-surface interface. The surfaces were heated during the test and the surface temperature was recorded until an adhesive failure occurred.

3.1 University of Alberta Cold Room Facilities

All of the experiments were performed in a refrigerated cold room manufactured by Foster. The cold room is one of three cold room facilities in the Mechanical Engineering Building at the University of Alberta. The cold room has a 4 m² floor area and a ceiling height of 2.15 m. The cooling unit is capable of maintaining the average room temperature between -5°C and -23°C, $\pm 1^\circ\text{C}$. The room was separated into two smaller compartments using plastic baffles to dampen circulation air currents, and to contain the humidity generated by the fog spray system. The tests were performed at average room temperatures of -8°C and -15°C.

Figure 3-1 illustrates the location of the experimental apparatus in the cold room. Sections 3.3 and 3.4 detail the operation of the two major components: the supercooled fog spray system and the adhesion strength centrifuge. Both the spray system and the adhesion strength centrifuge were designed and built at the University of Alberta. A detailed description of the experimental methodology is described in Section 3.5.

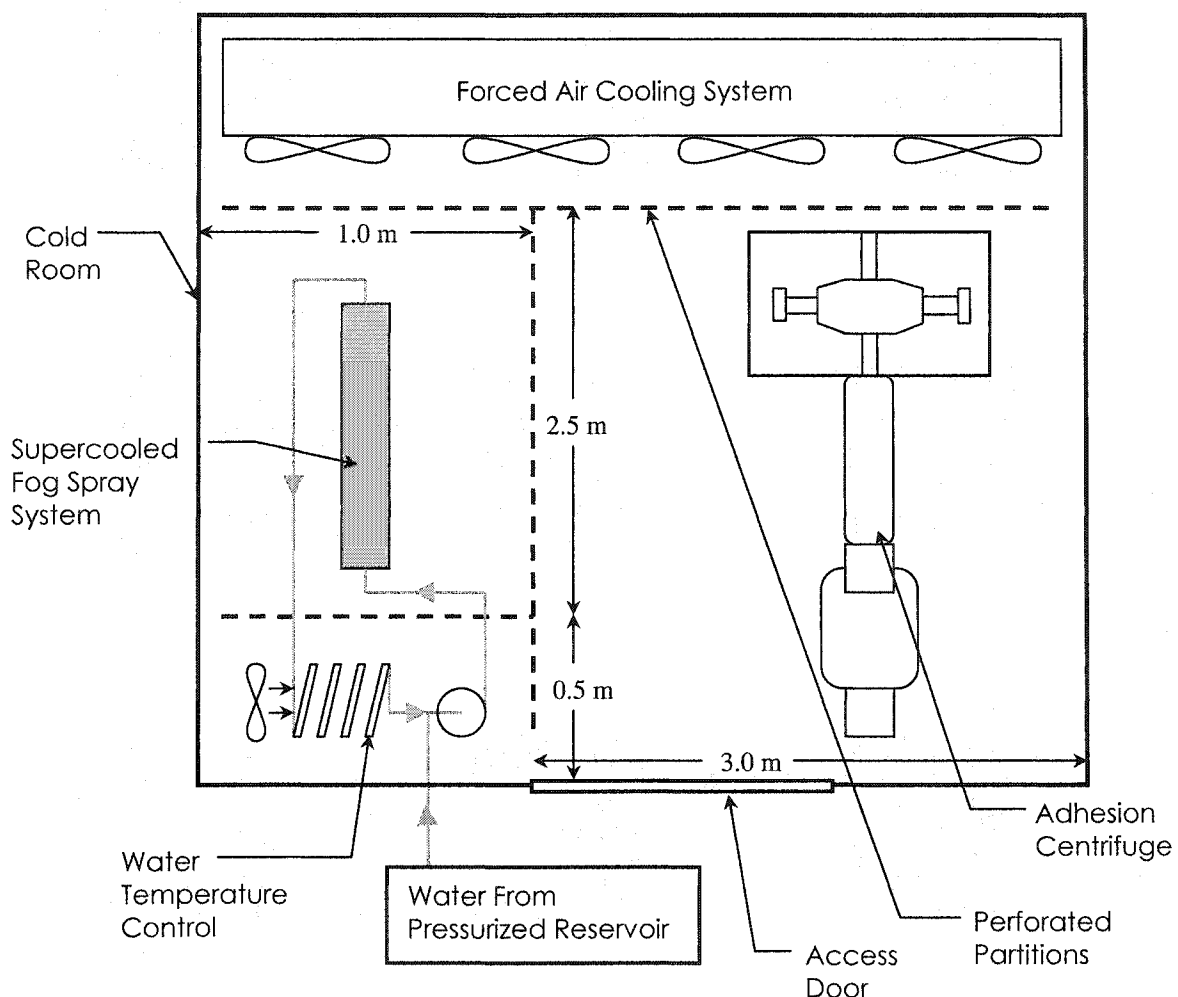


Figure 3-1: Cold Room Setup (Plan View)

3.2 Surface Characteristics of Samples

Aluminum plates were used as the base material for the surface coatings. Aluminum was chosen as all of the test surfaces bonded well to aluminum, and aluminum provides a good weight to strength ratio; which is critical for an object placed at the tip of a high-speed centrifuge. Aluminum also has a high thermal conductivity, so that the surface temperatures of the samples would be nearly uniform. Figure 3-2 outlines the design of the aluminum base plates.

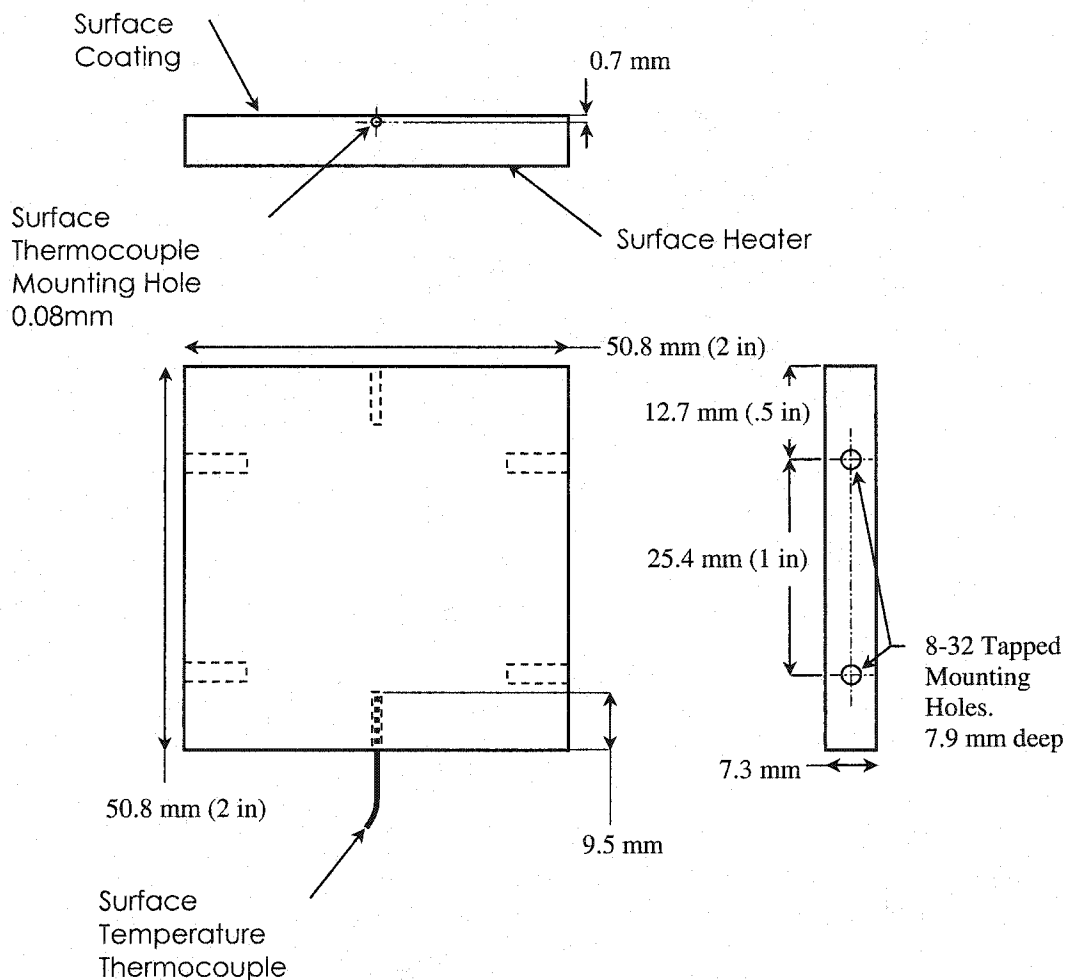


Figure 3-2: Surface Sample Base Plate Design

Two K-Type thermocouples were mounted inside each plate just below the coated surface, to monitor the surface temperature rise as the plates were heated during testing. The thermocouple tips were coated with heat sink compound and affixed inside the plates using epoxy. A 2580 mm², 17.8 Ω surface heater manufactured by Minco was attached to the bottom of each plate. The heater power is controlled independently of the centrifuge, and can deliver up to 50 W.

Four surface coatings were available for the adhesion testing, two of which are coatings currently used as blade gelcoats by wind turbine manufacturers, and two are surfaces with low surface tensions designed for water and ice shedding. Ameron and Progress Plastics supplied the gelcoats used on production wind turbines and 21st

Century Coatings supplied both of the low surface tension coatings. Relevant thermal and physical properties for the current experiment are listed in Table 3-1.

Table 3-1: Test Surface Characteristics

Manufacturer Name	Base Material	Average Surface Roughness (μm)	Average Coating Thickness (μm)	Thermal Conductivity (W/m-K)	Advancing Contact Angle
Ameron PSX700	Engineered Siloxane	0.27	110	0.22	77°
Progress Plastics 20-4969FX Gelcoat	Isophthalic Polyester	0.32	100	0.29	112°
21 st Century Coatings PC100	Fluorinated Polyurethane	0.18	75	0.20	81°
21 st Century Coatings PC200	Fluorinated Polyurethane with Silicon Additives	0.11	75	0.20	85°

The coating properties were obtained from the manufacturers except for the advancing contact angle, which was measured at the University of Alberta. A 0.65 mm diameter needle was used to create a droplet of distilled water on each of the surface coatings. Five digital images were taken of the advancing contact angle as the droplet grew, and the average value is listed above. Contact angle photos of each of the surfaces can be found in Appendix A, there was up to a 2° variation within each set of images. The surface manufacturers' data sheets can be found in Appendix B.

The aluminum plates were coated with one of the four selected surface coatings by the coating manufacturer. Four samples of each coating were made, two were intended for testing and two were used as spares when the testing surfaces became accidentally damaged.

Polished aluminum samples were also prepared at the University of Alberta to serve in comparison and calibration tests. The original design of the centrifuge

predicted that stresses on the order of 700 kPa could be induced, as it was estimated that such stresses would be likely necessary to cause ice-aluminum adhesion failures. It was later found that rotational speed limitations prevented the centrifuge from producing stresses large enough that the ice samples would release from the aluminum surfaces without melting the interface. It should be noted that a contact angle of 61° was measured on the aluminum surface.

3.3 Cloud Simulation

In order to produce repeatable samples of rime ice, a fog spray system was designed to spray supercooled water droplets onto the test surfaces in order to simulate possible in-cloud operating conditions. Figure 3-3 is a schematic of the spray system.

Atmospheric icing varies from location to location, depending on ambient air temperature, cloud droplet size distribution, wind speed and liquid water content. It was therefore necessary to choose a representative set of conditions to form rime ice. Pruppacher and Klett (1978) report that cloud droplet diameters may vary between 10-80 μm , for non-tropical clouds. Finstad and Makkonen (1993) estimate that the median volume droplet diameter in typical icing clouds for wind turbines, ranges between 10-30 μm with the cloud's liquid water content ranging between 0.1-1 g/m^3 .

To produce droplet size distributions similar to mountain-top in-cloud rime icing conditions, Bete PJ8 nozzles were selected for the water spray system. At 345 kPa (50 psi), the manufacturer lists the droplet distribution diameter between 0-100 μm , with a volume mean diameter of 65 μm . Given the natural variability of droplet sizes and distributions, and the fact that larger droplets tend to have higher collision probabilities with a turbine blade, this spray distribution falls within an acceptable range for the purposes of this experiment, although it is on the upper end of the droplet size distribution compared with icing clouds. The detailed setup of the spray system is shown in Figure 3-4.

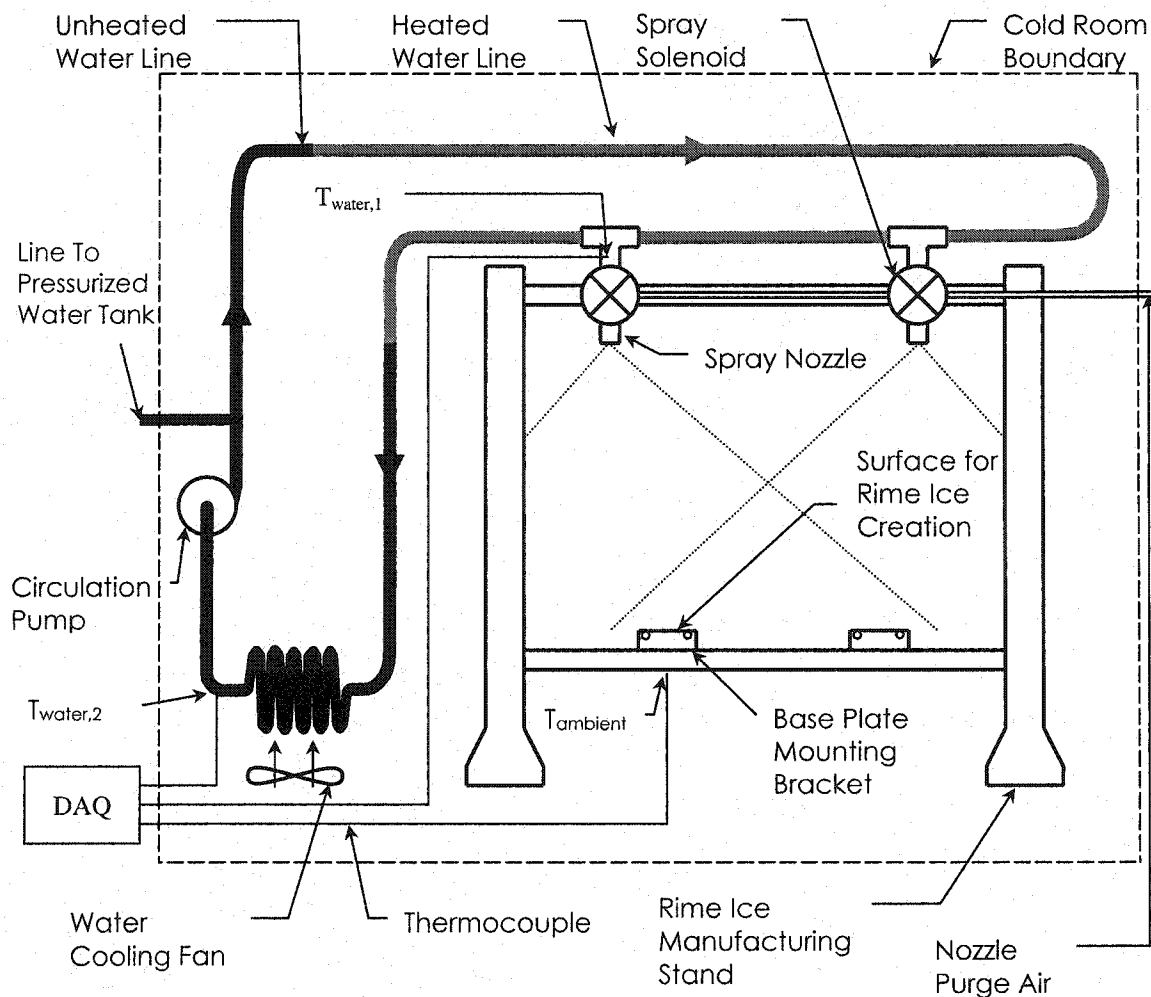


Figure 3-3: Cloud Simulation Spray System Schematic and Thermocouple Locations

The spray nozzles were located 229 mm (9 in) apart such that their sprays overlap to produce a uniform mist at the test surface location. The test surfaces were located 229 mm (9 in) below the spray nozzles, and 38 mm (1.5 in) apart. The aluminum base plates were held with four bolts to a mounting bracket (see Figure 3-4). A 3 mm (0.1275 in) air gap was designed between the samples and the bracket to ensure that the accreting ice formed only directly above the test surface.

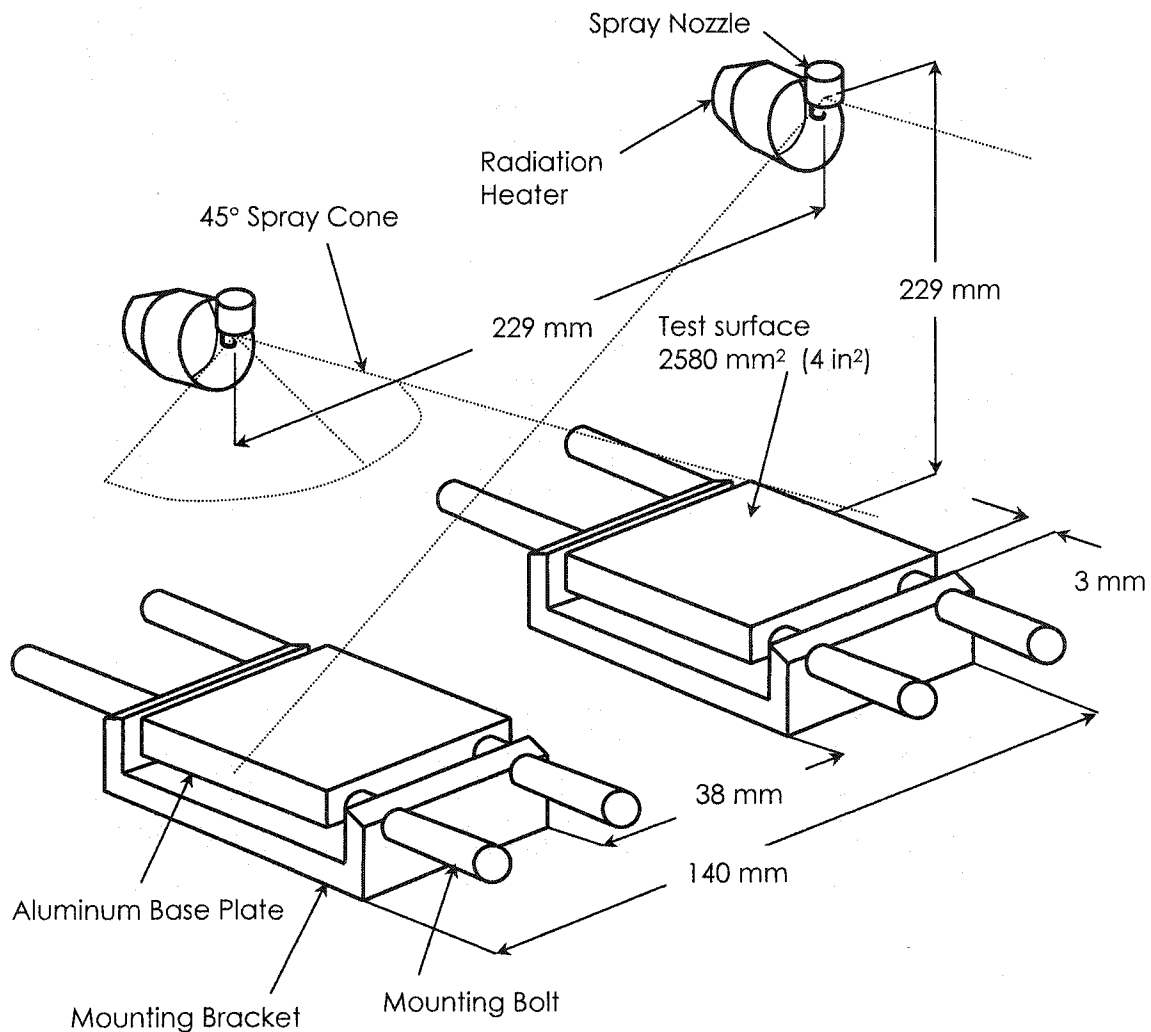


Figure 3-4: Spray Nozzle Setup

Cycling the spray nozzles on and off was required to maintain a constant ambient air temperature during the ice accretion process. Between water spray cycles, pressurized air was used to purge the nozzles in order to prevent freezing. In addition, heat lamps were used as radiation heaters between spray cycles to prevent ice build-up on the spray nozzles. They shut off one second before each spray cycle to ensure that the falling droplets would not be heated as they approached the test surfaces.

Distilled water was used in the system. This prevented mineral deposition on the nozzles and mimicked atmospheric water droplets more closely than standard tap water. The water was continually circulated through the spray lines in order to avoid

freezing, and was pressurized by an upstream reservoir to ensure that the spray was at 345 kPa (50 psi). A cooling fan and coil along with a line heater along the water line were used to control the water temperature.

During the spraying process, the water temperature was kept between 0°C and -0.5°C such that the droplets would be supercooled at impact, while ensuring that the spray system did not freeze. Additional droplet supercooling occurred as the droplets fell through the ambient air, so that the droplets would have been very close to the ambient temperature when they impacted on the test surface (see Appendix C for temperature estimate).

The ambient air temperature was monitored below the sample mounts to ensure that it did not significantly rise during the ice manufacturing process. Supercooling of the water droplets before impingement was necessary in order to get the freezing fraction as close to 1 as possible, that is to say the water freezes quickly on impact, resulting in rime ice.

This system was able to produce repeatable rime ice samples at -8°C and -15°C. The resulting rime ice formed with uniform thickness on the test surfaces. The samples were weighed and the thickness measured, and it was found that the rime ice samples had densities ranging between 550-600 kg/m³, which is within the range of rime ice density experienced on wind turbines in operation (Makkonen 1991). Figure 3-5 shows a typical sample accretion manufactured with the spray system.

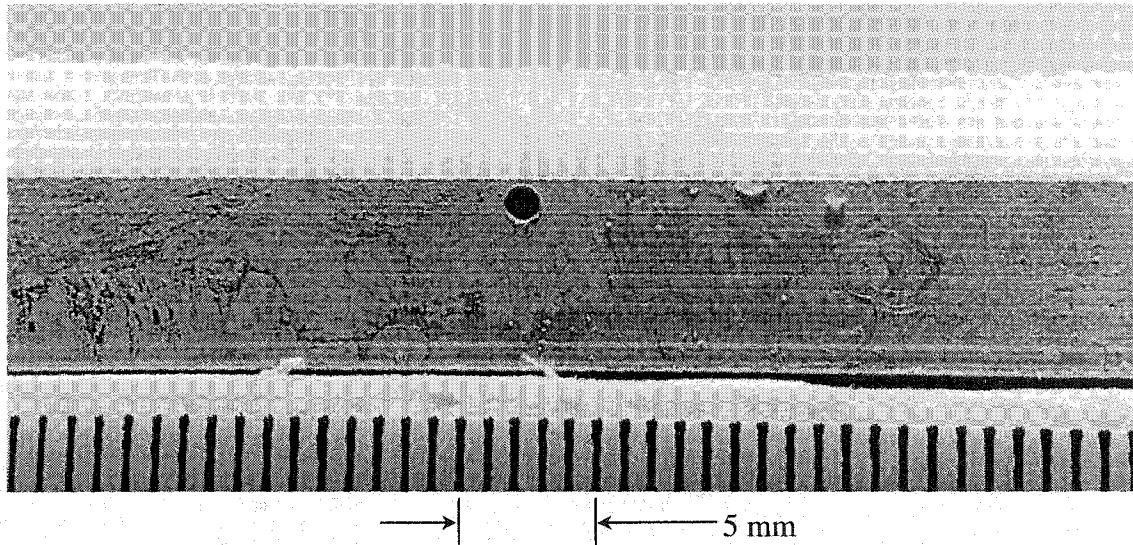


Figure 3-5: Rime Ice Accretion on Test Surface

3.4 Adhesion Strength Centrifuge

3.4.1 Forces on a Wind Turbine Blade

Three-bladed horizontal axis wind turbines (HAWT) have become the most common commercially available wind-energy systems. Such turbines range in size from small-scale community systems with 10-100 kW outputs, to large offshore 3 MW turbines as part of national power grids. Wind turbines that are commonly found in mountainous regions, and thus may be subjected to in-cloud icing are in the 660 kW – 1 MW range, with 50 m rotor diameters and 60 m tower heights being typical dimensions. These turbines operate with average wind speeds in the range of 5-10 m/s and rotate typically at 20-30 rpm. The turbine blades, and any ice forming on them are therefore subjected to a variety of external loads; loads resulting from the impinging wind, centripetal loads from the rotation of the blades, as well as wind gusts and blade flex.

At wind speeds of 10 m/s and rotational speeds of 30 rpm, turbine tip speed can reach relative wind speeds approaching 100 m/s, close to a Mach number of 0.3. These speeds are comparable to small aircraft speeds. Therefore the forces exhibited on the blades can be compared to work done by Scavuzzo et al. (1994) who investigated the

aerodynamic forces involved with ice shedding. Scavuzzo et al. list three major stresses at the ice interface that are caused by the aerodynamic forces on the airfoil; inertial forces due to the rotation of the blades (or propeller), pressure induced forces, and blade (or wing) flexing. Figure 3-6 illustrates these forces acting on ice accreted to a turbine blade.

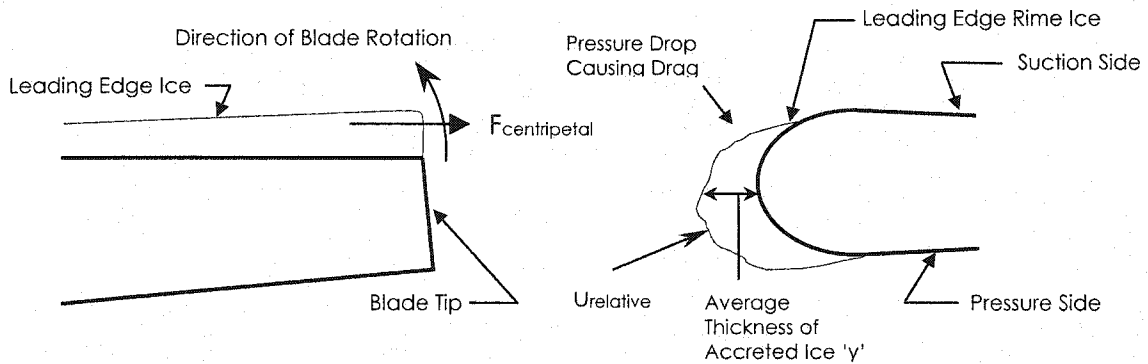


Figure 3-6: Body Forces Induced on Accreted Rime Ice

The inertial force caused by the rotation of the turbine blades will induce a shear stress on the ice that increases with the radius of the blade. The magnitude of the shear force resulting from centripetal loading can be estimated as:

$$F_c = m_{ice} \omega^2 r \quad (3.1)$$

where ω = turbine rotational speed (radians/sec),

r = radial position along blade (m),

m_{ice} = mass of rime ice (kg):

$$m_{ice} = \rho_{ice} A y \quad (3.2)$$

where ρ_{ice} = rime ice density (kg/m³),

A = surface area of ice accretion (m²),

y = average thickness of ice accretion (m).

The shear stress τ , can therefore be estimated as:

$$\tau = \frac{F_c}{A} = \rho_{ice} \omega^2 r y \quad (3.3)$$

Using the typical dimensions for a turbine listed earlier, if 5 cm of rime ice accretes with a density of 600 kg/m³, the rotation of the turbine at 30 rpm will induce shear stresses of 0.8 kPa, 3 m from the rotor hub and up to 7.4 kPa at the blade tip 25 m from the rotor hub.

Scavuzzo et al. (1994) used a two-dimensional finite element model, developed using ANSYS finite element software, to predict the stresses induced on an ice accretion on a NACA 0012 airfoil by aerodynamic forces. Equation 3.4 was used to calculate the pressure distribution around the accreted ice profile to determine the induced stresses.

$$P = C_p \frac{1}{2} \rho_{air} u_{relative}^2 \quad (3.4)$$

where P = surface pressure (Pa),

C_p = coefficient of pressure,

$u_{relative}$ = relative speed of wind and airfoil (m/s).

Table 3-2 lists the peak stresses at the ice interface determined by Scavuzzo et al. using this program.

Table 3-2: Peak Stresses at the Ice Interface with an Airfoil

Mach Number	Angle of Attack (°)	Peak Tensile Stress (kPa)	Peak Shear Stress (kPa)
0.3	0	12.9	12.8
0.12	0	8.9	1.4
0.12	2	2.6	2.7
0.12	4	3.3	3.4
0.12	6	3.4	2.8

It is important to note that the pressure decreases with the square of velocity, so that the interface stress drops quickly as the relative wind speed decreases, which is towards the rotor hub in the case of wind turbines. Furthermore, the peak shear stresses were found

to occur only over short distances along the interface of the accreted ice, while the average interface stress was typically a factor of 2 less than the peak stress. Therefore, in the case of rotating wind turbine blades, the combined effects of centripetal and aerodynamic forces may cause peak shear stresses that can reach almost 20 kPa at the blade tip, and diminishing to approximately 2 kPa at the blade stem. The average shear stress along the ice interface however is more likely to range from 13 kPa to 1 kPa along the length of the blade.

Normal stresses are not induced on the ice by the rotation of the turbine blades, but Scavuzzo et al. found that tensile and compressive stresses can be induced due to the aerodynamic pressure forces. Compressive stresses arise due to the impinging air, but they do not cause adhesive failures. A tensile stress is induced in the ice due to the pressure difference on the pressure and suction sides of the airfoil. The surface of the airfoil becomes more and more normal to the streamlines downstream of the stagnation point. This curvature of the airfoil may cause ice adhered to the blade to be in tension due to pressure drops on the suction side of the blade shown in Figure 3-7. As seen in Table 3-2, the peak tensile force can be as large as the peak aerodynamic shear forces. However, this was found only at the extremity of the ice accretion on the suction side of the airfoil, and quickly dropped by approximately a factor of 4 along the remainder of the ice interface. Normal forces therefore are much less significant than shear forces in adhesive failures of ice from an airfoil, rotating or otherwise.

Forces induced by wind gusts and the flexing of turbine blades were ignored in these estimates, as they are unpredictable and therefore unreliable as a mechanism for ice removal. Blade flexing is also not uniform from one blade to the next and can result in unbalanced ice loads, if it were relied upon as the mechanism for ice removal.

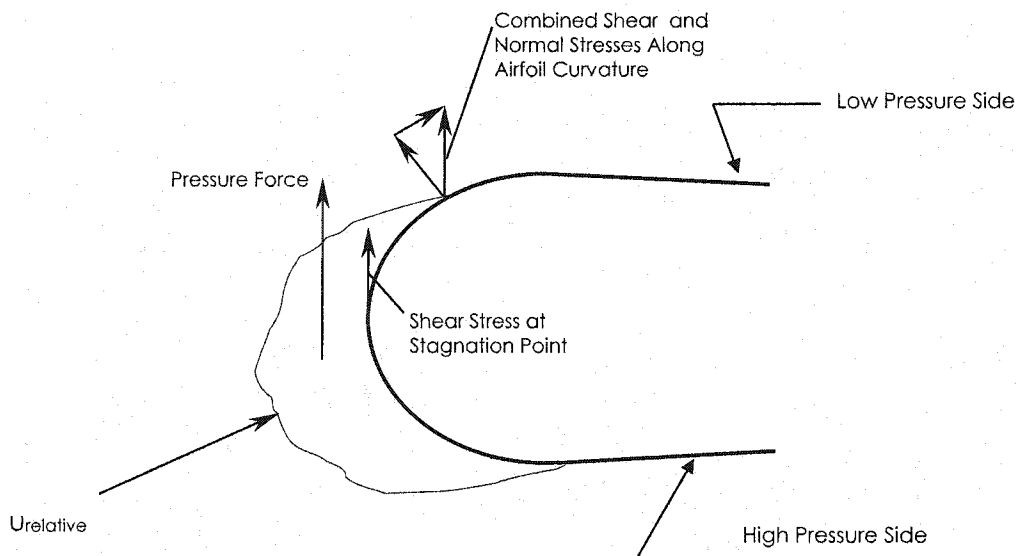


Figure 3-7: Stresses at Ice-Airfoil Interface

3.4.2 Adhesion Centrifuge Design

Figure 3-8 is a schematic of the centrifuge system. The adhesion centrifuge was designed to induce uniform body forces on the rime ice that would be on the order of those exerted on rime ice accreted on wind turbine blades. Temperature, motor speed and heater voltage signals were monitored and recorded using a *Datataker 500* data acquisition system (DAQ) manufactured by Data Electronics. The DAQ was used for both the rime ice creation process and the centrifuge and it was controlled with a QuickBasic interface which sampled all signals at approximately 1 Hz. The control code for the DAQ can be found in Appendix D.

The 240 V/30 A direct current WER Industrial motor was controlled by an Emerson Industrial controller, with a manual speed control dial. A General Electric permanent magnet generator was used as a tachometer. The tachometer signal was calibrated using a variable frequency strobe light to measure the rotor's rotational speed.

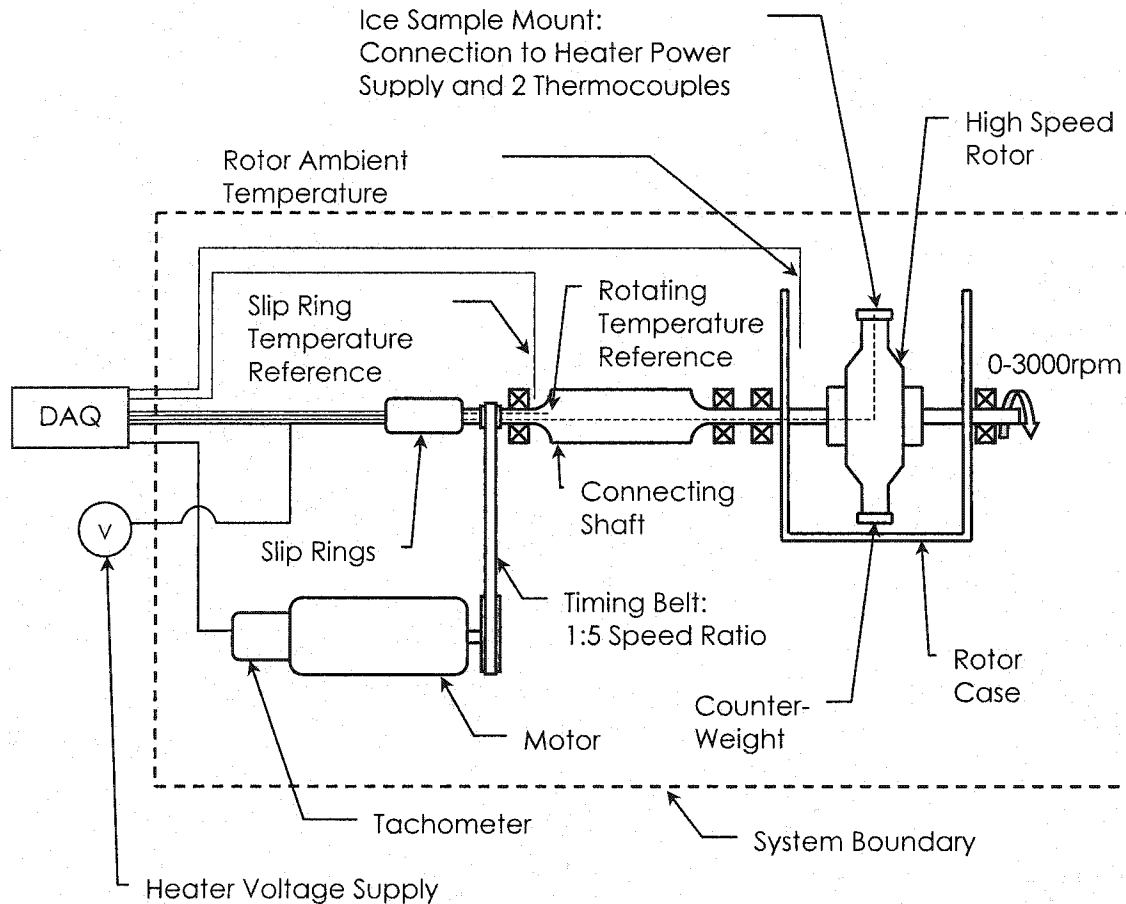


Figure 3-8: Adhesion Strength Centrifuge System Schematic

All thermocouple signals were referenced to an ice bath, and the temperatures were obtained using a K-type thermocouple calibration chart. All of the temperature outputs were calibrated at 20°C and -15°C to be within 0.2°C using a Fluke 2180 RTD digital thermometer with the rotor not turning. Difficulties arose in the temperature measurements, as the temperature readings began to decrease from the steady ambient value when rotation of the centrifuge commenced due to frictional heating of the slip ring rotor. The slip ring temperature reference and the rotating temperature reference were used to correct the errors. The correction method is discussed further in Section 3.6.

The ice sample mount on the ends of the centrifuge rotor could be interchanged such that the test surface was either perpendicular or parallel to the radius, thereby inducing either a normal or a shear body force respectively. Figure 3-9 and Figure 3-10

are detailed drawings of the rotor hub set up for normal and shear stress tests respectively.

After a rime ice sample was created in the fog spray system, it was weighed and fastened into the centrifuge mount at the end of the rotor hub. A counterweight was placed in the opposite mount to minimize vibrations during the tests. The centrifuge was designed to rotate at a given steady speed to create a steady force on the ice before a voltage was applied to the sample heater to raise the surface temperature. The surface temperature rise was monitored by the thermocouples embedded in the aluminum base plates until the ice released from the surface. The temperature at the time the ice failure occurred was recorded and the stress (v_b) induced by the centripetal body force was calculated from the rotational speed, the mass of ice and the length of the rotor arm using Equation 3.5:

$$v_b = \frac{m_{ice} \omega_r^2 \bar{r}}{A_p} \quad (3.5)$$

where m_{ice} = mass of rime ice (kg),

ω_r = rotor rotational speed (radians/sec),

\bar{r} = average radial distance from sample plate to axis of rotation (m),

A_p = surface area of test surface (m²).

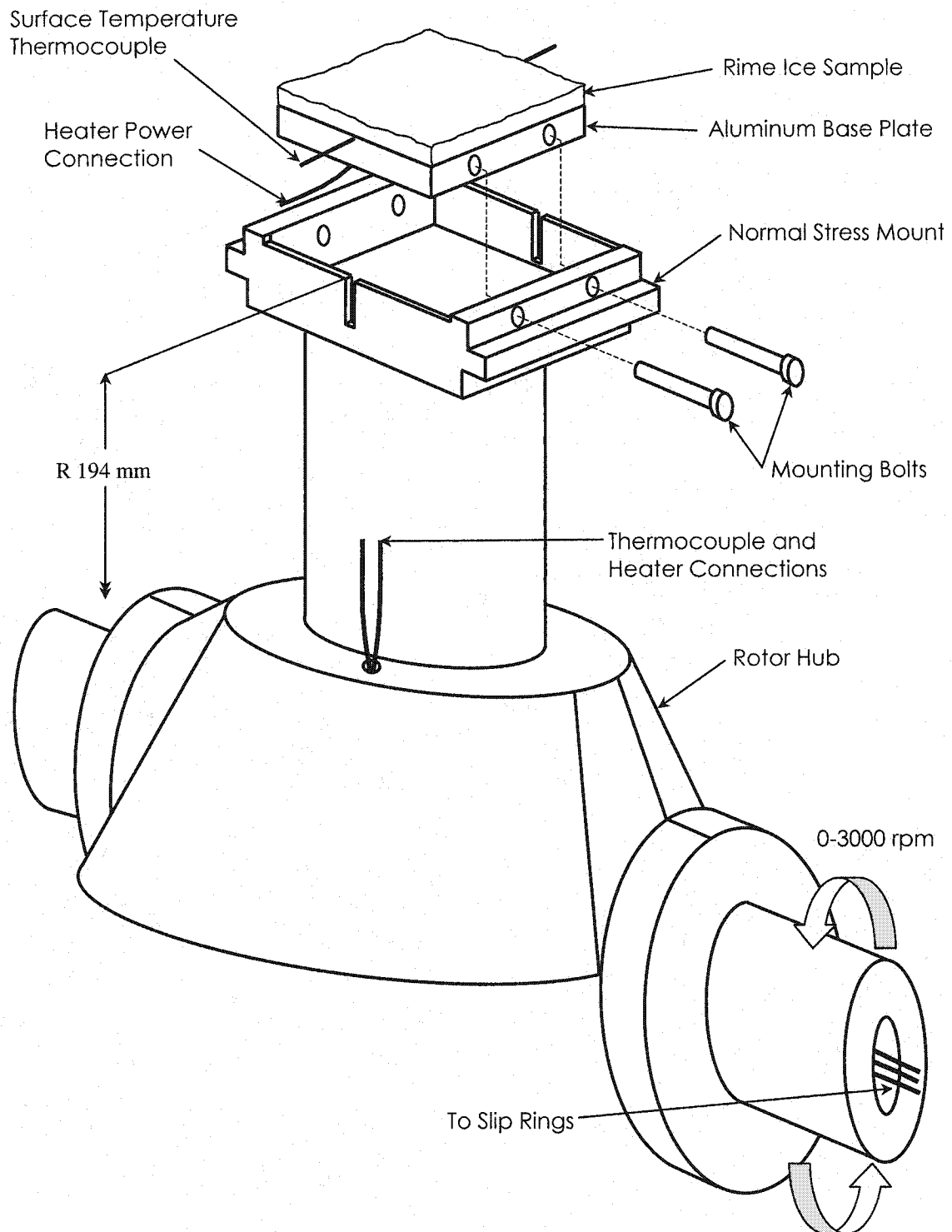


Figure 3-9: Centrifuge Hub Setup For Normal Stress Tests

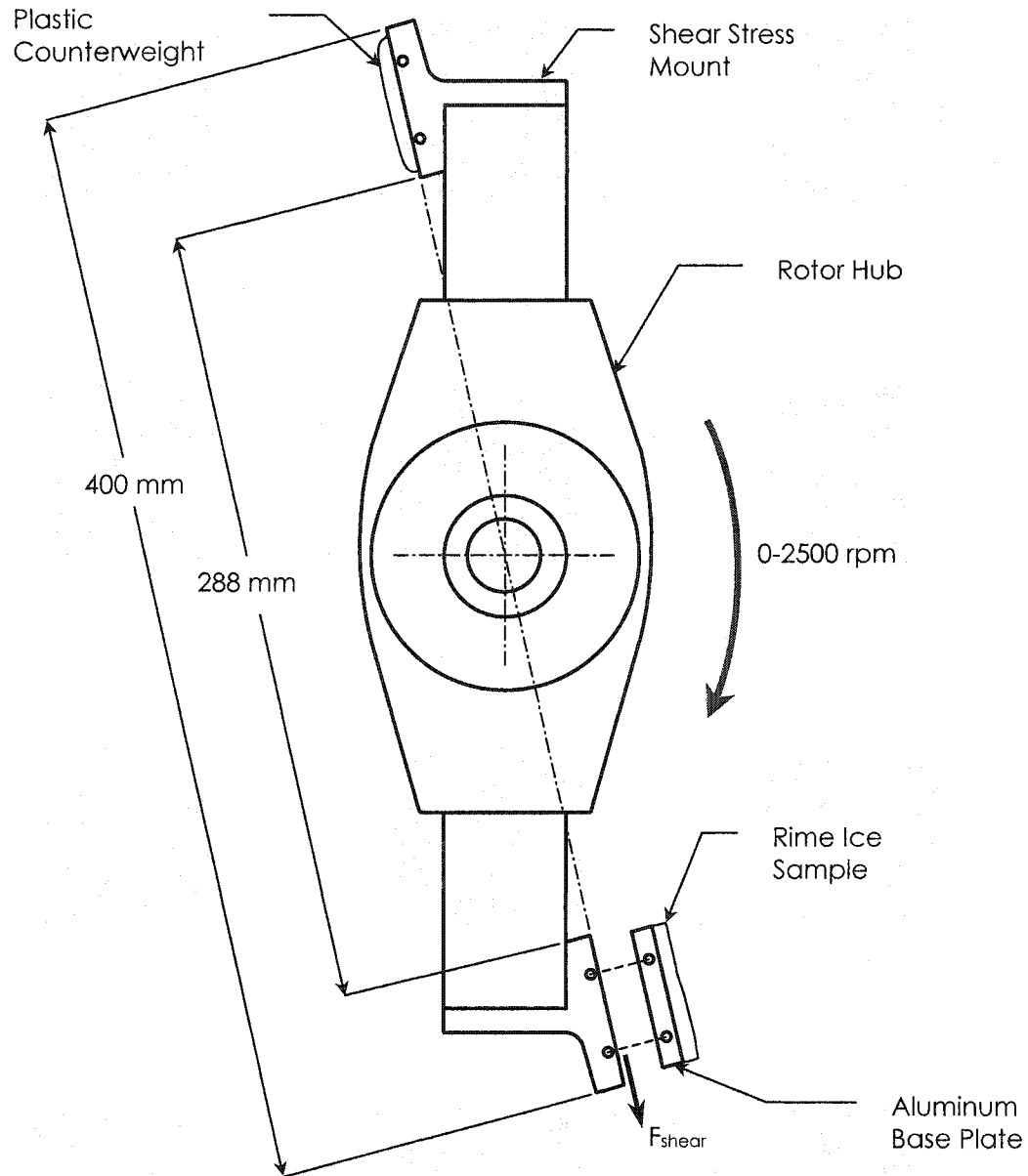


Figure 3-10: Shear Stress Centrifuge Setup

3.5 Experimental Methodology and Data Collection

3.5.1 Rime Ice Creation Procedure

Each test consisted of two parts: creating the rime ice with the fog spray system and testing its adhesion strength in the centrifuge. The spray system was capable of

creating two rime ice samples at once. Typically, two plates with the same surface coating were used in the spray system together. The cold room was set to an ambient temperature of -8°C or -15°C and allowed to reach a steady temperature before testing to ensure that the sample plates and the testing equipment had uniformly reached the ambient temperature.

As mentioned earlier it was necessary to cycle the spray system on and off in order to create rime ice, such that the enthalpy added to the system by the spray water and the latent heat of freezing did not significantly elevate the ambient air temperature and the surface temperature respectively during the process. Although surface warming due to the latent heat of freezing occurs naturally, it is assumed that the high relative wind speeds that wind turbine blades are subjected to quickly remove this heat such that the surface temperature of turbine blades is close to uniform. Makkonen et al (2001) have shown the friction caused by the air flowing over the airfoil can generate a notable amount of heat, warming the leading edge of the blade. The amount of heating depends on the relative airspeed and thus the radial distance along the blade. Therefore, although the temperature of the leading edge of the blade will be above the ambient air temperature, it can be assumed to be uniform during the icing process.

The spray cycle times were chosen by trial and error, by monitoring the ambient air temperature below the plate mounting bracket and the test surface temperature as the ice was created. It was desirable that neither of these temperatures rose more than 1°C above the inherent fluctuations in ambient temperature (about 1°C above and below the average) during the duration of the spraying cycles. For the tests performed at an ambient air temperature of -15°C , the spray was on for 0.5 seconds and off for 9 seconds. For the tests performed at -8°C , the spray lasted for 0.5 seconds and was off for 30 seconds. Figure 3-11 is a time trace of the relevant temperatures during an ice spraying process at an average ambient air temperature of -15°C . Figure 3-11 shows the cyclical ambient air temperature change, the control on the spray water temperature close to 0°C and the surface temperature of the sample remaining close to the average ambient temperature during the ice creation process.

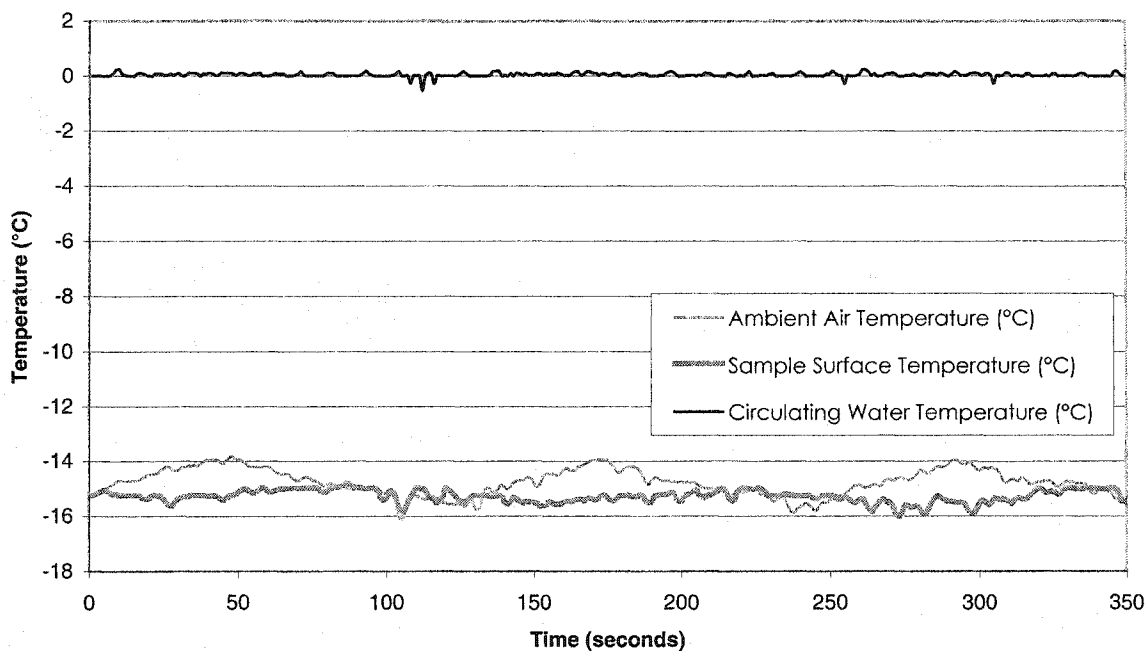


Figure 3-11: System Temperatures During Rime Ice Creation

The number of cycles selected determined the thickness of rime ice that was created. On average 250 cycles were chosen, which produced approximately 6.5 g of rime ice on any of the test surfaces. The average ice density was consistently between 550-600 kg/m³, and as seen in Figure 3-12, it formed approximately uniformly and directly above the test surface. Larger and smaller numbers of cycles were also used to create larger and smaller sample masses of ice. If too large a number of spray cycles were used, the thickness of the ice samples became increasingly less uniform. If too few cycles were used the surface would not be completely or uniformly coated. It was found that uniform samples could be created with masses between 3-9 g.

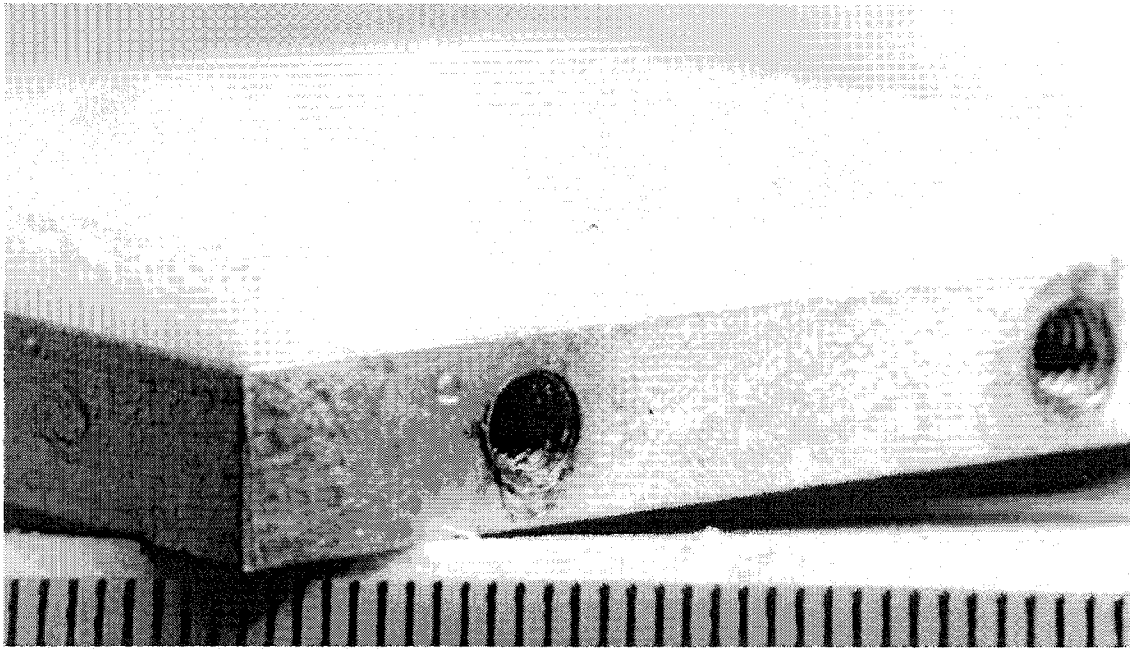


Figure 3-12: Uniform Rime Ice Sample Above Test Surface

3.5.2 Adhesion Test Procedure

With an ice mass of 6.5 g and an average radial distance of 172 mm, the rotor is required to rotate at approximately 1500 rpm to produce stresses on the order of 10 kPa, based on Equation 3.5. For the majority of the tests, 2000 rpm was chosen as the rotational speed as it was found to be a stable, repeatable speed for the motor. Because of the poor aerodynamics of the rotor, rotational speeds beyond 3,500 rpm created noticeable vibrations, and speeds above 4,000 rpm could not be achieved with either the shear force or the normal force sample mount in place. This speed limitation, combined with the mass restriction of the ice samples, limited the stresses that could be induced on the ice samples. The adhesion strength between ice and the aluminum samples could not be measured, as the necessary forces required to cause adhesive fractures could not be achieved due to the aforementioned limitations.

After the ice was created, the samples were weighed and the thickness was measured before they were placed into the adhesion centrifuge. A permanent counterbalance was made from an epoxy of approximately the same height and weight as the average ice sample, and it was fixed in the opposite sample mount. Once

fastened onto the centrifuge, the ice samples were spun to a steady rotational speed. The rotation of the rotor caused a temperature drop inside the rotor case. This can be seen in Figure 3-13, which illustrates the adhesion testing process. This temperature drop was due to the fact that the cooling fans were located directly above the centrifuge rotor case. The thermal mass of the case would ensure that the temperature inside the case was typically very close to the prescribed average ambient temperature when the rotor was not turning. Spinning the rotor would draw in the cooler air directly from the cooling fans, which was colder than the ambient temperature, and normally would not have directly entered the rotor case. The sample was allowed to reach the new lower temperature before the test began. When a steady temperature was achieved, a voltage was applied to the resistance heater such that surface began to warm until the ice failed.

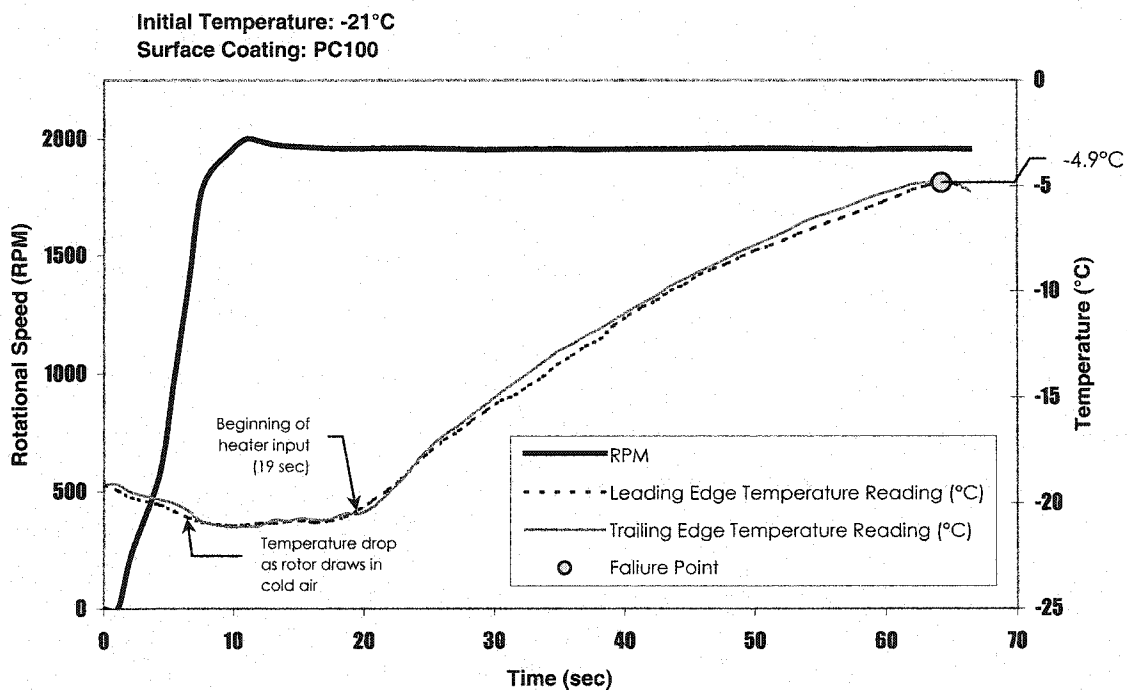


Figure 3-13: Adhesion Strength Test Process

The failure was detected, by visually observing the ice failure and striking an input key so that the data file was marked at the time where the ice released. The system was originally designed with an accelerometer mounted on the rotational axis of the connecting shaft, which would detect heightened accelerations due to rotor

imbalance when the ice failed. The accelerometer could clearly detect excessive vibrations if the system was unbalanced; however, due to the inertia of the rotor, the accelerometer did not detect vibration spikes until well after the ice had released. Because the DAQ could only sample at 1 Hz, a manual response was an adequate replacement for the accelerometer in terms of response time to the ice failure.

3.6 Temperature Measurement Error

3.6.1 Thermal Contact

To verify that there was good thermal contact between the thermocouples embedded in the aluminum base plates, calibration tests were performed by insulating the coated side of the sample base plates. The results are shown in Figure 3-14 which compares the measured temperature to the theoretical temperature rise (dT/dt) described in Equation 3.6, of a mass (m_{Al}) of aluminum being uniformly heated (q):

$$q = m_{Al} c_p \frac{dT}{dt} \quad (3.6)$$

where c_p = specific heat of aluminum 2024 = 875 J/kg·K.

Also shown in Figure 3-14 are the results of an explicit numerical scheme to calculate the temperature within the aluminum base plate. This scheme is further discussed in Section 4.1; suffice to say for the time being that the embedded thermocouples corresponded very well with the expected calculated values so long as the rotor was not turning.

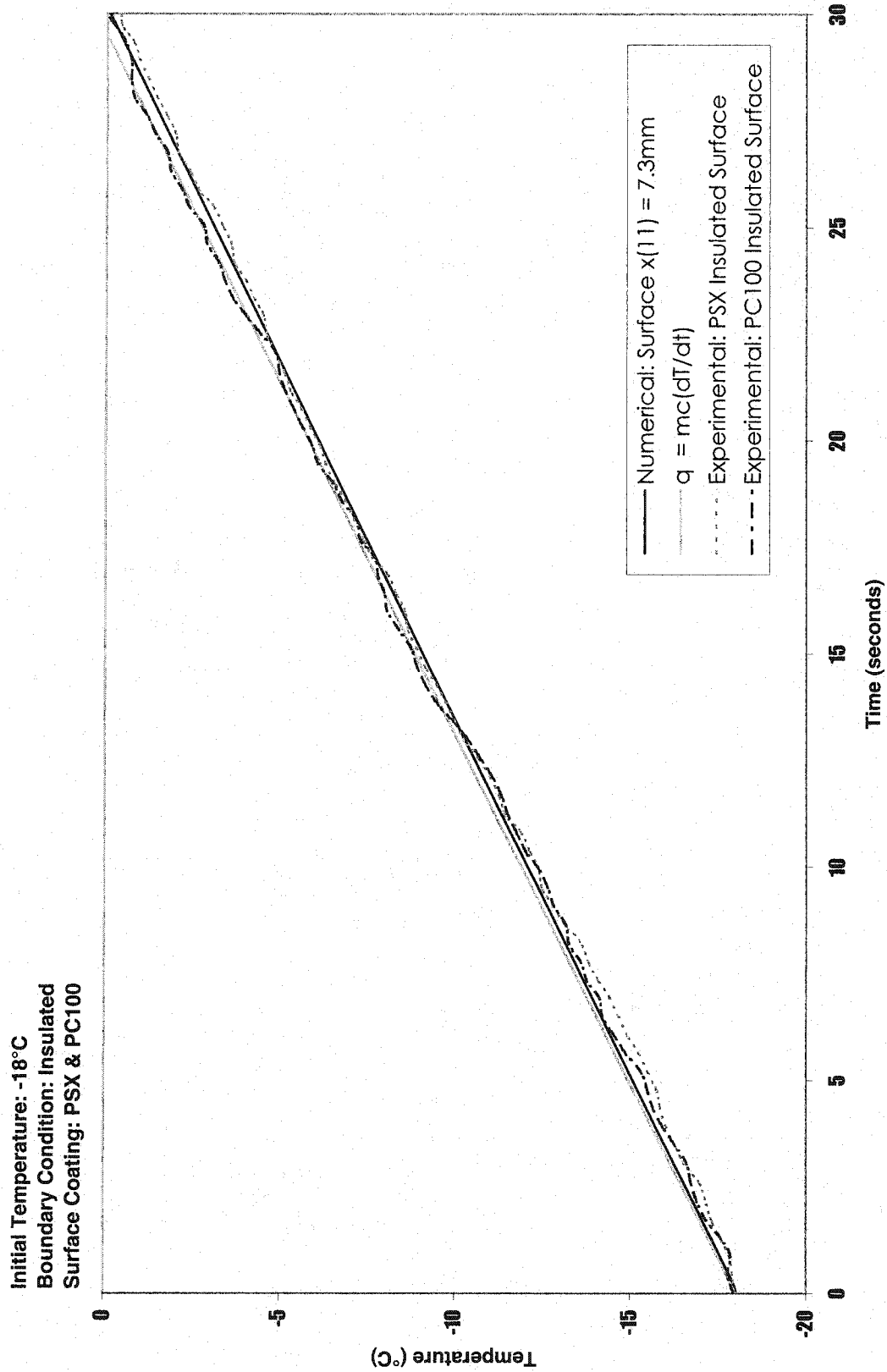


Figure 3-14: Experimental and Theoretical Surface Temperature Rise in Heated Aluminum Base Plates

3.6.2 Slip Ring Errors

Difficulties arose in reading the output from the embedded thermocouples when the centrifuge began to rotate, due to errors induced by the slip rings. A 12 channel silver rotor set of slip rings manufactured by IDM Electronics was used to transmit the signal between the rotor and the DAQ. The silver that is used for the rotor rings adds an additional metal into the thermocouple circuit, as seen in an equivalent circuit schematic of the rotor thermocouples in Figure 3-15.

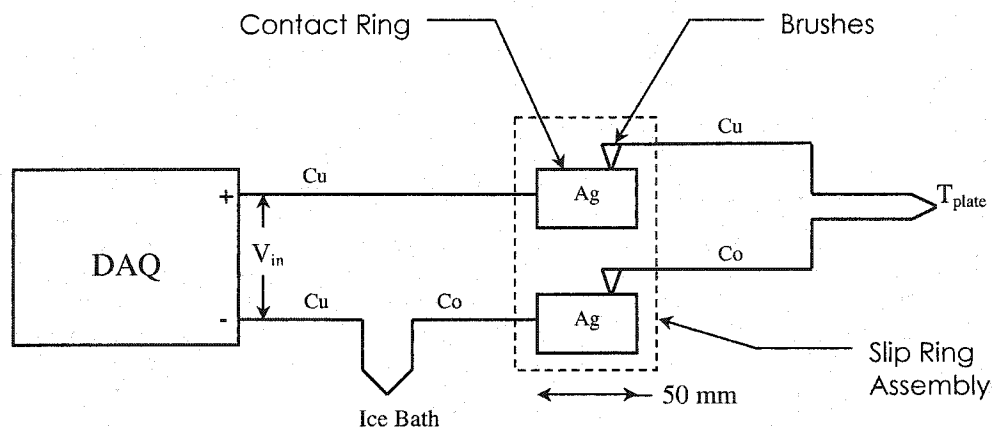


Figure 3-15: Thermocouple Slip Ring Circuit Diagram

The 'law of intermediate metals' states that inserting a third metal between the two dissimilar metals of a thermocouple circuit will have no effect on the output so long as both ends of third metal are isothermal. Therefore the silver rotor would not cause any interference in the circuit so long as it was isothermal. Friction between the brushes and the ring during the rotation of the slip rings inherently generates heat. The output ring is approximately 50 mm from the heat generated at the brushes, the silver cannot be assumed to be isothermal. Thus, the rotation of the slip rings induces unwanted voltages into the system. The problem became obvious during the testing as the temperature reading of the thermocouples connected though the slip rings would drop significantly more than the expected drop due to the mixing of cooler air discussed in Section 3.5.2. Furthermore, for the duration of the test, the temperature reading would continue to drop so long as the rotor was turning, and for a period after the motor was

stopped, likely as the heat diffused into the shaft, until eventually the signal would return to the ambient temperature.

In order to compensate for this problem, two additional thermocouples were added to the system and used as references as shown in Figure 3-8. The *slip ring temperature reference* was secured to the steel centrifuge frame and the *rotating temperature reference* was connected through the slip rings and secured inside the stainless steel connecting shaft. Both temperature reference thermocouples were connected to objects of high thermal mass, within close proximity to one another (5 cm) and were therefore assumed to be isothermal. Any difference in signal outputs between these two thermocouples could therefore be attributed to the internal heating of the slip rings. The aluminum base plate temperatures were corrected using the voltage difference between the slip ring temperature reference and the rotating temperature reference.

The temperature signal problem and correction can be seen in Figure 3-16 which illustrates the thermocouple output signal through the slip rings as well as a thermocouple measurement of the ambient air temperature inside the rotor case which was not connected through the slip rings as a comparison.

Internally cooling the slip rings may have been an alternative solution to the intermediate metal problem posed by them; however, as the referencing method showed good agreement with the ambient thermocouple, this method was deemed adequate. The reference thermocouple inside the centrifuge rotor case was monitored for each test to ensure that it agreed with the aluminum base plate readings before any heat was applied to the samples.

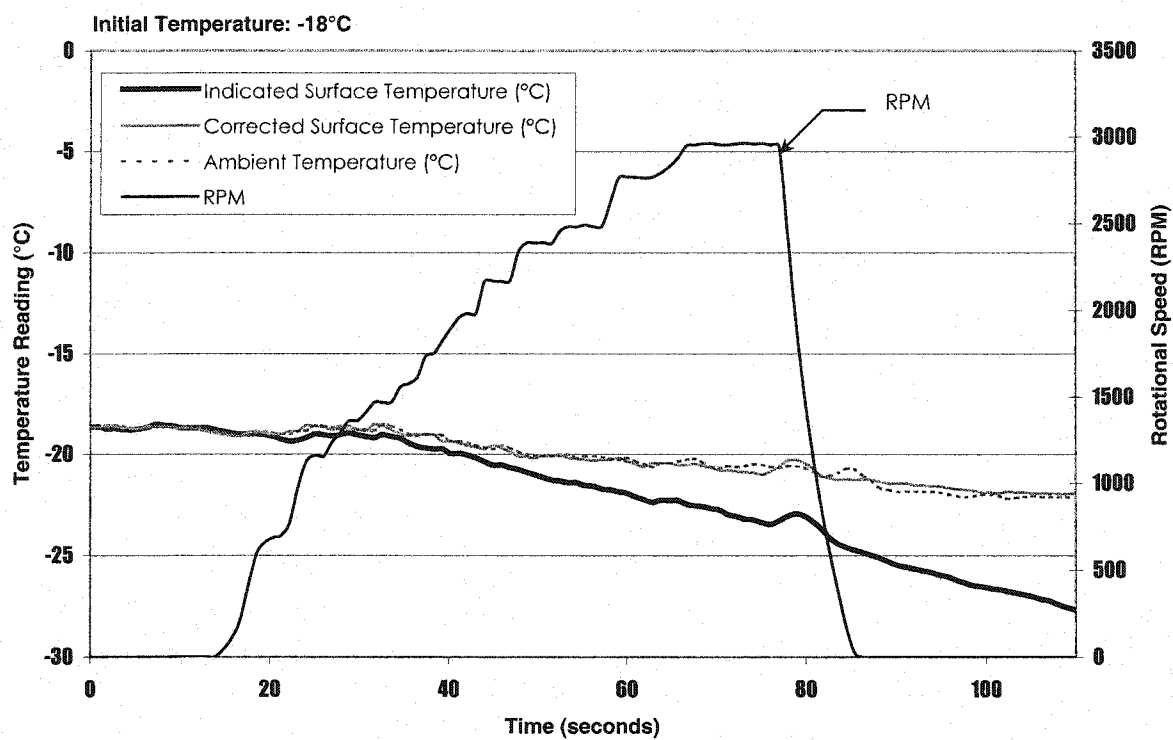


Figure 3-16: Rotor Speed Influence on Indicated and Corrected Surface Temperature

Chapter 4

EXPERIMENTAL RESULTS AND ANALYSIS

The temperatures measured by the thermocouples embedded in the aluminum plates are related to the ice interface temperature. The data were processed using a numerical code to predict the surface interface temperature based on the thermocouple's output. The results are correlated with the contact angles that distilled water makes on the test surface, and how the adhesion strength relates to wind turbine blades.

4.1 Results

4.1.1 Numerical Determination of Surface Temperature

Due to the fact that the thermocouples were embedded inside the aluminum base plates, the surface temperature at the ice interface could not be measured directly. Between the ice interface and the thermocouple, there were the surface coating, the aluminum above the thermocouple hole and the heat sink compound surrounding the thermocouple, all of which are thermal resistors. It was therefore necessary to determine the significance of the temperature differences across these resistors to relate the measured temperature to the desired interface temperature. A numerical scheme was developed to predict the temperature at the ice interface based on the temperature measured by the embedded thermocouples.

Since the length to thickness ratio of the aluminum plates is 7.5:1, a one-dimensional approximation of the heat transfer process was used. The scheme explicitly solves the one-dimensional transient heat diffusion equation:

$$\frac{\partial^2 T}{\partial x^2} = \frac{1}{\alpha} \frac{\partial T}{\partial t} \quad (4.1)$$

where α = thermal diffusivity of material (m^2/s),

x = distance from heater (m),

t = time (s),

T = local temperature (K).

The system is initially uniformly at the ambient temperature, such that at $t = 0$, $T = T_o$ for all x . A constant heat flux is input at the heater boundary, meaning that

$$-k \frac{dT}{dx} \Big|_{x=0} = q''(0), \text{ and an overall heat transfer coefficient } (U) \text{ is assumed at the other}$$

boundary, so that $q''_{outer} = U(T_{11} - T_{\infty})$.

When writing numerical code it is common practice to non-dimensionalize all variables and equations to improve accuracy and avoid overflow errors. In order to non-dimensionalize Equation 4.1, the thickness of the aluminum plate ($L_o = 7.3$ mm) and the initial temperature (T_o in K), were used as reference values for length and temperature respectively. Equation 4.1 can therefore be non-dimensionalized using the following non-dimensional numbers:

$$Fo = \frac{t\alpha}{L_o^2} \quad ; \quad x^* = \frac{x}{L_o} \quad ; \quad \theta = \frac{T - T_o}{T_o} \quad (4.2)$$

where Fo is commonly called the Fourier number. Substituting these non-dimensional numbers into Equation 4.1 yields:

$$\frac{\partial^2 \theta}{\partial x^{*2}} = \frac{\partial \theta}{\partial Fo} \quad (4.3)$$

By central differencing the $\partial^2 \theta / \partial x^{*2}$ term, θ can be explicitly solved for:

$$\theta^{n+1} = \theta^n + \left[\frac{\theta^n_{x^*+1} - 2\theta^n_{x^*} + \theta^n_{x^*-1}}{(\Delta x^*)^2} \right] \cdot \Delta Fo \quad (4.4)$$

where n denotes the non-dimensional time step. If the previously mentioned initial and boundary conditions can be determined, Equation 4.4 can then be solved in a

spreadsheet for the temperature distribution within the aluminum plate. This code was used with an insulated boundary condition instead of a convection boundary condition, for the numerical reference in Figure 3-15.

Assuming that all of the energy input into the resistance heater is transferred into the aluminum plate ($q''(0) = q''_h$), therefore only the overall heat transfer coefficient (U) need be determined as a boundary condition for the ice-interface side of the plate. The process of determining the overall heat transfer coefficient boundary condition is explained later in this section. When appropriate boundary conditions are determined for the various experimental conditions, it can be shown, using Equation 4.4, that the temperature within the plate at the location of the embedded thermocouple is insignificantly different from that at the edge of the aluminum plate. This is due to the fact that aluminum has a very high thermal conductivity (167 W/m·K), and the thermocouple is only 0.7 mm below the surface. Figure 4.1 illustrates this internal temperature stratification as the plate is heated.

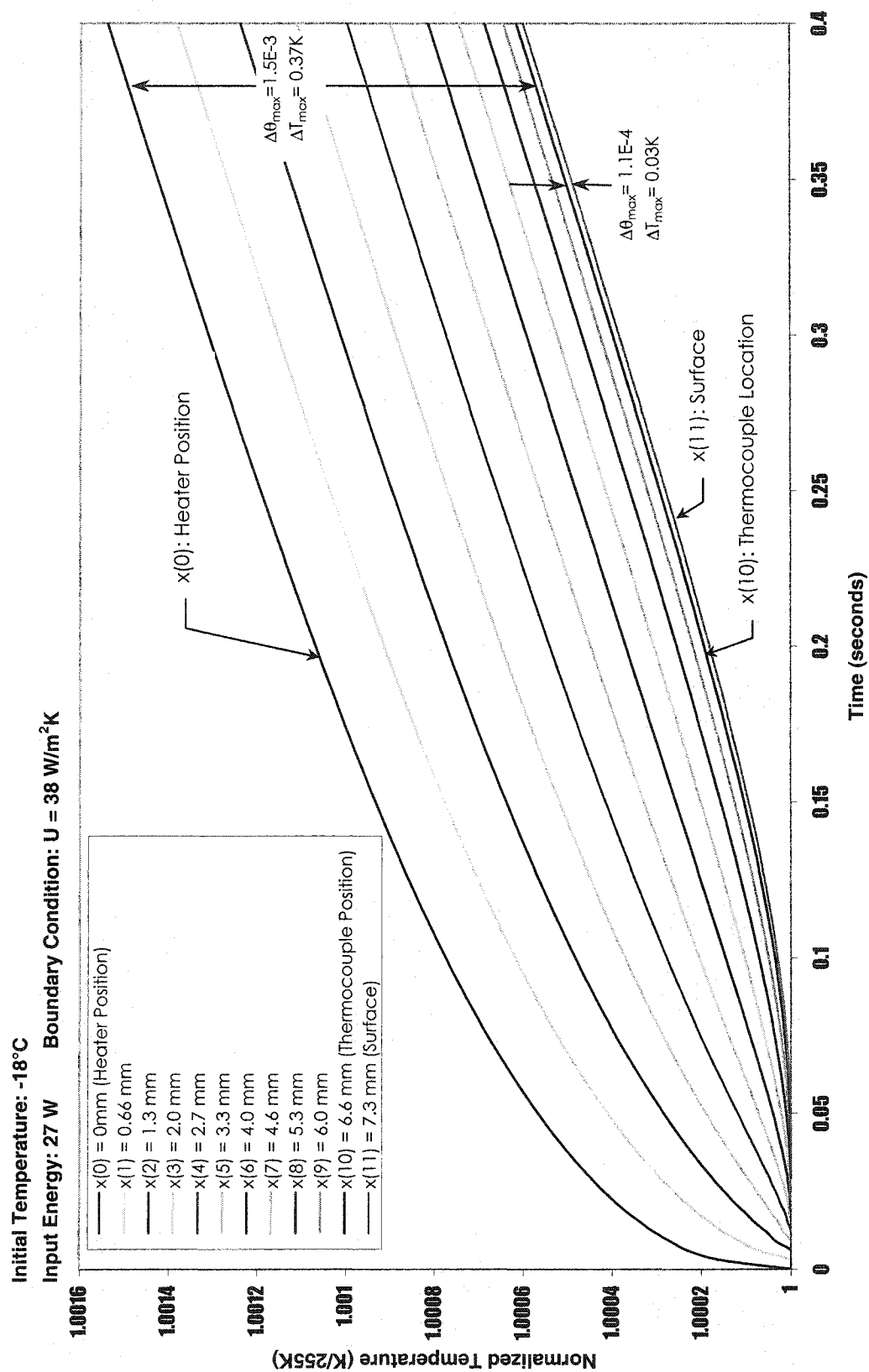


Figure 4-1: Numerical Simulation of Temperature Distribution in Aluminum Plate During Heating

Figure 4-1 shows that a temperature gradient develops within the plate during the first 0.2 seconds after the heat is applied to the system, and that major changes in the temperature profile do not occur beyond this initial transient stage. So long as the steady heat source is applied, the temperature stratification remains almost constant with time, such that after 50 seconds – the duration of a typical adhesion experiment – the temperature difference between the thermocouple position and the outer temperature of the aluminum is only 0.03°C. This difference is below the resolution of the thermocouples used in the experiments so that the thermocouple temperature reading can be assumed to be that of the outer edge of the aluminum plate. This assumes that the thermal conductivity of the aluminum remains constant during the heating process, which is a good approximation over the small temperature changes involved (at most a 20°C temperature rise from the beginning of the test to ice failure).

As mentioned earlier, the negligible temperature difference between the thermocouple position in the aluminum and the aluminum surface is due to the high thermal conductivity of the aluminum. The coatings used in the experiments however, have thermal conductivities four orders of magnitude lower than the aluminum, and although the coatings were very thin (70-110 µm), a significant temperature gradient can occur across the coatings due to their low thermal conductivity. It was therefore necessary to develop a means of calculating the surface-ice interface temperature based on the embedded thermocouple reading.

By assuming a quasi-steady state at each time step, the temperature gradient across the coating shown in Figure 4-2 can be determined by solving Fourier's Law:

$$q'' = -k \frac{\Delta T}{\Delta x_c} \quad (4.5)$$

where: q'' = heat transfer through the coating (W/m²),

k = thermal conductivity of the coating (W/m·K),

Δx_c = coating thickness (m).

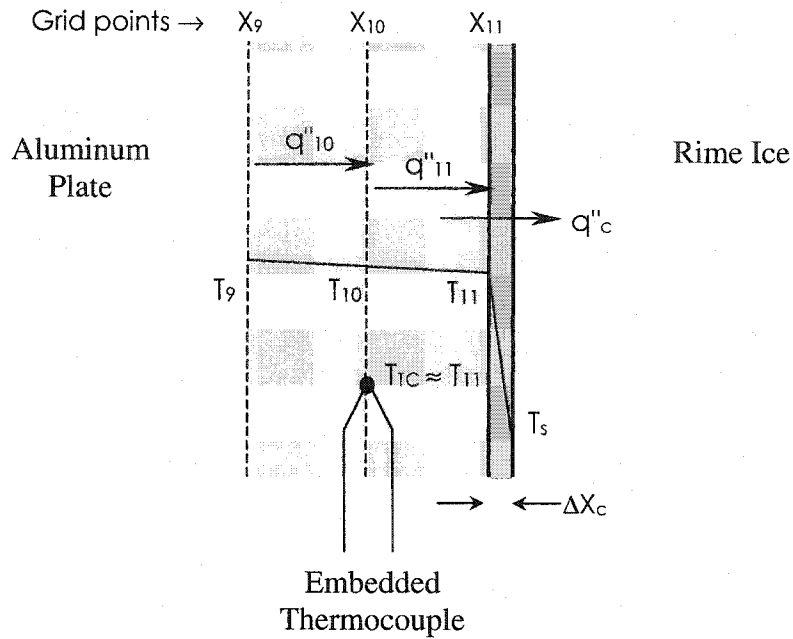


Figure 4-2: Heat Transfer Across Surface Coating

Equation 4.5 can then be re-arranged to determine the surface temperature of the coating based on the inner temperature measured by the embedded thermocouple as shown in Figure 4-2:

$$T_s = T_{TC} - \frac{q''_c \cdot \Delta x_c}{k_c} \quad (4.6)$$

The only unknown in Equation 4.6 is the heat transfer rate across the surface coating, q''_c , as it is not a constant across the aluminum plate during transient heating. The heat transfer rate at the surface coating depends on the input heat transfer as well as the boundary condition, which in this case includes the thermal resistance (R) of the rime ice layer as well as its thermal storage capacity and the convective heat transfer coefficient between the rime ice and the surrounding air. The input heat transfer is a known parameter based in the input voltage, so that only the overall heat transfer coefficient boundary condition needs to be determined in order to calculate the desired surface temperature.

The overall boundary condition can be determined indirectly for each individual test by comparing the experimentally measured thermocouple output over time, with the numerical code. Because the temperature difference between the thermocouple and surface temperature are negligible, both sets of data trace the surface temperature of the aluminum plate at the interface with the coating. The overall boundary condition can thus be set in the numerical code such that it matches the temperature rise in the experimental data; an example of this is shown in Figure 4-3. The overall boundary condition ranged between 30-50 $\text{W/m}^2\text{K}$ depending on the rotational speed and the orientation of the sample.

In Figure 4-3, an overall boundary condition of 38 $\text{W/m}^2\text{K}$ was used for a tensile test at 2000 rpm. At 2000 rpm, the airspeed at the surface of the plate is 40 m/s. By assuming a turbulent flow heat transfer correlation over a flat plate it can be shown that the average heat transfer coefficient would be on the order of 150 $\text{W/m}^2\text{K}$. Assuming that there is no thermal storage within the rime ice, this would mean that the rime ice has a thermal conductivity of 0.25 W/mK for an overall boundary condition of 38 $\text{W/m}^2\text{K}$. The thermal conductivity of rime ice depends greatly on the air trapped within the ice, but Hobbs (1973) has stated the thermal conductivity of glaze ice to be on the order of 2 W/mK at temperatures between -20°C and 0°C . Due to the air pockets, one would expect that the thermal conductivity of rime ice to be lower than glaze ice, therefore, the aforementioned thermal conductivity of 0.25 W/mK for rime ice is within a reasonable range. It is important that the overall boundary condition be approximated with some degree of accuracy, as it influences the predicted surface temperature. For example, when the overall boundary condition is 38 $\text{W/m}^2\text{K}$, the predicted temperature difference across the surface coating is 2.0°C for the case shown in Figure 4-3. If an overall boundary coefficient of 1 or 100 were to be chosen, the predicted correction would be 0.3°C and 3.3°C respectively.

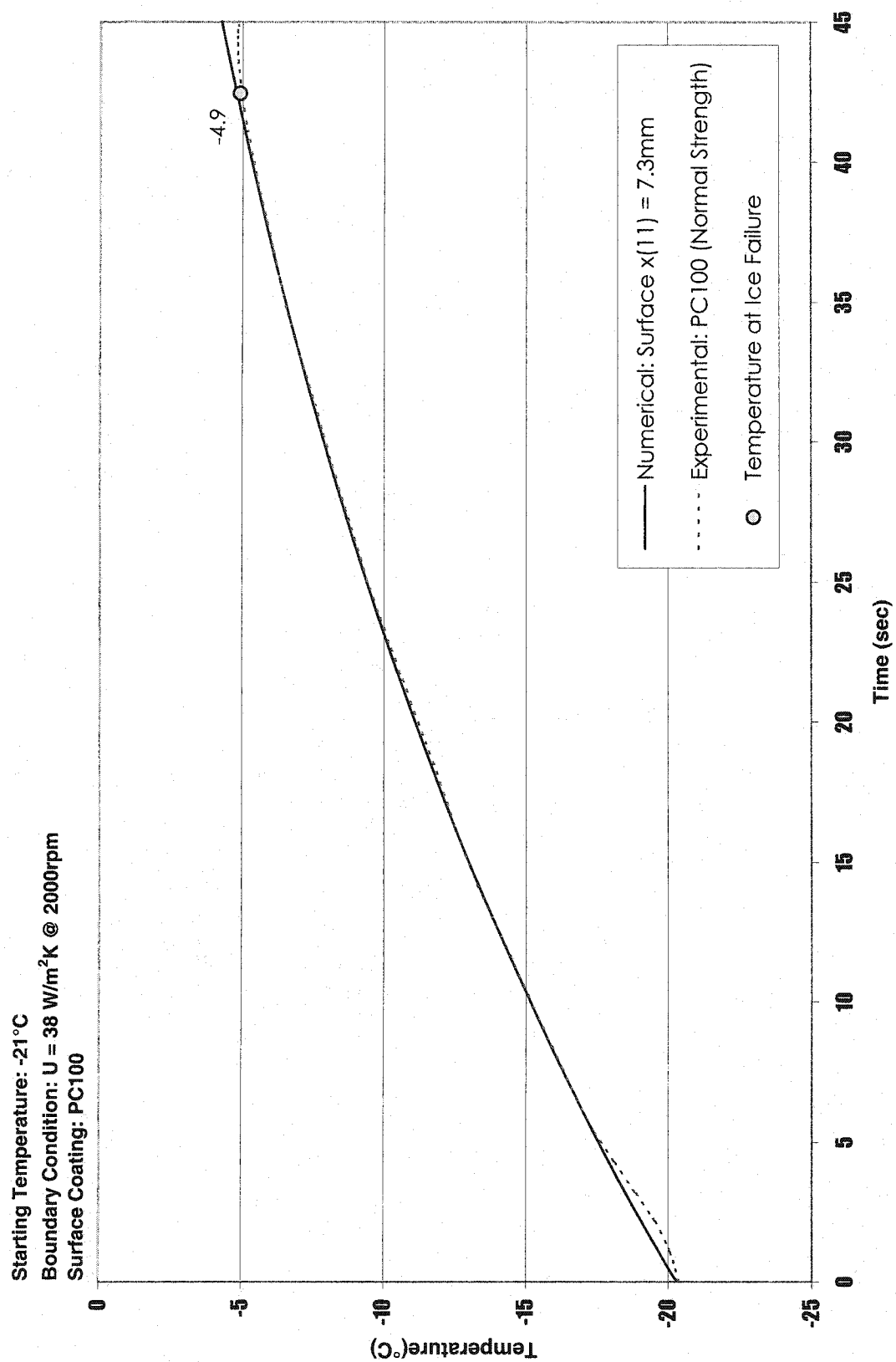


Figure 4-3: Experimental Temperature Rise Compared with Numerical Simulation to Determine Overall Boundary Condition

Because the numerical code predicts the temperature inside the aluminum plate only, the overall boundary condition consists of the surface coating, the rime ice layer and the forced convection due to the rotation of the system as shown in Figure 4-4.

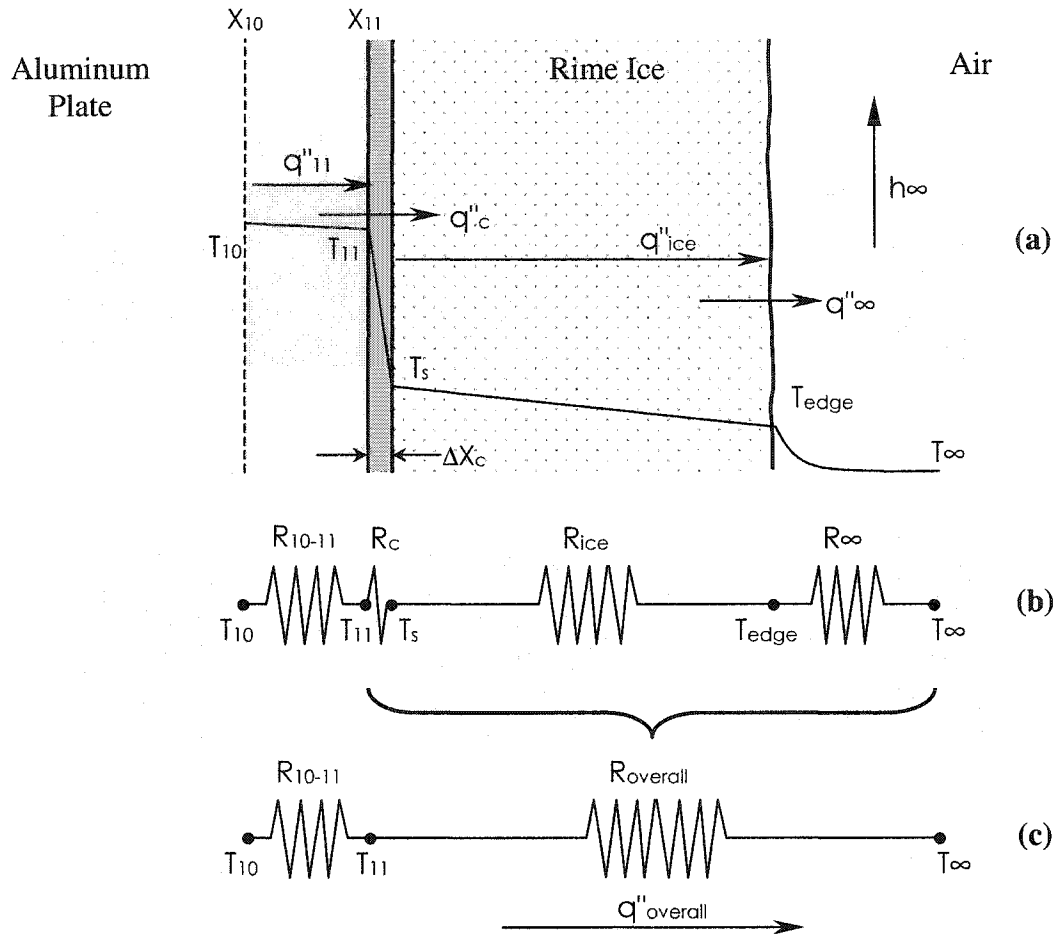


Figure 4-4: Equivalent Thermal Circuit of Ice Sample

Assuming that a negligible amount of energy is absorbed by the small mass of the surface coating as heat is applied, the system can be treated as if it were in a quasi-steady state so that q''_c can be approximated by the temperature gradient between x_{10} and x_{11} , that is $q''_c = q''_{11}$. Figure 4-5 shows the temperature gradient across each grid cell during the heating process.

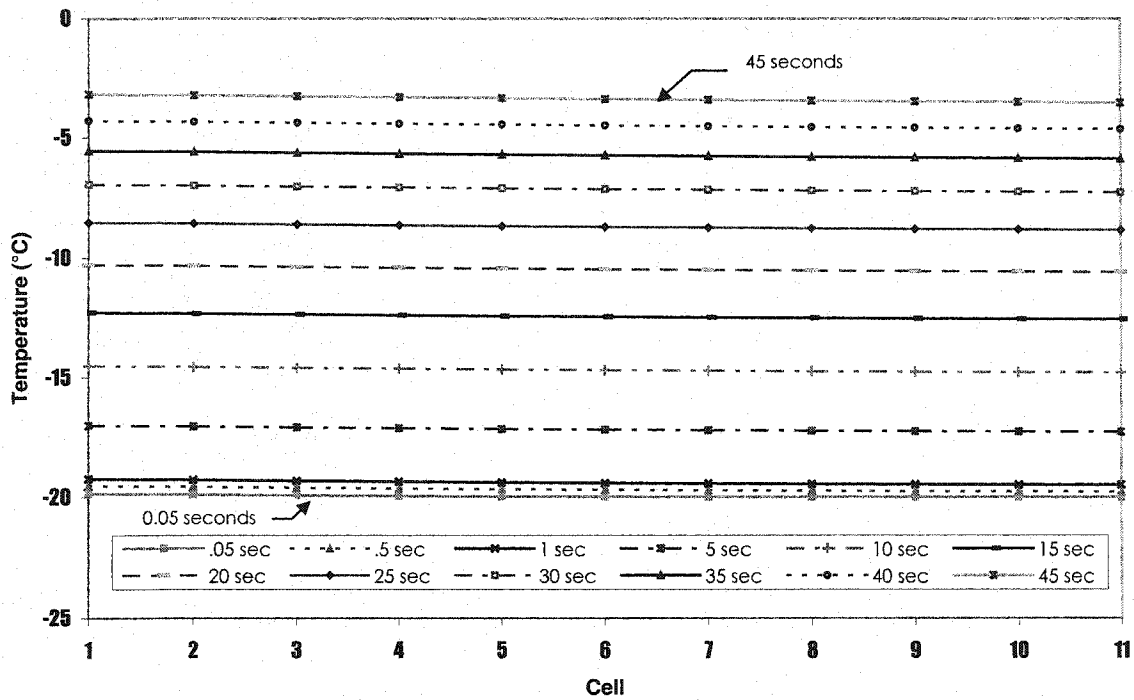


Figure 4-5: Predicted Plate Temperature Distribution During Heating

Because the temperature gradients are almost linear, determining q''_{11} from the slope of the temperature is a good approximation. Therefore, by letting $q''_c = q''_{11}$, Equation 4.6 can be re-written to find the surface temperature of the ice-coating interface as:

$$T_s = T_{TC} - \frac{q''_{11} \cdot \Delta x_c}{k_c} \quad (4.8)$$

The surface temperatures presented hereafter have all been processed in the preceding manner. Therefore the surface temperatures presented are all indirect measurements.

4.1.2 Adhesion Strength Results

The majority of the data was collected using ice samples that were created at an average ambient temperature of -15°C . This is because it became quickly apparent that the ice that was formed at -8°C yielded similar results, indicating that it was the surface temperature not the temperature at which the ice was created that lead to the adhesive failures. The bulk of the data are for the tests where the ice formed at -15°C ; tests with

ice formed at -8°C , if any, are indicated with a different symbol. The centrifuge was set to rotate at either 2000 or 2250 RPM for the experiments to produce a range of applied forces. A comparison between the forces generated at the different speeds is shown in Section 4.2.1. The heater power was set at 27 W for all of the experiments. As will be discussed in Section 4.2.1, tests were performed at a reduced power and it was found not to have a bearing on the release temperature. Therefore the maximum available heater power (27 W) was used in order to minimize the length of each test. A measurement error estimate is also presented on the individual test surface figures. The error estimate calculations are shown in Appendix E.

A best-fit line is drawn through each data set while forcing an intercept at the origin, as it is assumed that the adhesion strength at the melting point is close to zero, as Jellinek (1959) found in his experiments with glaze ice. Furthermore, at the melting temperature van Oss et al. (1992) found that the interfacial surface energy between ice and liquid water is 0.04 mJ/m^2 , practically zero for the present application. A slope was determined using the best-fit line that indicates the nominal stress increase per degree Celsius of surface temperature change.

Rime ice is a collection of individually frozen droplets. Consequently, there are inherent air gaps within the ice, as well as at the interface. The failure stress plotted on the figures was determined by dividing the centripetal force by the surface area of the sample. This surface area is not equal to the area of contact between the ice and the surface because of the aforementioned air pockets, seen in a top view of a rime ice sample in Figure 4-6.

Therefore, although the stresses presented may be practically useful as they are based on the geometry of the iced surface, they are not the true stress, which should be based on the actual area of contact between the surface and the ice droplets.

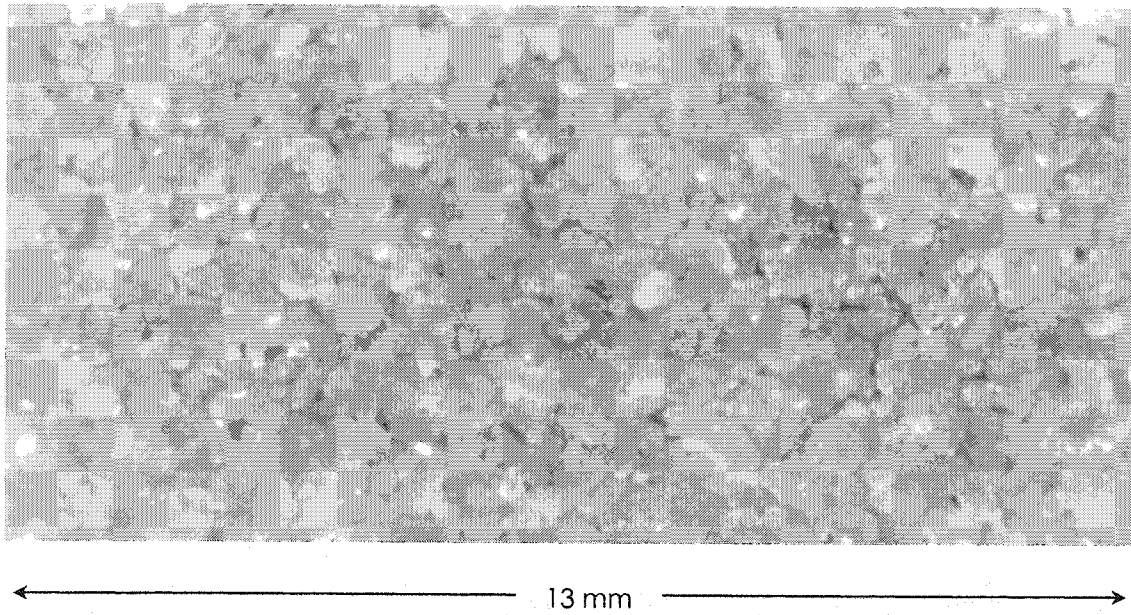


Figure 4-6: Rime Ice Structure Showing Voids

Throughout all of the testing, the rime ice consistently failed at the interface with the test surfaces. Although microscopic layers of ice may have been left on the test surfaces, to the naked eye it appeared as though the ice failed at the interface. Occasionally, a partial cohesive failure would occur around the edges of the plate, which would naturally be slightly cooler than the rest of the surface, as can be seen in Figure 4-7. Such failures were not common, but they suggest a sharp transition between the temperature at which failure does and does not occur. No total cohesive failures were noted throughout the tests.

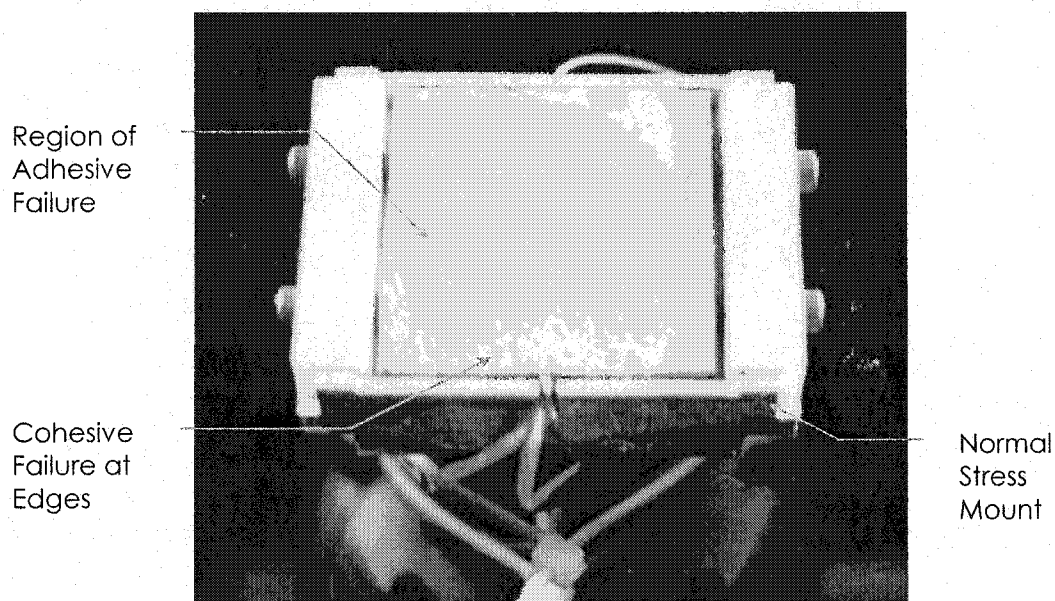


Figure 4-7: Main Adhesion Failure With Cohesive Failure Around Edges of the Sample

4.1.2.1 Normal Strength Results

Experimental results for the normal stress tests are presented for the four test surfaces in Figures 4-8 through 4-11. Figure 4-12 is a summary of the normal stress results for the four surfaces for comparison.

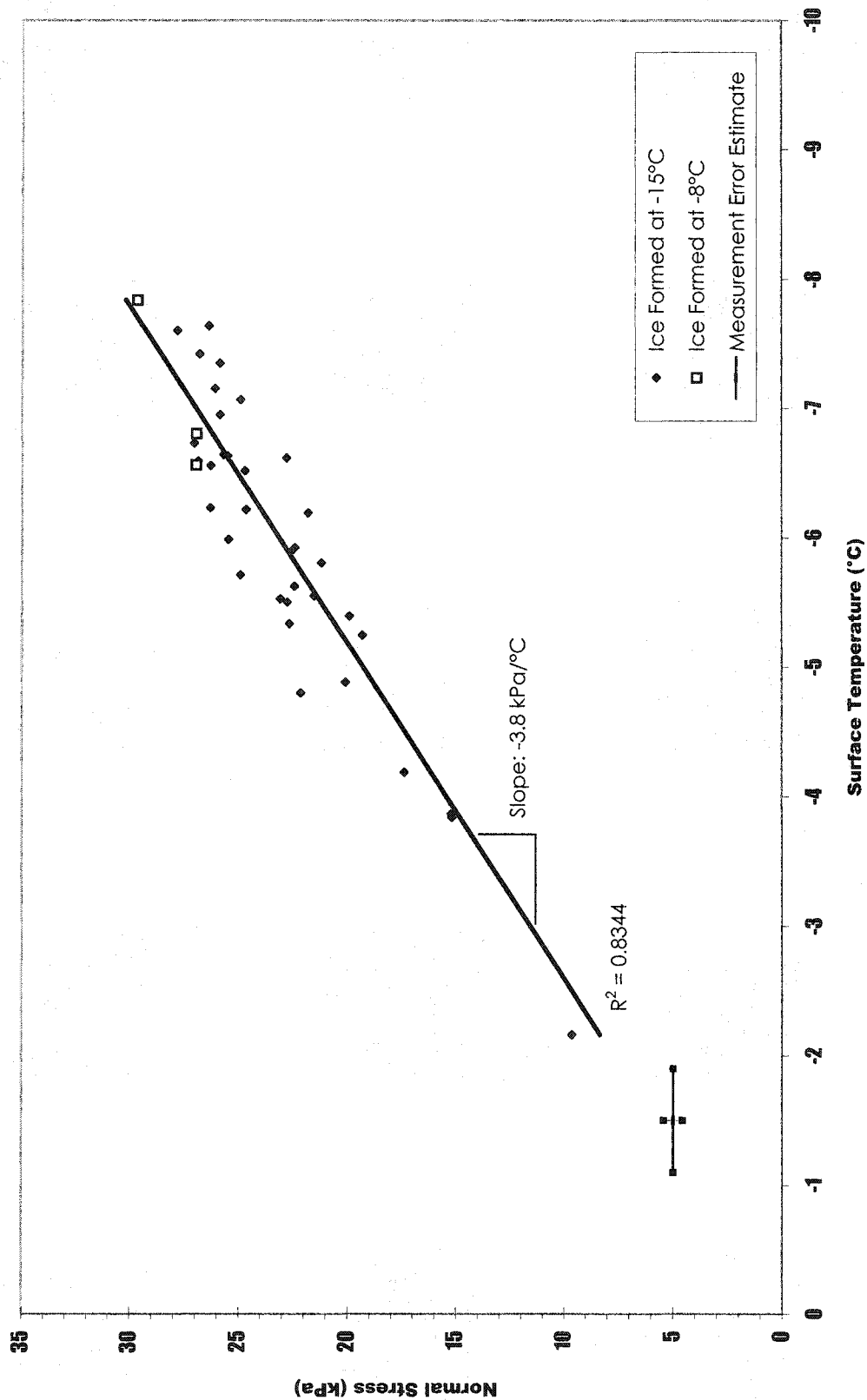


Figure 4-8: Tensile Adhesion Strength of Rime Ice to PC 100 Surface Coating

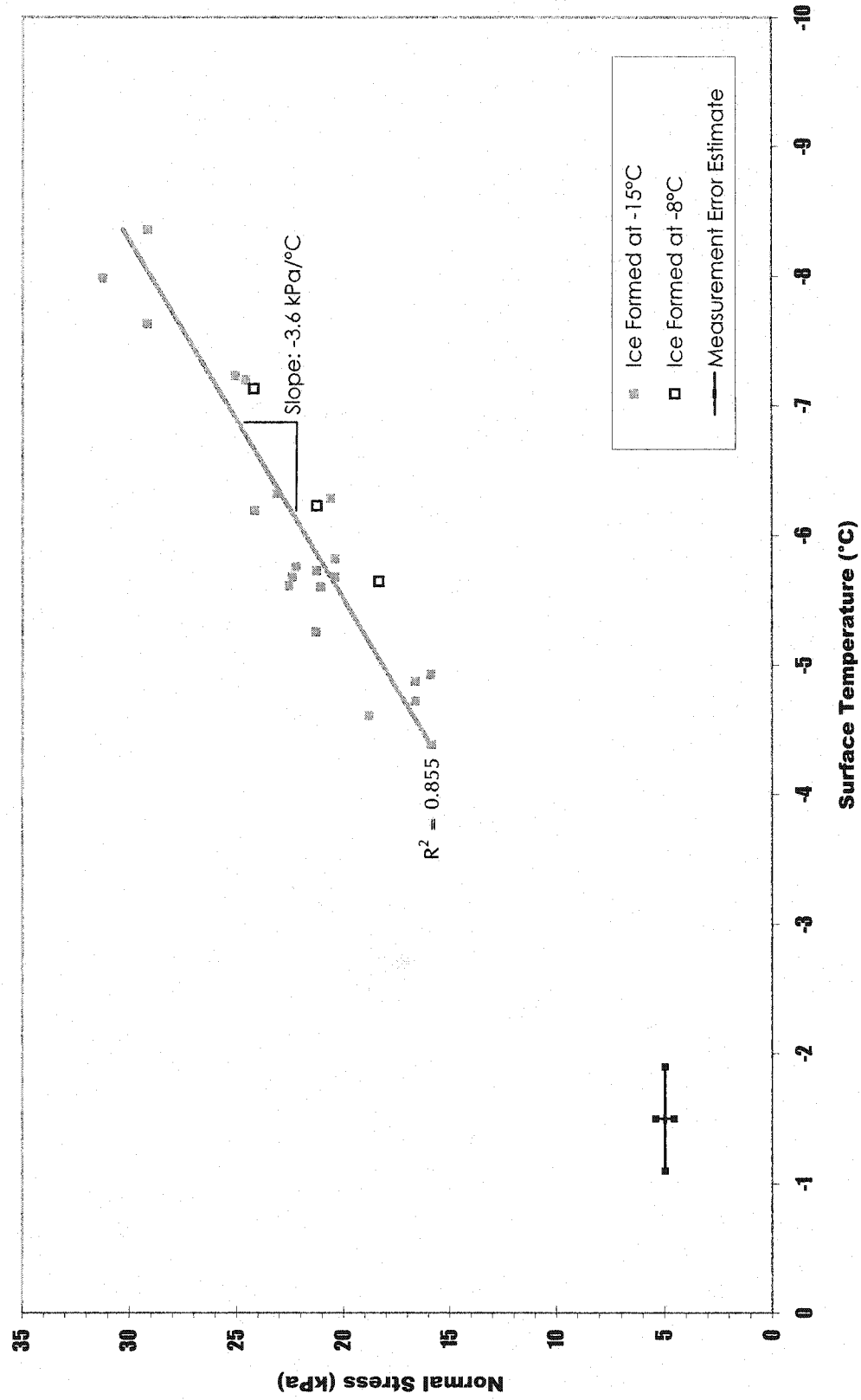


Figure 4-9: Tensile Adhesion Strength of Rime Ice to PC 200 Surface Coating

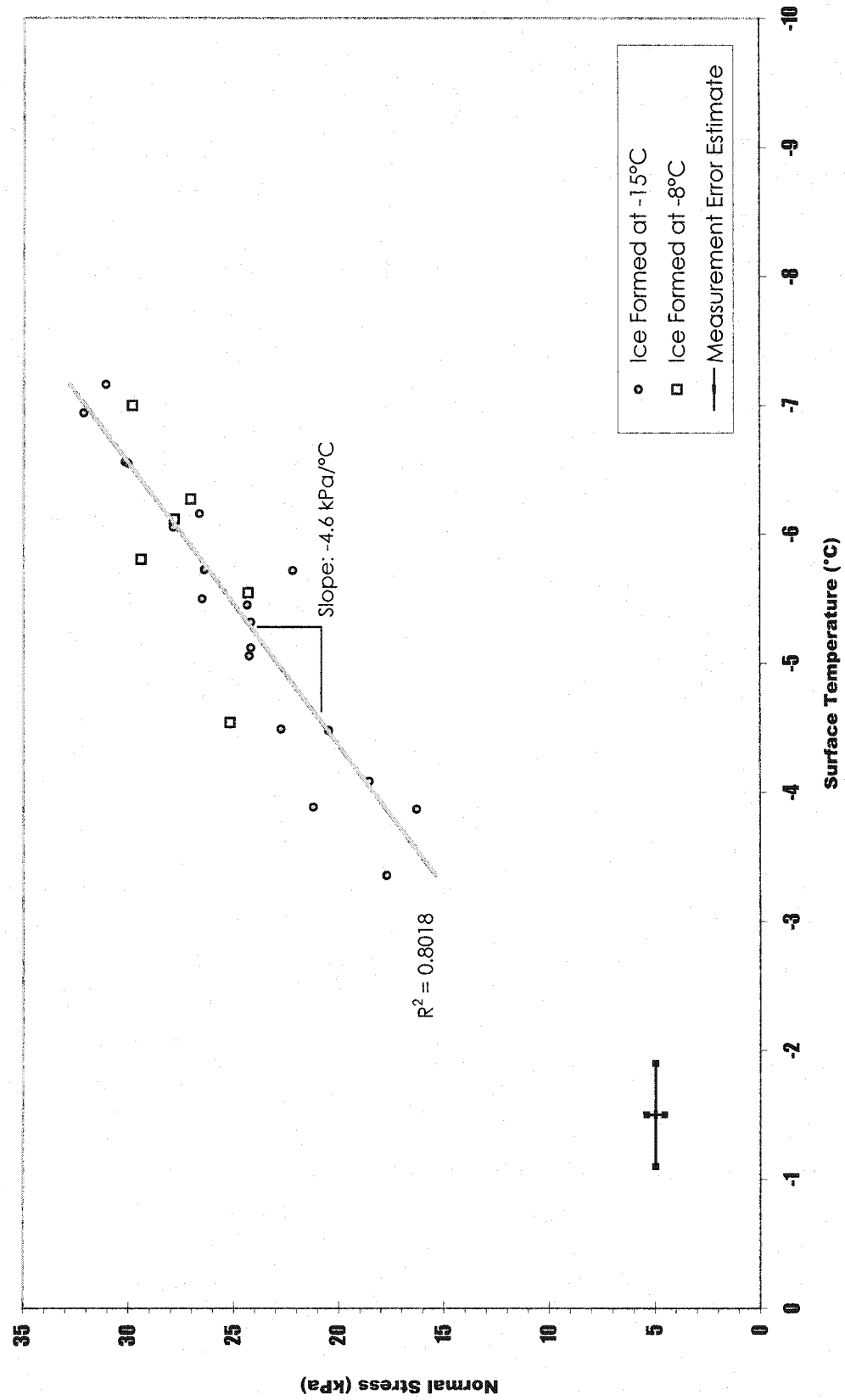


Figure 4-10: Tensile Adhesion Strength of Rime Ice to PSX 700 Surface Coating

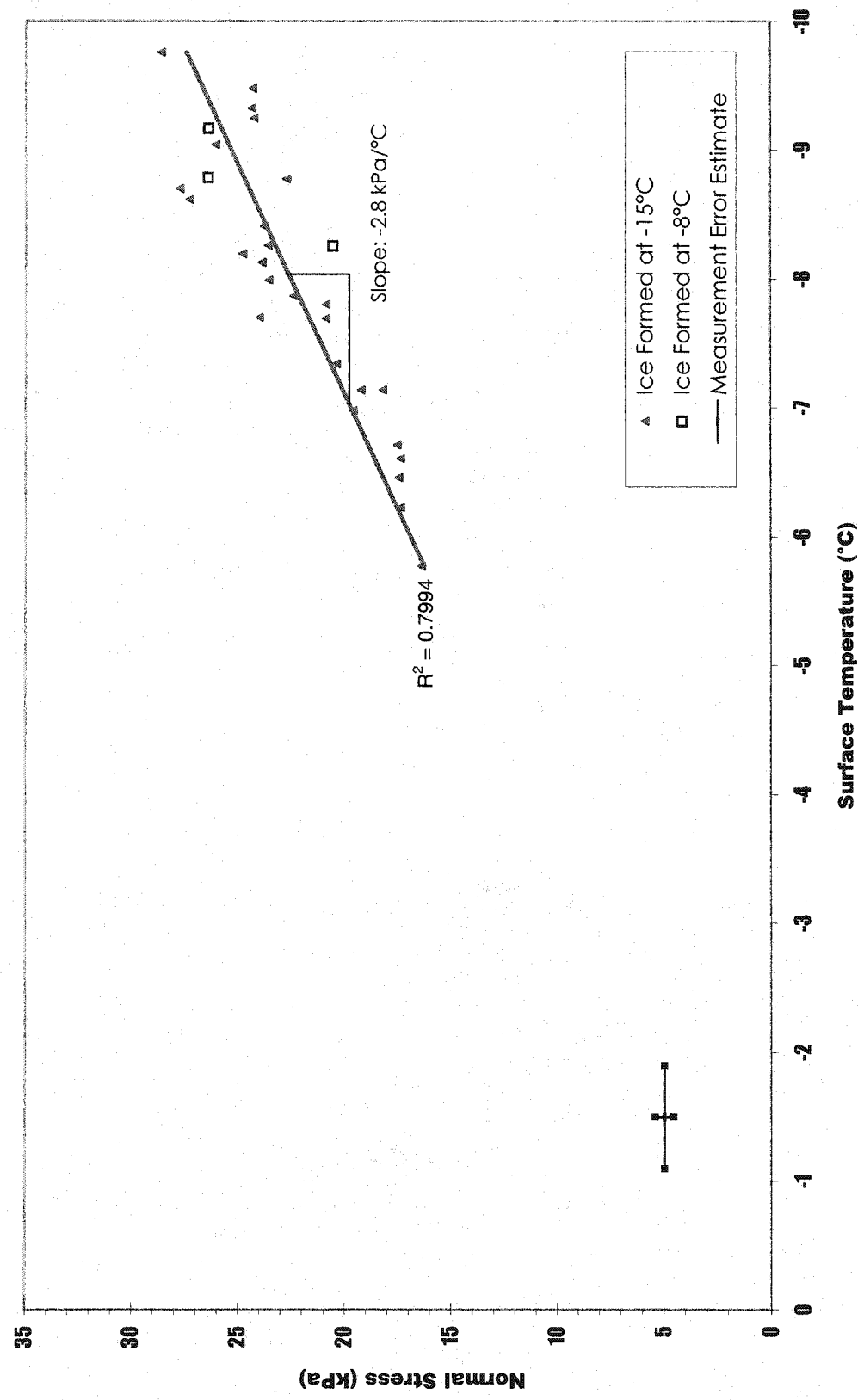


Figure 4-11: Tensile Adhesion Strength of Rime Ice to 20-4969FX Surface Coating

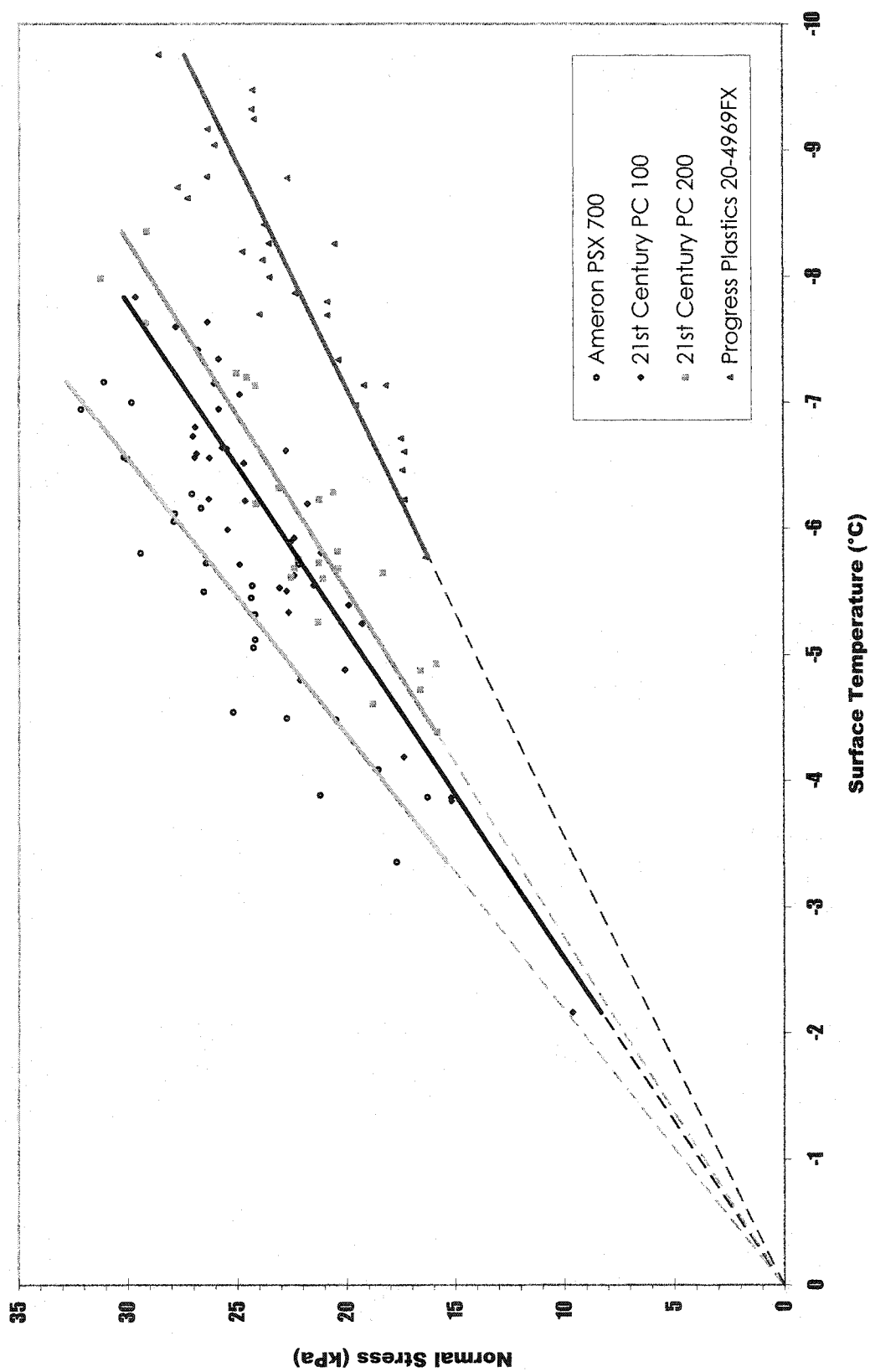


Figure 4-12: Tensile Stress Failures For All Surfaces

4.1.2.2 Shear Strength Results

The results of the shear tests are presented in the same manner as the normal strength tests. Preliminary tests were performed in shear for ice that was created at -8°C , which, like the normal stress tests did not demonstrate a noticeable difference from those performed at -15°C . Due to the fact that the tests took a significantly larger amount of time to carry out without yielding any new information, all of the presented data were performed at -15°C . Figures 4-13 to 4-16 are the results of the individual surfaces tests, and Figure 4-17 is an overall comparison of the four cases.

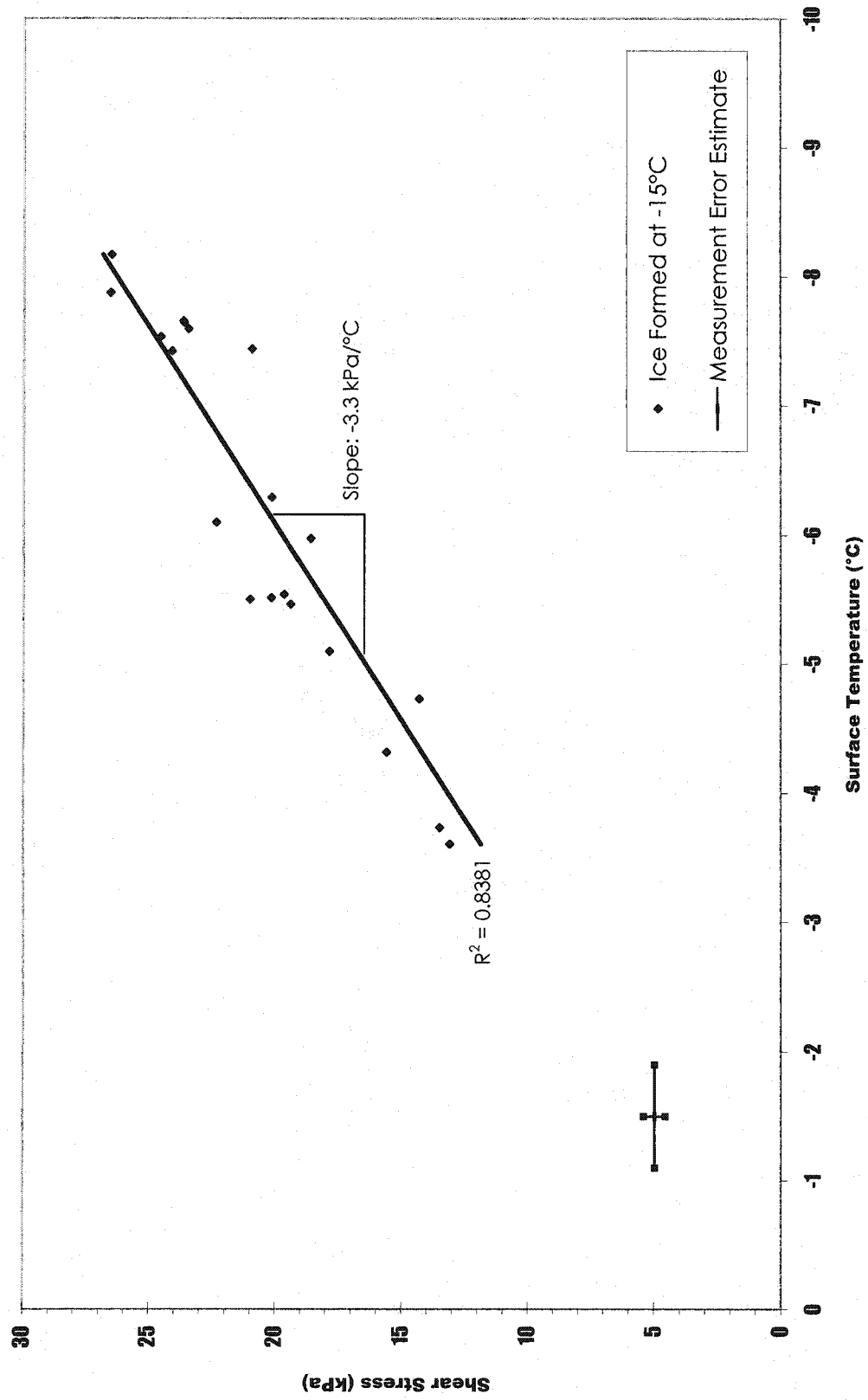
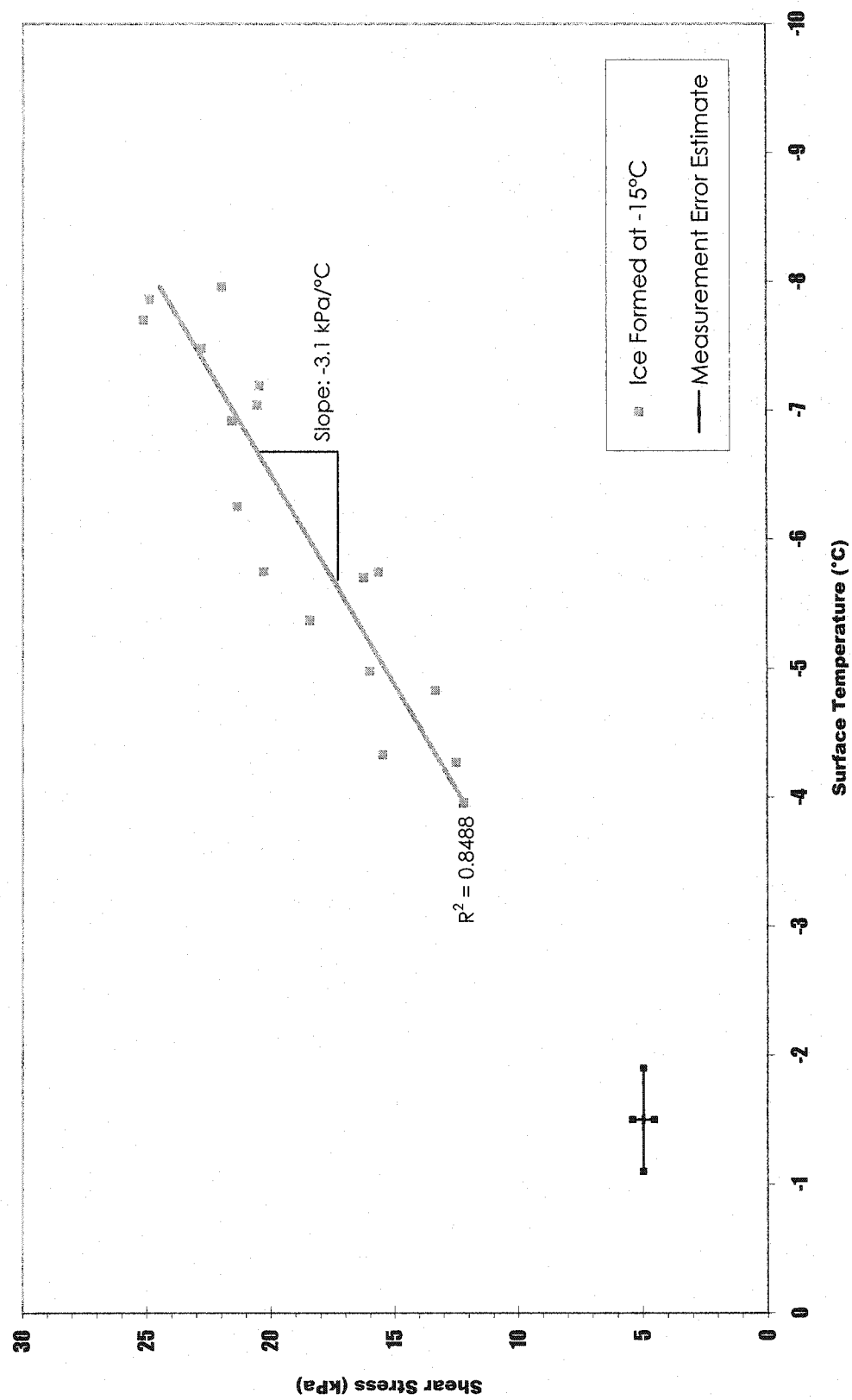


Figure 4-13: Shear Stress Adhesion Strength of Rime Ice to PC 100 Surface Coating



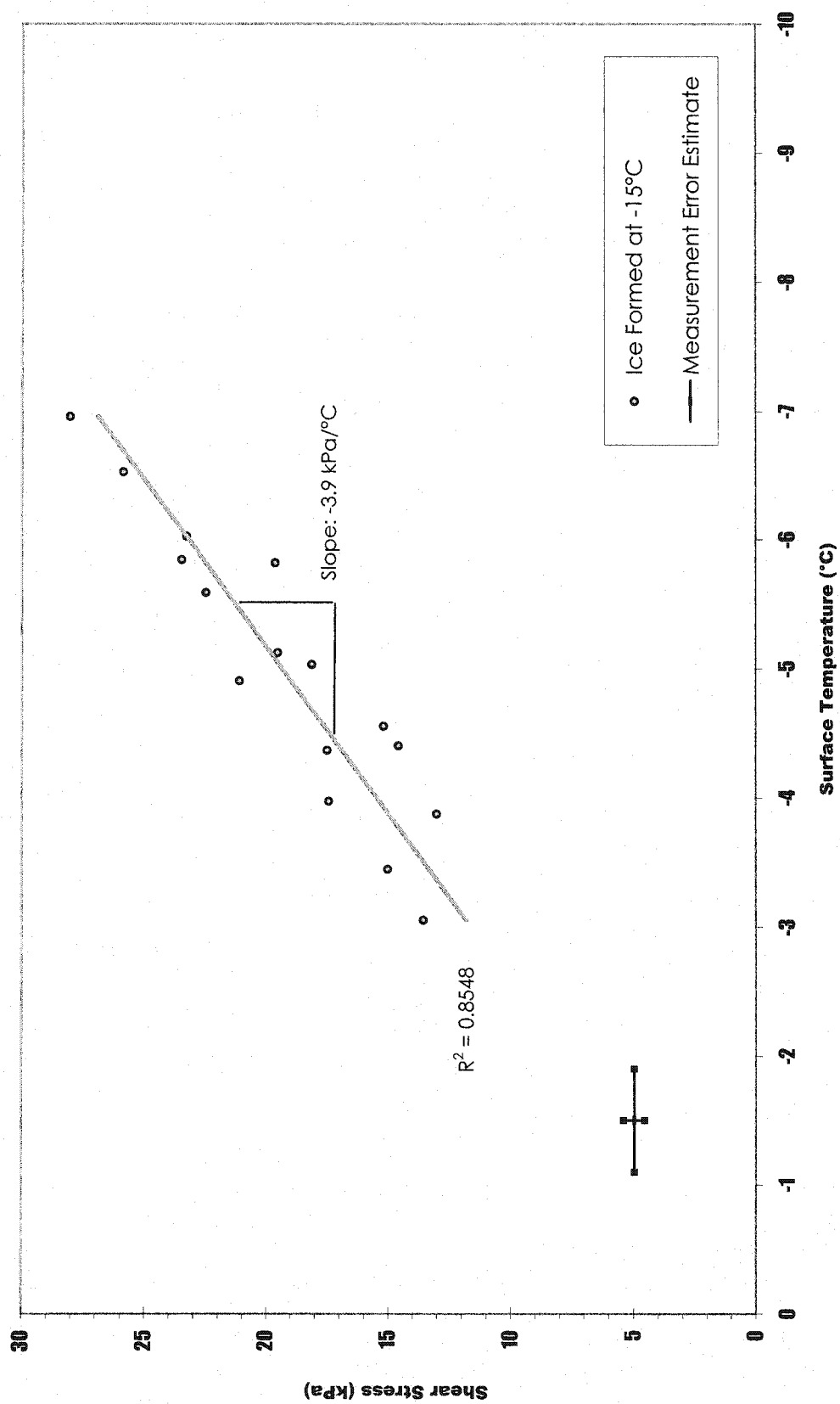


Figure 4-15: Shear Stress Adhesion Strength of Rime Ice to PSX 700 Surface Coating

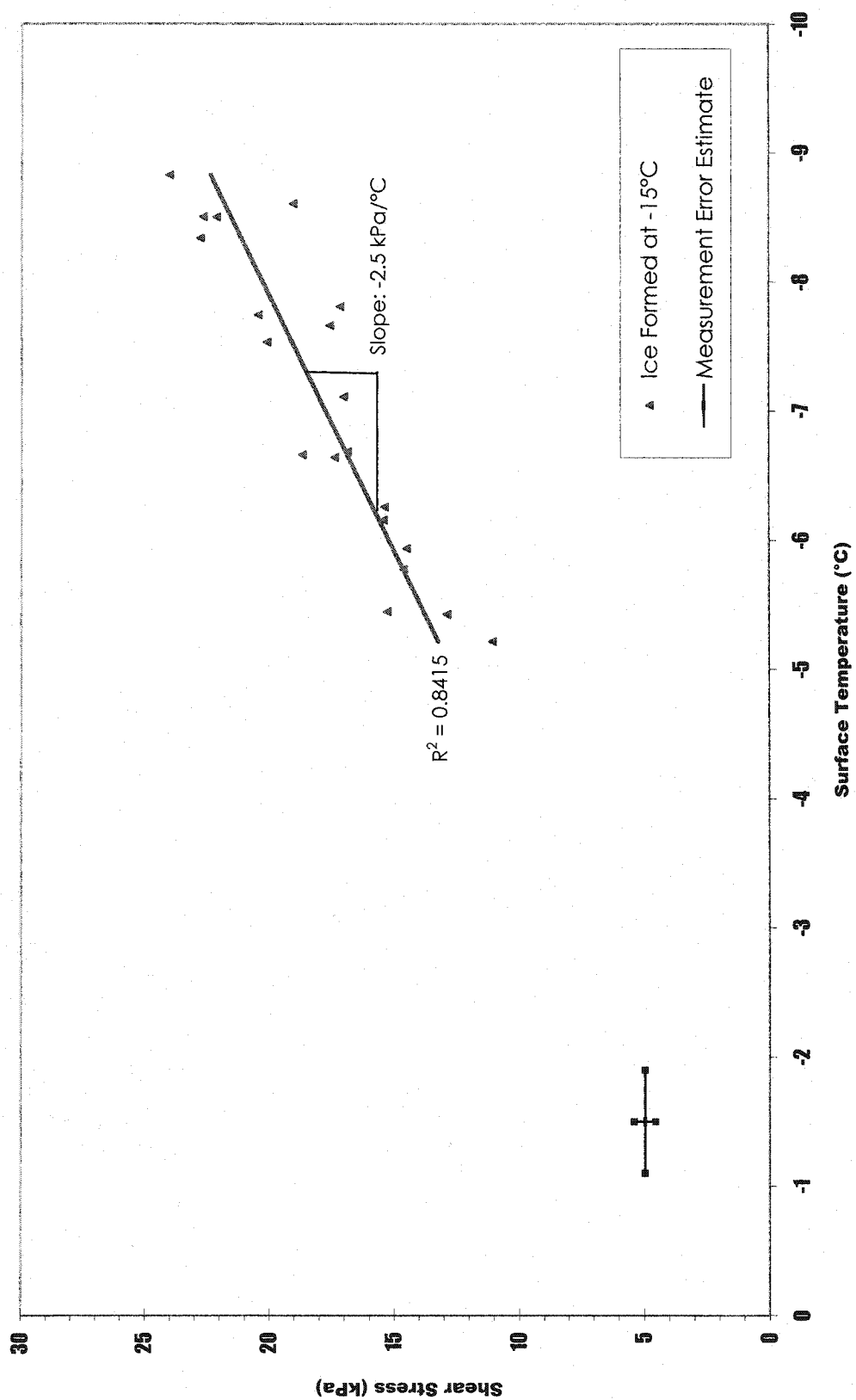


Figure 4-16: Rime Ice Adhesion Strength in Shear Stress to 20-4969FX Surface Coating

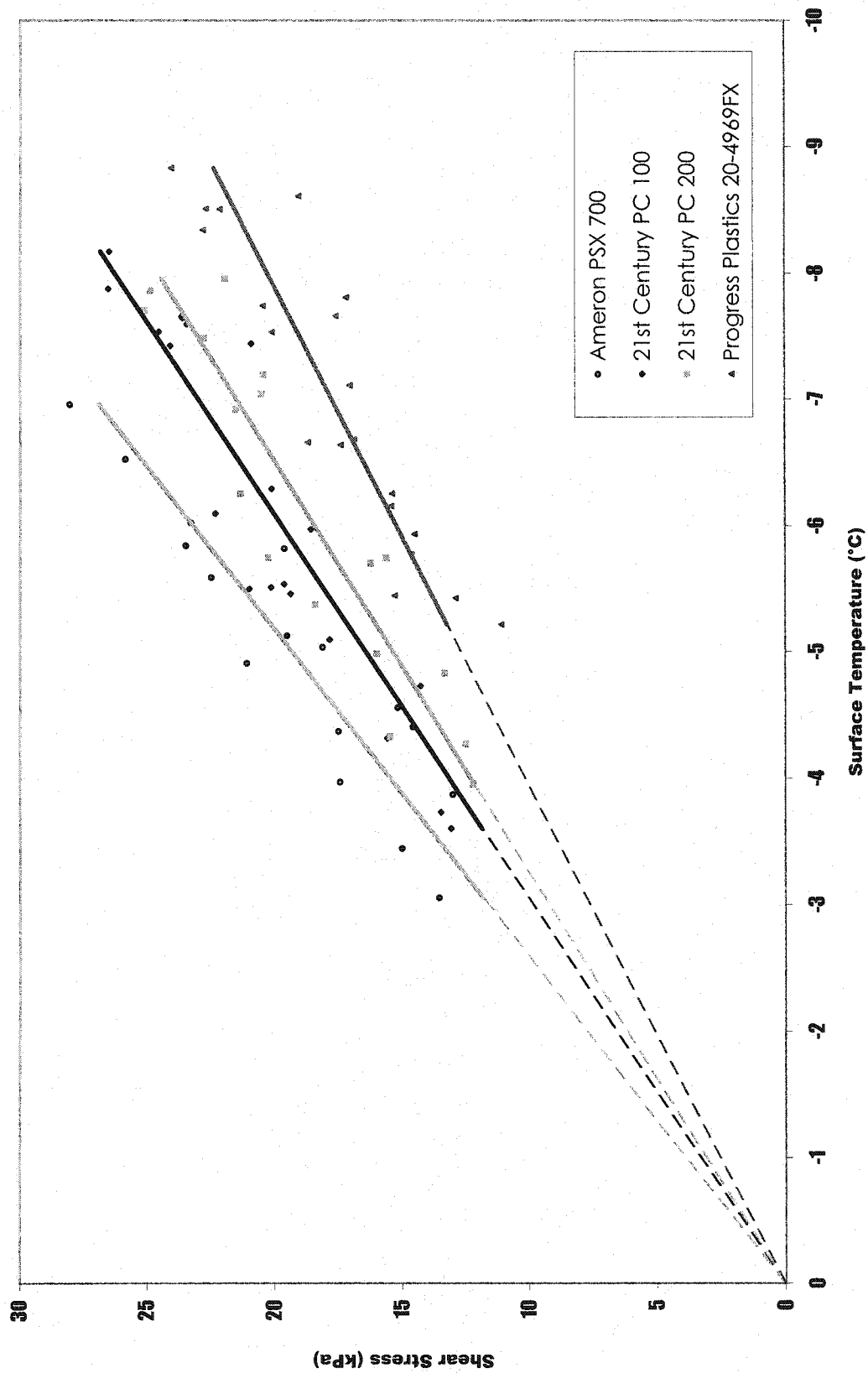


Figure 4-17: Shear Stress Failures For All Surfaces

4.2 Discussion of Results

4.2.1 System Performance

Although there is a fair amount of scatter in the data, given the measurement accuracy limitations and the difficulty inherent in producing repeatable ice samples, the data do appear to fall into distinct regions for both the normal and the shear strength tests. All the results show that the adhesion strength decreases with increasing temperature in normal and shear.

Calibration tests were performed on the system to determine the effects of rotational speed and heat transfer rate on the results. The tests were performed by using a smaller ice mass and an increased the rotational speed to produce the same centripetal force as the standard tests performed at 2000 rpm. The calibration tests were all performed using the PC 100 surface coating. Ice samples with a mass close to 8 g were used for the control tests at 2000 rpm, which would therefore have an interface stress of 26 kPa. The rotor speed was increased to 2250 rpm, and 4 g samples were used to create the same induced stress. Further tests were performed at 2000 rpm, using 8 g samples with the heater power reduced from 27 W to 20 W. The results of these tests, shown on Figure 4-18, compare the control tests with the other two calibration tests. The trendline shown on the figure is taken from the complete data set for the PC 100 samples.

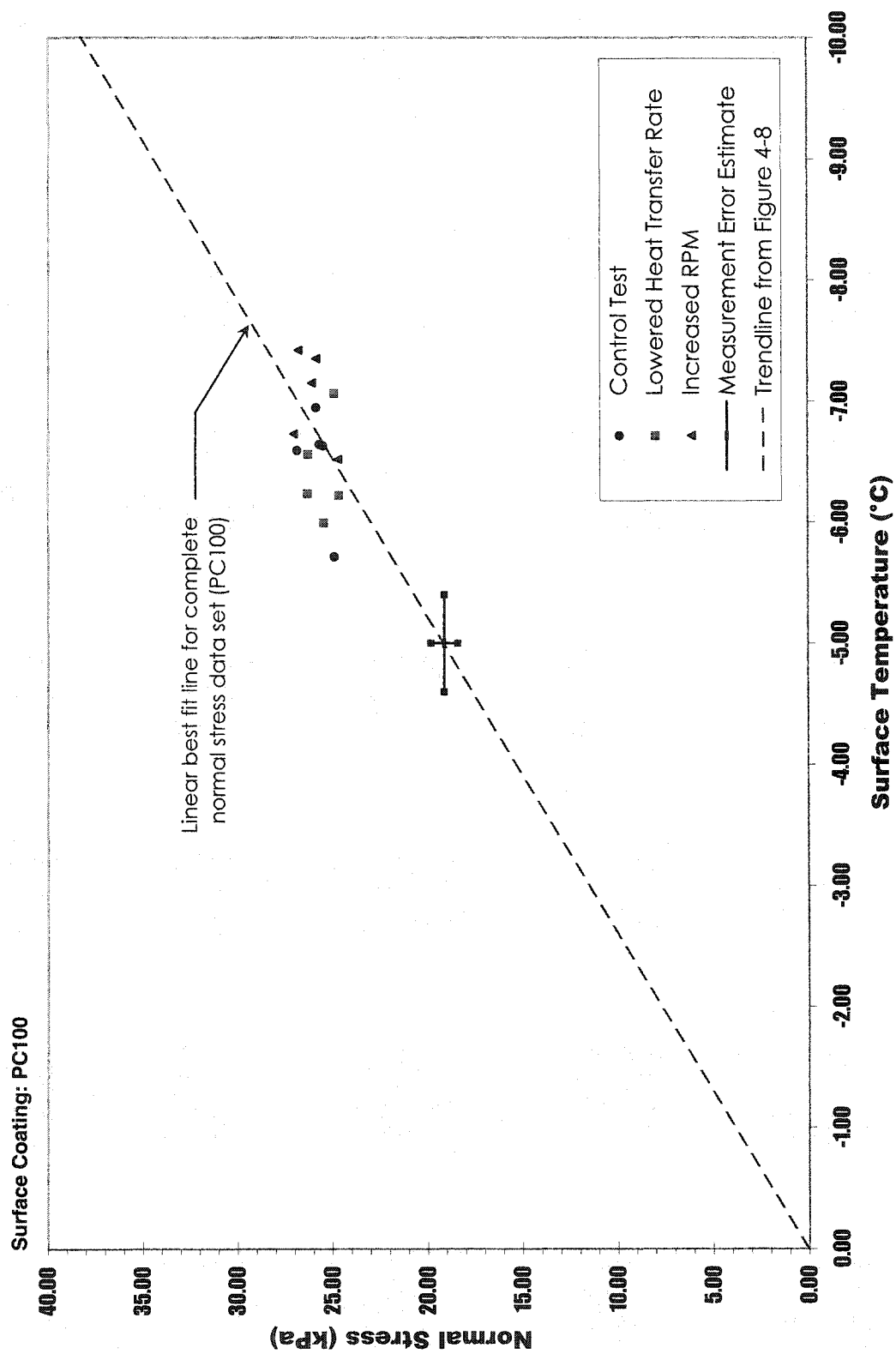


Figure 4-18: System Calibration Results

Figure 4-18 demonstrates that similar results were obtained by using either the mass or the rotational speed to apply a body force and by using different heating rates to reach a given temperature. This indicates that centrifuge system appears to be an appropriate method for applying body forces to adhesion samples, as the results are independent of the test method. Figures 4-12 and 4-17 indicate that the surface temperature is a governing factor in the adhesion strength of rime ice, while Figure 4-18 implies that it is the surface temperature as opposed to the rate of heat transfer that is causes the adhesive failure.

4.2.2 Analysis of Results

In normal and shear strength tests, the four surfaces ranked in the same order, with the Ameron PSX 700 Siloxane having the largest adhesion strength, the Progress Plastics 20-4969FX Polyester coating having the lowest adhesion strength, while both of the 21st Century Coatings PC 100 and PC 200 Fluorinated Polyurethane coatings showed almost identical performances relative to each other and to the other two coatings. Table 4-1 summarizes these results.

Table 4-1: Test Results Summary

Manufacturer Name	Base Material	Advancing Contact Angle	Normal Stress Slope (kPa/°C)	Shear Stress Slope (kPa/°C)	Difference Between Slopes in Normal and Shear
Ameron PSX700	Engineered Siloxane	77°	-4.6	-3.9	-15 %
21 st Century Coatings PC 100	Fluorinated Polyurethane	81°	-3.8	-3.3	-13 %
21 st Century Coatings PC 200	Fluorinated Polyurethane with Silicon additives	85°	-3.6	-3.1	-14 %
Progress Plastics 20-4969FX	Isophthalic polyester	112°	-2.8	-2.5	-11 %

The work of adhesion of a sessile droplet to each of the surfaces can be calculated using Equation 2.4:

$$W_{adh} = \gamma_{lv}(1 + \cos \phi), \quad (2.4)$$

by substituting $\gamma_{lv} = 72.9 \text{ mJ/m}^2$, the surface energy of distilled water in air. The work of adhesion is compared to the normal and shear strengths when the failure occurred at -4°C and -7°C in Table 4-2. This information is plotted in Figures 4-19 and 4-20. Given the limited data, a reasonably good correlation is shown.

Table 4-2: Work of Adhesion and Failure Strengths

Manufacturer Name	Base Material	Advancing Contact Angle	Work of Adhesion (mJ/m^2)	-4°C Surface Temperature		-7°C Surface Temperature	
				Normal Strength (kPa)	Shear Strength (kPa)	Normal Strength (kPa)	Shear Strength (kPa)
Ameron PSX700	Engineered Siloxane	77°	89	11.2	10.0	19.6	17.5
21 st Century Coatings PC 100	Fluorinated Polyurethane	81°	84	14.4	12.4	25.2	21.7
21 st Century Coatings PC 200	Fluorinated Polyurethane with Silicon additives	85°	79	15.2	13.2	26.6	23.1
Progress Plastics 20-4969FX	Isophthalic polyester	112°	46	18.4	15.6	32.2	27.3

Forest (1980) observed a similar trend with glaze ice tests, that contact angle or the work of adhesion plays an important role the adhesion strength of ice. He noted however, that other factors such as surface roughness may be equally important. For that reason, the surface roughnesses were similar for all of the test surfaces, and the figures show a good correlation at both temperatures for both the normal and shear stress modes.

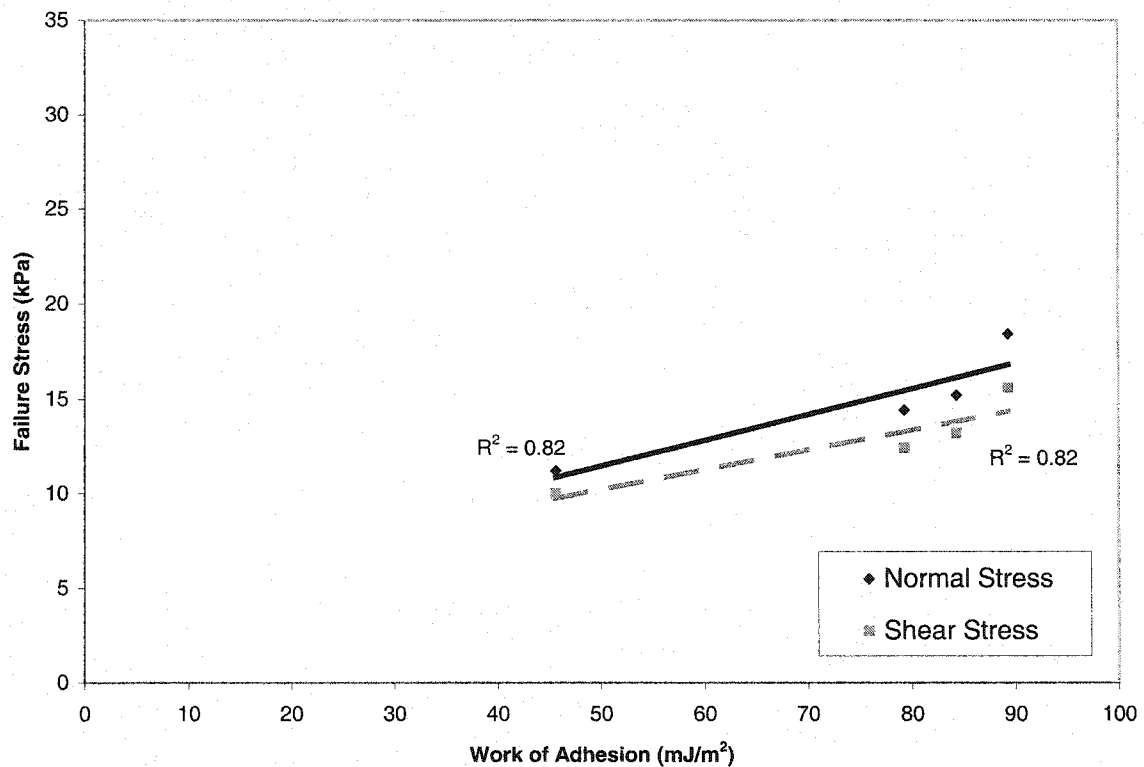


Figure 4-19: Work of Adhesion and Failure Stress at -4°C

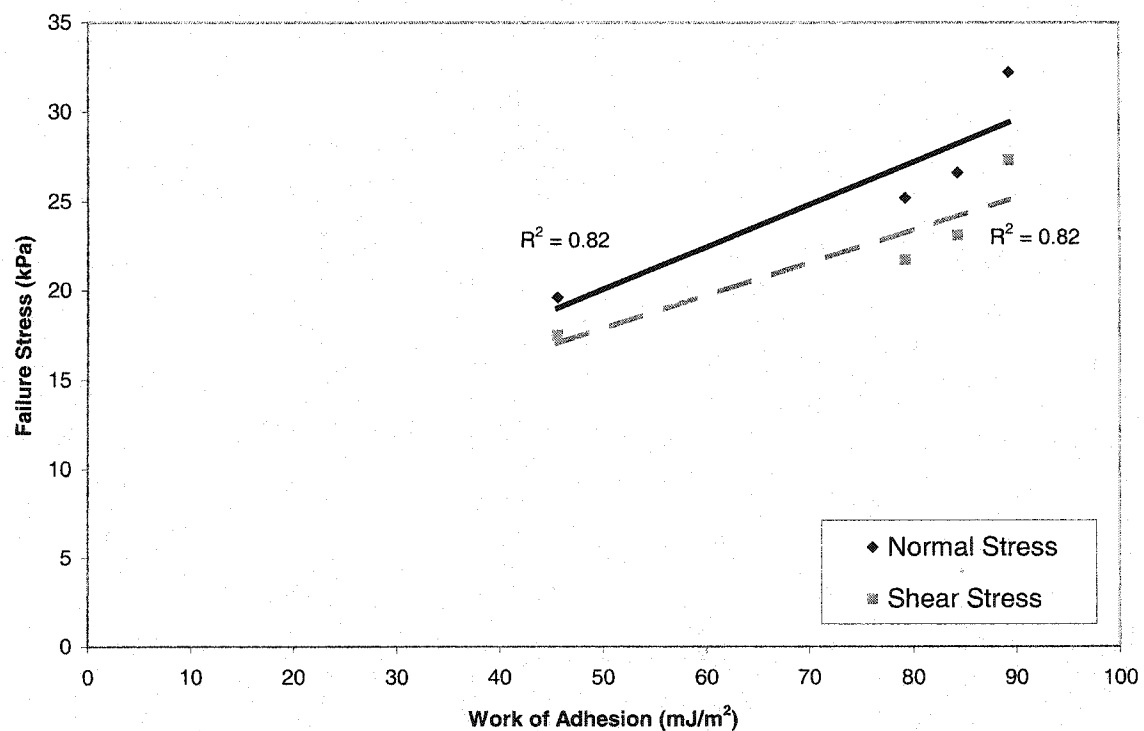


Figure 4-20: Correlation Between Work of Adhesion and Failure Stresses at -7°C

All of the surfaces in this work showed lower adhesion strength in shear than they did in normal stress, although the difference between shear and normal results was not much greater than the margin of experimental error. This difference was ranged between an 11-15% decrease from normal strength to shear strength for all of the specimens, while the experimental error in the slope is estimated to be 9% (see Appendix E). Jellinek (1959), however, found a very significant difference between the normal and shear strength of glaze ice interfaces. Using ice-polystyrene and ice-steel interfaces, he found that the normal adhesion strength was up to 14 times larger than the shear adhesion strength at -10°C (350 kPa in tensile and 25 kPa in shear for ice-polystyrene). Given the differences between the structure of glaze and rime ice, these results are not directly comparable, although one may expect to see a similarly large magnitude difference between the normal and shear stresses for rime ice as was observed for glaze ice. Little or no adhesion testing has been done using rime ice in normal and shear and therefore, despite the apparent discrepancy between the glaze ice and rime ice normal to shear adhesion stress ratio, it would be necessary to attempt to repeat similar results with an independent test setup. The porous physical structure of rime ice may account for the observed similarities between shear and normal failure strength, not observed with glaze ice. Jellinek (1959) proposed a quasi-liquid layer that exists between the surface and the ice, which would present large surface tension necessary to overcome in tensile loading, with significantly smaller strength in shear. The porosity of rime ice may reduce the surface tension of this layer by providing numerous discontinuities and non-uniformities. The rime droplets also trap air pockets within the ice structure, which serve as stress concentrations, reducing the overall normal adhesion strength of the rime ice such that it is similar to the shear strength.

As discussed in Section 3.4.1, the dominant force likely to cause ice shedding of rime ice on a wind turbine blade is the shear force induced by the rotation of the blades. This body force is a function of the mass of accreted ice, the rotational speed and the radial distance from the rotor hub. Assuming a typical rotation speed of 20 rpm, a rime ice density of 600 kg/m^3 and a problematic ice accretion height of 5 cm, the rime ice

shear strength for the tested surfaced is compared to the centripetal shear stress along the length of a wind turbine blade in Table 4-3.

Table 4-3: Adhesion Strength Along Wind Turbine Blade

Shear Stress (kPa)	Blade Distance Wind Turbine Hub (m)	Surface Temperature for Rime Ice Release in Shear			
		Ameron PSX 700	21 st Century Coatings PC 100	21 st Century Coatings PC 200	Progress Plastics 20-4969FX
0.0	0.0	0.0	0.0	0.0	0.0
1.0	3.4	-0.3	-0.3	-0.3	-0.4
3.0	10.1	-0.8	-0.9	-1.0	-1.1
5.0	16.9	-1.3	-1.5	-1.6	-1.9
7.0	23.6	-1.8	-2.1	-2.2	-2.7
9.0	30.4	-2.3	-2.8	-2.9	-3.4

Modern wind turbines often have blades as long as 30 m. Even towards the blade tips where the centripetal forces are the highest, the surface of the blades would need to be heated to between -2°C and -3°C for the accreted rime to self-shed depending on the surface coating. This temperature would need to be increased towards the centre of the blades as the body and aerodynamic forces on the ice decrease with radial length. Although this is an incremental difference, considering that heaters are often used continuously for winter as long as 6 months, small savings will be compounded, especially for installations with numerous turbines. However, in order for the ice to release due to the centripetal force caused by its own mass, it would be necessary to allow a certain amount of ice to build up before sufficient mass had accumulated to induce the necessary centripetal force. Power losses would certainly occur due to the increased surface roughness and altered geometry of the blade. Depending on the rate of ice accretion and the duration of the icing events, the production loss, as the necessary mass accretes, could easily offset any energy saving by using blade heaters as de-icers rather than anti-icing.

4.2.3 Limitations of the Results

The results presented in this work using the new test equipment and experimental method appear to demonstrate the utility of the centrifuge design. There

exist limitations to the applicability of the results, as well as with the system itself to further understand ice adhesive failures.

In previous ice adhesion experiments, great pains have been taken in order to produce ice free of defects and air pockets. This was intentionally avoided in the present experiment, since rime ice is of much greater significance to wind turbines and has not been thoroughly examined in the past. The difficulty this presents for the current work is that although the glaze ice research provides an indirect comparison, there is no frame of reference to directly compare the present results with.

Lock (1990) reported that rime ice has a lower adhesion strength than glaze ice, and rime ice formed at increasingly colder temperatures has decreasing adhesion strengths. Although experiments for the current study were carried out at two distinct temperatures (-15°C and -8°C), it is important to note that the failures occurred at similar surface temperatures for both cases. This suggests that the surface temperature is a more dominant cause of failure than the temperature at which it was created. Ultimately, additional experiments need to be conducted to verify the present results, as well as to determine the repeatability and variability of rime ice adhesion strength under different ambient conditions, particularly conditions with ambient wind speeds greater than zero.

The current test method cannot be used to monitor the failure mechanism due to the high speeds at which the failures occur. Investigation of the failure surface can only be examined after the heat supply is removed from the surface and the rotation of the system has stopped. This may allow for changes to the ice interface between the time of failure and the investigation of the surface. The vast majority of tests resulted in a completely adhesive failure. That is, there appeared to be no ice remaining on the surface. There was no way to tell whether the ice released simultaneously or as numerous fragments, some triggered by others.

Although the centrifuge is able to create stresses comparable to those experienced on modern wind turbines, it would be advantageous to create a larger range of induced stresses to allow for a greater spread in the data further from the origin. It

would also have been useful to reach the cohesive limit of the rime ice, where cohesive failures occur before adhesive failures at sufficiently low temperatures and high stresses. The ability to induce larger stresses would also allow tests to be performed on uncoated surfaces for comparison purposes.

Lastly, the centrifuge design does not test the rate of applied stress. Although this is not necessary in the case of wind turbines, as they tend to operate at steady speeds, it may be an area of interest for other applications, as ice is known to creep. This effect cannot be handled with the current design.

Chapter 5

CONCLUSIONS AND RECOMMENDATIONS

5.1 Adhesion Strength of Rime Ice

Based on the experiments performed, it can be concluded that centrifugal testing appears to be a useful tool for testing the adhesion strength of materials that could not be tested otherwise due to physical constraints, such as rime ice, which would otherwise crush if laterally or torsionally loaded.

The adhesion strength of rime ice to a polymer surface was found to decrease linearly as the surface temperature is increased, when loaded in tension or in shear. The adhesion strength of rime ice was found to be similar whether it was loaded in tension and in shear. The contact angle that water makes with a surface is a qualitative indicator of the adhesion strength that ice will have on that surface. Using the four cases in the present study, the adhesion strength of rime ice correlated well with the work of adhesion of a water droplet. More than four data points are needed to verify this relationship. There are also many other important factors such as surface roughness and the freezing process that also likely influence with adhesion strength.

Comparing the results of this work, which involves rime ice to previous adhesion studies using glaze ice, it appears that the process under which the ice is created has a major influence on adhesion strength. Previously, it has been found that glaze ice has far greater adhesion strength in tension than it does in shear. The current work found that the strength of rime ice in tension was very similar to shear.

5.2 Applicability to Wind Turbines

The results of the experiments show that it will be difficult to shed ice from the blades of a modern wind turbine without heating the surface close to the melting temperature. If blade heaters were used as de-icers, rime ice would be allowed to collect on the blades before it was thermally removed. The energy savings that would be accrued by the slight reduction in power supplied to the de-icing heaters by avoiding melting the ice will most likely be offset by the production losses associated with allowing a mass of ice to build-up on the blade. The only advantage to this technique would be that it avoids run-back of melted ice. If run-back is found to be a significant problem in the future, this technique may be important to investigate further.

5.3 Future Work

In order to verify the validity of the results, the centrifuge could be used to test glaze ice samples as a comparison with other traditional adhesion strength methods. A re-design of the rotor could also be done to either improve the aerodynamics of the system or an increase of the rotor's radial length such that higher stresses could be achieved. This would allow for a comparison to materials such as aluminum with higher adhesion strengths that have been more thoroughly studied in the past.

Further investigations into how adhesion bond strength changes depending on the process under which the ice is formed are warranted to determine the applicability of the present results. The variability of rime properties depending on such factors as droplet size, spray liquid water content and impact speed would help qualify the breadth of conditions under which tests such as these are valid.

REFERENCES

1. Ah-You, K. and Leng, G. (1999) "Renewable Energy in Canada's Remote Communities", Renewable Energy for Remote Communities Program, Natural Resources Canada.
2. Bascom, W.D., Cottingham, R.L. and Singleterry, C.R. (1969) "Ice Adhesion to Hydrophilic and Hydrophobic Surfaces", *Journal of Adhesion*, Vol. 1, pp. 246-263.
3. Bose, N. (1992) "Icing on a small horizontal-axis wind turbine – Part 2: Three dimensional ice and wet snow formations", *Journal of Wind Engineering and Industrial Aerodynamics*, Vol. 45, No. 1, Dec. 1992, pp. 87-96.
4. Brothers, C. (2001) Personal Communication. Site Manager, Atlantic Wind Test Site, North Cape, Prince Edward Island, Canada.
5. BTM-Consult ApS (2000) "International Wind Energy Development. World Market Update 1999".
6. Canadian Wind Energy Association; CanWEA (2001) "Wind Vision for Canada. 10,000 MW by 2010 (10 X 10). Recommendations for Achieving Canada's Wind Energy Potential".
7. Edworthy, J. (2002) Personal Communication. Executive Director – Marketing, Vision Quest Windelectric Inc., Calgary, Alberta, Canada.
8. Craig, D.F. and Craig, D.B. (1996) "An Investigation of Icing Events on Haeckel Hill", *Wind Power in Cold Climates BOREAS III Conference Proceedings*, Finnish Meteorological Institute, Helsinki, pp. 169-191.
9. Environment Canada (2000) "Canada's Greenhouse Gas Inventory, 1990-1998 Final Submission to the UNFCCC Secretariat".
10. Eskin, S.G., Fontaine, W.E. and Witzell, O.W. (1957) "Strength Characteristics of Ice in Contact With Various Kinds of Surfaces", *Refrigerating Engineering*, Vol. 65, pp. 33-38.
11. Finstad, K. and Makkonen, L. (1993) "Modelling of Rime Icing of Wind Turbines", *Proceedings of the 6th International Workshop on the Atmospheric Icing of Structures*, Budapest, Hungary, pp.79-83.
12. Forest, T.W. (1980) "The Adhesion of Ice to Low Energy Solids", ASME-Paper No. 80-WA/HT-19 for Winter Annual Meeting Nov 16-21 1980.

13. Hobbs, P.V. (1973) Ice Physics, Clarendon Press, Oxford, pp. 392-474.
14. Incorpera, F.P. and DeWitt, D.P. (1996) Introduction to Heat Transfer, John Wiley and Sons, Inc., pp. 212-223.
15. Jellinek, H. H. G. (1959) "Adhesive Properties of Ice", *Journal of Colloid Science*, Vol.14, pp. 245-254.
16. Jellinek, H.H.G. (1970) "Ice Adhesion and Abhesion: A Survey", US Army CRREL
17. Kimura, S., Seifert, H. and Tammelin, B. (1994) "Effect of ice accretion on elasticity of the rotor blade", *Wind Power in Cold Climate BOREAS II Conference Proceedings*, Finnish Meteorological Institute, Helsinki, pp. 231-253.
18. Kimura, S., Seifert, H. and Tammelin, B. (1997) "Effect of Ice Accretion on the Turbine Rotor", *Proceedings of the International Conference on Fluid Engineering* pp. 1533-1538.
19. Lock, G.S.H. (1990) The Growth and Decay of Ice, Cambridge University Press, Cambridge, pp. 167-228.
20. Lodge, M.A. (1996) "Natural Resources Canada (NRCan) Wind Energy Research & Development Activities and Remote Community Initiatives", *Wind Power in Cold Climates BOREAS III Conference Proceedings*, Finnish Meteorological Institute, Helsinki, pp. 52-59.
21. Loughborough, D.L. and Haas, E.G. (1946) "Reduction of the Adhesion of Ice to De-Icer Surfaces", *Journal of Aeronautical Sciences*, Vol. 13, pp. 126-134
22. Maisson, J.F. (2000) Personal Communication. Director, Technical Services, Yukon Energy Corporation, Whitehorse, Yukon, Canada.
23. Maisson, J.F. (2001) "Wind Power Development in Sub-Arctic Conditions with Severe Rime Icing", Presented at the Circumpolar Climate Change Summit and Exposition, Whitehorse, Yukon, March 19-21.
24. Makkonen, L. and Autti, M. (1991) "The Effects of Icing on Wind Turbines", *EWEC Conference Proceedings*, Wind Energy: Technology and Implementation, pp. 575-580.
25. Makkonen, L. and Finstad, K. (1996) "Improved Numerical Model for Wind Turbine Icing", *7th International Workshop on Atmospheric Icing of Structures*, Chicoutimi, Québec, June 3-7, pp. 373-378.

26. Makkonen, L., Laakso, M.M. and Finstad, K. (2001) "Modeling and Prevention of Ice Accretion on Wind Turbines", *Journal of Wind Engineering*, Vol. 25, No.1, pp. 3-21.
27. Oksanen, P. (1983) "Adhesion Strength of Ice", 7th International Conference on Port and Ocean Engineering under Arctic Conditions, Helsinki, Finland, Vol. 2, pp. 710-719.
28. Petrenko, V.F. and Whitworth, R.W. (1999) Physics of Ice, Oxford University Press, New York, pp. 314-318.
29. Pruppacher, H.R. and Klett, J.D. (1978) Microphysics of Clouds and Precipitation, D. Reidel Publishing Company, London, pp. 9-21.
30. Raraty, L.E. and Tabor, D. (1958) "The Adhesion and Strength Properties of Ice", *Proceedings of the Royal Society of London. Series A*, Vol. 245, pp. 184-201.
31. Raynolds, M. and Pape, A. (2000) "The Pembina Institute Green Power Guidelines for Canada", July 2000.
32. Rogers, R.R. and Yau, M.K. (1989) A Short Course in Cloud Physics, 3rd Edition, Pergamon Press, pp. 75-76.
33. Ross, M., Martel, S. and Usher, E. (1998) "Photovoltaics in Canada's North", *GEOS Vol. 1 No. 2*, Natural Resources Canada.
34. Scavuzzo, R.J., Chu, M.L. and Ananthaswamy, V. (1994) "Influence of Aerodynamic Forces in Ice Shedding", *Journal of Aircraft*, Vol. 31, No. 3, pp. 526-530.
35. Seifert, H. and Richert, F. (1998) "A Recipe to Estimate Aerodynamics and Loads on Iced Turbine Blades", *Wind Power in Cold Climates BOREAS IV Conference Proceedings*, Finnish Meteorological Institute, Helsinki, pp. 305-316.
36. Seifert, H. and Tammelin, B. (1996a) "Icing of Wind Turbines in Europe", *Wind Power in Cold Climates BOREAS III Conference Proceedings*, Finnish Meteorological Institute, Helsinki, pp. 43-49.
37. Seifert, H. and Tammelin, B. (1996b) "Icing of Wind Turbines", *Proceedings of the European Union Wind Energy Conference*, Gothenborg, Sweden, May 20-24, pp. 1059-1062.
38. Seifert, H., Molly, J.P., Rehfeldt, K. (1998) "The Newest Wind Energy Statistics in Germany", *Wind Power in Cold Climates BOREAS IV Conference Proceedings*, Finnish Meteorological Institute, Helsinki, pp. 40-49.

39. Tammelin, B. and Sääntti, K. (1994) "Effect of Rime Accretion on Wind Energy Production in the Top Areas of Fells", Wind Power in Cold Climates BOREAS II Conference Proceedings, Finnish Meteorological Institute, Helsinki, pp. 265-275.
40. Tammelin, B., Cavaliere, M., Hannele, H., Morgan, C., Seifert, H., and Sääntti, K. (2000) Wind Energy Production in Cold Climates, European Commission DG XII, Non Nuclear Energy Programme, Finnish Meteorological Institute Publication, 41 Pages.
41. Thomas, S.K., Cassoni, R.P. and MacArthur, C.D. (1996) "Aircraft Anti-Icing and De-Icing Techniques and Modeling", Journal of Aircraft, Vol. 33, No. 5 pp. 841-854.
42. van Oss, C.J., Giese, R.F., Wentzek, R., Norris, J. and Chuvilin, E.M. (1992) "Surface tension parameters of ice obtained from contact angle data and from positive and negative particle adhesion to advancing freezing fronts", Journal of Adhesion Science and Technology, Vol.6, pp. 503-516.
43. Vølund, P. (1998) "Measured Ice Loads on Avedore 1MW Test Turbine", BOREAS IV: Wind Power in Cold Climates Conference Proceedings, Finnish Meteorological Institute, Helsinki, pp. 293-302.
44. Wind Power Monthly (2000) Volume 12, Number 3, March 2000.
45. Yekutieli, O. and Clark, R.N. (1987) "Influence of Blade Surface Roughness on the Performance of Wind Turbines," 6th ASME Wind Energy Symposium, Dallas, TX, February 15-18, pp. 181-187.
46. Yukon Development Corporation (1999) The Yukon Green Power Initiative, Implementation Strategy.

APPENDIX A: SURFACE CONTACT ANGLES

A.1 Advancing Contact Angles With Distilled Water

A 0.65 mm diameter needle was used to create a droplet of distilled water on each of the surfaces used for testing. Five digital images were taken the advancing contact angle as the droplet was grown on the surface. The contact angles were measured from the collected images using in-house software to measure the contact angle of the digitized image at the Surface Analysis and Imaging Laboratory in the University of Alberta Department of Mechanical Engineering. An example of each image is shown in figures A-1 to A-5.



Figure A-1: Contact Angle of Water on Fluorinated Polyurethane & Silicone PC100 Coating

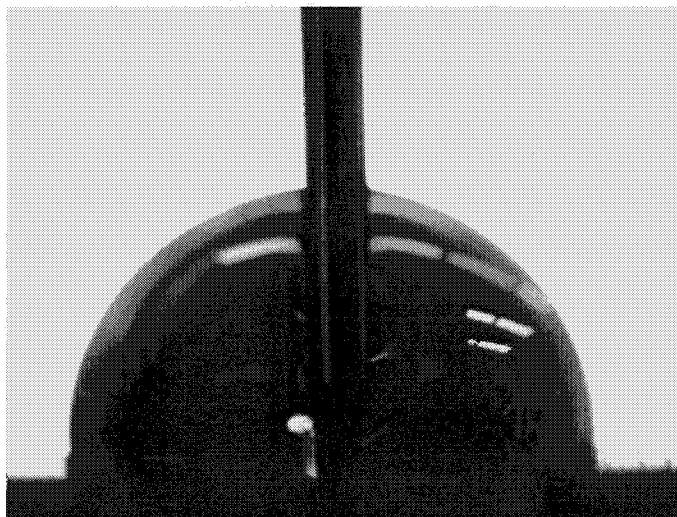


Figure A-2: Contact Angle of Water on Fluorinated Polyurethane PC200 Coating

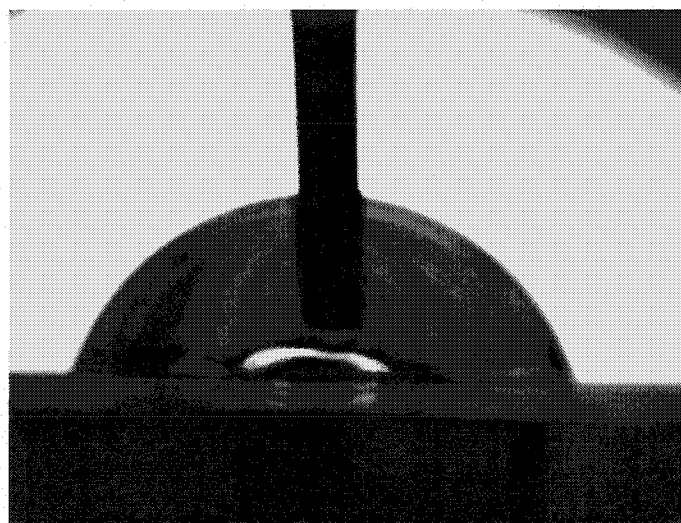


Figure A-3: Contact Angle of Water on Siloxane PSX700 Coating

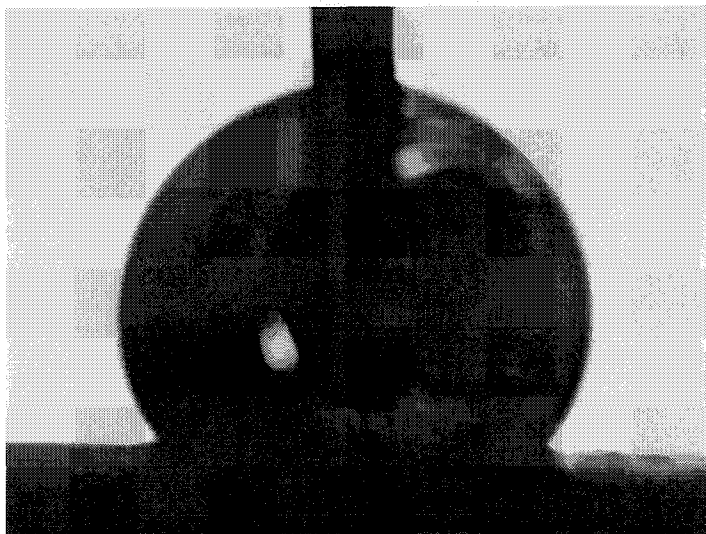


Figure A-4: Contact Angle of Water on Isophthalic Polyester 20-4969FX Coating

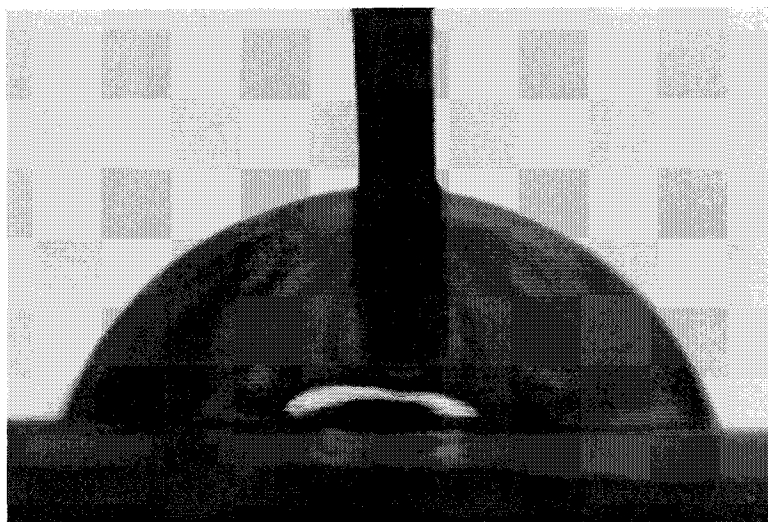


Figure A-5: Contact Angle of Water on Polished Aluminum 2024

APPENDIX B: DATA SHEETS FOR EXPERIMENTAL SURFACES

A data sheet was made available from each of the surface coating manufacturers except for the Progress Plastics 20-4969FX coating. 21st Century Coatings has renamed WC-1E and WC-2E, PC 100 and PC 200 respectively since the printing of these data sheets.

B.1 21st Century Coatings Data Sheets

FPU® Fluorinated Polyurethane**WC-1E****PRODUCT DESCRIPTION**

WC-1E is a high-performance, highly fluorinated polyurethane top coat formulated for thin film applications, offering general ease of handling and application. It is a two-component, solvent based, high solids enamel system which exhibits outstanding performance properties, compared to higher build, multi-coat premium systems.

The patented "fluoroshield" protection of WC-1E makes it virtually impervious to moisture and oxygen permeation. WC-1E exhibits unsurpassed performance for all physical properties as well as resistance to chemicals, weathering and uv degradation. WC-1E and its special additive provides low surface tension properties also make it an ideal coating for water shedding and anti-graffiti applications.

**CHARACTERISTICS**

A high performance, inert topcoat system designed to overcoat virtually any surface and make it resistant to corrosion, UV breakdown, abrasion, graffiti and chemical attack. FPU® coatings exhibit outstanding weathering characteristics. Developed over two decades of research and development, FPU® has a proven service history.

WC-1E is ideal for limited immersion service on marine, aerospace, architectural, industrial and automotive equipment, ferrous and non-ferrous metals, masonry, timber, fiberglass and carbon fiber. It provides a high quality finish, and offers exceptional all round performance with an expected life span exceeding 20 years.

- ☒ Outstanding Hydrophobic and Oleophobic surface properties
- ☒ Impervious to moisture and oxygen permeation (Osmotic barrier)
- ☒ Highly flexible and outstanding impact and abrasion resistance
- ☒ Low surface energy which resists soiling and marking
- ☒ Highly resistant to attack by hydrocarbons and chemical products
- ☒ Completely insensitive to UV radiation
- ☒ Meets or exceeds all US Military industrial coating specifications

**Application**

For optimum appearance properties, WC-1E should be spray applied in two to three coats to a minimum of 2 mils DFT / 50 microns DFT. Always allow each coat to "flash off" to a tacked state prior to a following coat.

WC-1E may also be spray applied, brushed or rolled in one coat, unreduced to the recommended DFT.

FPU® coatings must not be applied to surfaces at ambient temperatures above 35°C / 95°F. For optimum application properties, the temperature of the material should be between 10°C and 25°C / 50°F and 80°F prior to mixing and application. Apply the coating only when the surface temperature is more than 5°F or 3°C above the dew point temperature of the surrounding air and relative humidity is below 85%, in order to prevent moisture condensation on the surface.

**Mixing & Activation**

Mixing ratio 2:1 by volume (2 parts base to 1 part activator)

Reduction: T-102 - Slow reducer
T-059 - Fast reducer

Spray Viscosity: 21-25 seconds #2 Zahn

WC-1E is a two component coating system supplied in two separate containers. Part A is the base and Part B is the activator. Prior to activation, Base component (Part A) must be thoroughly mixed by mechanical agitation. Following agitation, with a paint stick, ensure all settled material is removed from the can bottom. After activation of Component A and Component B together, agitate for approximately 1-2 minutes. Reduce activated WC-1 to a maximum of 15% if required with recommended reducer and use immediately. WC-1 requires no induction period.

FPU® Fluorinated Polyurethane

WC-1E⁰**Pot Life**

3 Hours @ 21°C / 70°F
1 1/2 Hours @ 32°C / 90°F

However, these times may vary with environmental or climatic conditions

This material and its components are moisture sensitive. The product should be kept covered at all times after mixing and during application to prevent contamination and prevent moisture absorption.

**Curing**

Dry time @ 21°C / 70°F ambient air cure
Tack free: 4-6 Hours
Hard Cure: 24 hours
Full Cure: 3-5 days
Elevated Curing 40°C - 60°C / 105°F - 140°F for 40 minutes

**Colors & Finishes**

White, Clear and a full range of colors are available including metallic and pearlescent finishes.

High Gloss - > 90 / 60°
Semi-Gloss - 50-60 / 60°
Low Sheen - 30-40 / 60°

**Surface Preparation**

Suitable substrates for WC-1E include ferrous metal, galvanized metal, aluminum, fiberglass, carbon fiber, concrete and wood. Good surface preparation and cleaning of all substrates to be coated is essential for optimum performance of the coating system. All surfaces to be coated should be clean, dry and free from contaminants. For old or previously finished surfaces, the degree of preparation and cleaning required, is dependent upon the condition of the substrate.

Consult your 21st Century Coatings (Canada) Ltd. representative for recommended surface preparation procedures for your specific project.

**Coverage**

WC-1E exhibits excellent opacity and coverage when spray applied. If applying colors by means other than spray, test opacity over a small section to ensure adequate coverage prior to general application.

Solids content (+/- 2%)	60% by volume - White 50% by volume - Clear
Number of Coats	2-3 coats at 50 microns / 2 mils DFT - White 2-3 coats only at 37.5 microns / 1 1/2 mils DFT - Clear
Coverage (theoretical)	19.66 m ² per litre @ 25 microns / 1 mil DFT - White 963 ft ² per gallon @ 25 microns / 1 mil DFT - White 16.39 m ² per litre @ 25 micron / 1 mil DFT - Clear 803 ft ² per gallon @ 25 microns / 1 mil DFT - Clear

**Storage & Handling**

Hazardous Goods: Paint, Flammable Liquid, UN1263 Class III Hazchem 3YE

Shipping Information: 8.30 kg/18.25 lbs. per gallon unit including container - White
6.76 kg/14.9 lbs. per gallon unit including container - Clear

VOC content: 335 grams per liter / 2.8 lbs. per gallon - White

419 grams per liter / 3.5 lbs. per gallon - Clear

Flash Point (Seta Flash): 34°C / 93°F

Storage - FPU® coatings must be stored and handled in compliance with all current local regulations applying to flammable, or highly flammable liquids. Store in cool, dry, protected storage, well ventilated, between 5°C-35°C / 40°F-95°F and out of direct sunlight, moisture or rain. Maintain unmixed material in sealed containers at all times.

Shelf Life - FPU® has a minimum shelf life of 12 months from the date of manufacture if stored as indicated above, unopened in sealed containers. Ensure both components are consistent in appearance and thickness after stirring, and ensure that the activator (Part B) is clear and transparent before mixing the components together.

Do not use activator that is not visually clear.



FPU® Fluorinated Polyurethane

WC-2E[®]**Pot Life**

3 Hours @ 21°C / 70°F
 1 1/2 Hours @ 32°C / 90°F However, these times may vary with environmental or climatic conditions

This material and its' components are moisture sensitive. The product should be kept covered at all times after mixing and during application to prevent contamination and prevent moisture absorption.

**Curing**

Dry time @ 21°C / 70°F ambient air cure
 Tack free: 4-6 Hours
 Hard Cure: 24 hours
 Full Cure: 3-5 days
 Elevated Curing 40°C-60°C / 105°F-140°F for 40 minutes

**Colors & Finishes**

White, Clear and a full range of colors are available including metallic and pearlescent finishes.

High Gloss - > 90 / 60°
 Semi-Gloss - 50-60 / 60°
 Low Sheen - 30-40 / 60°

**Surface Preparation**

Suitable substrates for WC-2 include ferrous metal, galvanized metal, aluminum, fiberglass, carbon fiber, concrete and wood. Good surface preparation and cleaning of all substrates to be coated is essential for optimum performance of the coating system. All surfaces to be coated should be clean, dry and free from contaminants. For old or previously finished surfaces, the degree of preparation and cleaning required, is dependent upon the condition of the substrate.

Consult your 21st Century Coatings (Canada) Ltd. representative for recommended surface preparation procedures for your specific project.

**Coverage**

WC-2E exhibits excellent opacity and coverage when spray applied. If applying colors by means other than spray, test opacity over a small section to ensure adequate coverage prior to general application.

Solids content (+/- 2%)	60% by volume - White 50% by volume - Clear
Number of Coats	2-3 coats at 50 microns / 2 mils DFT - White 2-3 coats at 37.5 microns / 1 1/2 mils DFT - Clear
Coverage (theoretical)	19.66 m ² per litre @ 25 microns / 1 mil DFT - White 963 ft ² per gallon @ 25 microns / 1 mil DFT - White 16.39 m ² per litre @ 25 micron / 1 mil DFT - Clear 803 ft ² per gallon @ 25 microns / 1 mil DFT - Clear

**Storage & Handling**

Hazardous Goods:	Paint, Flammable Liquid, UN1263 Class III Hazchem 3YE
Shipping Information:	8.30 kg/18.25 lbs. per gallon unit including container - White 6.76 kg/14.9 lbs. per gallon unit including container - Clear
VOC content:	335 grams per liter / 2.8 lbs. per gallon - White 419 grams per liter / 3.5 lbs. per gallon - Clear
Flash Point (Seta Flash):	34°C / 93°F

Storage - FPU® coatings must be stored and handled in compliance with all current local regulations applying to flammable, or highly flammable liquids. Store in cool, dry, protected storage, well ventilated, between 5°C-35°C / 40°F-95°F and out of direct sunlight, moisture or rain. Maintain unmixed material in sealed containers at all times.

Shelf Life - FPU® has a minimum shelf life of 12 months from the date of manufacture if stored as indicated above, unopened in sealed containers. Ensure both components are consistent in appearance and thickness after stirring, and ensure that the activator (Part B) is clear and transparent before mixing the components together.

Do not use activator that is not visually clear.

FPU® Fluorinated Polyurethane**WC-2E®****PRODUCT DESCRIPTION**

WC-2E containing PTFE and silicon additives, is a high-performance, highly fluorinated polyurethane top coat formulated for thin film applications, offering general ease of handling and application. It is a two-component, solvent based, high solids enamel system which exhibits outstanding performance properties, compared to higher build, multi-coat premium systems.

The patented "fluoroshield" protection of WC-2E makes it virtually impervious to moisture and oxygen permeation. WC-2E exhibits unsurpassed performance for all physical properties as well as resistance to chemicals, weathering and uv degradation. WC-2E with its' PTFE and silicon additives makes it an ideal coating for water & ice shedding as well as non-stick applications.

**CHARACTERISTICS**

A high performance, inert topcoat system designed to overcoat virtually any surface and make it resistant to corrosion, UV breakdown, abrasion, graffiti and chemical attack. FPU® coatings exhibit outstanding weathering characteristics. Developed over two decades of research and development, FPU® has a proven service history.

WC-2E contains PTFE and silicon additives and is ideal for limited immersion service on marine, aerospace, architectural, industrial and automotive equipment, ferrous and non-ferrous metals, masonry, timber, fiberglass and carbon fiber. It provides a high quality finish, and offers exceptional all round performance with an expected life span exceeding 20 years.

- ☒ Outstanding Hydrophobic and Oleophobic surface properties
- ☒ Impervious to moisture and oxygen permeation (Osmotic barrier)
- ☒ Highly flexible and outstanding impact and abrasion resistance
- ☒ Low surface energy which resists soiling and marking
- ☒ Highly resistant to attack by hydrocarbons and chemical products
- ☒ Completely insensitive to UV radiation
- ☒ Meets or exceeds all US Military industrial coating specifications

**Application**

For optimum appearance properties, WC-2E should be spray applied in two coats to a minimum of 2 mils DFT / 50 microns DFT. Always allow each coat to "flash off" to a tacked state prior to a following coat.

WC-2E may also be spray applied, brushed or rolled in one coat, unreduced to the recommended DFT.

FPU® coatings must not be applied to surfaces at ambient temperatures above 35°C / 95°F. For optimum application properties, the temperature of the material should be between 10°C and 25°C / 50°F and 80°F prior to mixing and application. Apply the coating only when the surface temperature is more than 5°F or 3°C above the dew point temperature of the surrounding air and relative humidity is below 85%, in order to prevent moisture condensation on the surface.

**Mixing & Activation**

Mixing ratio 2:1 by volume (2 parts base to 1 part activator)

Reduction: T-102 - Slow reducer
T-059 - Fast reducer

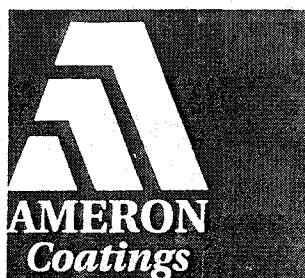
Spray Viscosity: 21-25 seconds #2 Zahn

WC-2E is a two component coating system supplied in two separate containers. Part A is the base and Part B is the activator. Prior to activation, Base component (Part A) must be thoroughly mixed by mechanical agitation. Following agitation, with a paint stick, ensure all settled material is removed from the can bottom. After activation of Component A and Component B together, agitate for approximately 1-2 minutes. Reduce activated WC-2 to a maximum of 15% if required with recommended reducer and use immediately. WC-2 requires no induction period.



21st Century Coatings (Canada) Ltd. 12074-86th Avenue, Surrey, BC, Canada V3W 3H7
Phone: (604) 204-0075 * Fax (604) 204-0003 * Email: info@21st-century-coatings-canada.com

B.2 Ameron PSX 1 Data Sheet



PSX[®] 700

Engineered Siloxane[®] coating Patent Nos. 5,618,860 and 5,275,645

Application Instructions

Refer to the Product Data sheet for properties and uses.

Adhere to all application instructions, precautions, conditions, and limitations to obtain the maximum performance. For conditions outside the requirements or limitations described, contact your Ameron representative.

Surface Preparation

Coating performance is, in general, proportional to the degree of surface preparation. Refer to specifications for the specific primer being used. Prior to coating, primed surface must be clean, dry, undamaged and free of all contaminants including salt deposits. Round off all rough welds and remove all weld spatter.

Steel - Remove all loose rust, dirt, grease or other contaminants by one of the following depending on the degree of cleanliness required: SSPC-SP6 or 10. The choice of surface preparation will depend on the system selected and end-use service conditions.

Concrete - Acid etching (ASTM D4260) or abrasive blast (ASTM D4259) new concrete before priming.

Aluminum - Remove oil, grease or soap film with neutral detergent or emulsion cleaner; treat with Alodine[®] 1200, Alumiprep[®] or equivalent or blast lightly with fine abrasive.

Galvanizing - Remove oil or soap film with detergent or emulsion cleaner, then use zinc treatment such as Galvaprep[®] or equivalent or blast lightly with fine abrasive.

Aged coatings - Contact your Ameron representative. A test patch of PSX 700 over intact clean coating and observation for firm defects for over a period of 3 to 6 months may be required.

Repair - Prepare damaged areas to original surface preparation specifications, feathering edges of intact coating. Thoroughly remove dust or abrasive residue before touch up.

Application Equipment

The following is a guide; suitable equipment from other manufacturers may be used. Changes in pressure, hose and tip size may be needed for proper spray characteristics.

Airless spray - Standard equipment such as Graco Bulldog Hydra-Spray or larger with a 0.015- to 0.021-in. (0.38 to 0.53 mm) fluid tip.

Conventional spray - Industrial equipment such as DeVilbiss MBC or JGA spray gun with 78 or 765 air cap and "E" fluid tip, or Binks No. 18 or 62 gun with a 66 x 63 PB nozzle set up. Separate air and fluid pressure regulators, mechanical pot agitator, a moisture and oil trap in the main air supply line are recommended.

Power mixer - Jiffy Mixer powered by an air or an explosion-proof electric motor.

Brush - Natural bristle. Maintain wet edge.

Roller - Use industrial roller. Level any air bubbles with bristle brush.

Environmental Conditions

Temperature	°F	°C
air	40 to 120	4 to 49
surface	40 to 120	4 to 49
Relative humidity	40% minimum	

Surface temperatures must be at least 5°F (3°C) above dew point to prevent condensation during application and initial dry through. Relative humidity lower than 40% will extend dry times.

Heat curing

Allow 700 or 700FD to dry to touch before exposing to curing temperatures above 140°F.

Application Procedure

1. Flush equipment with thinner or Amercoat[®] 12 before use.
2. Mix to a uniform consistency.
3. Add PSX 700 cure to 700 resin. Mix thoroughly until uniformly blended.

Pot life (hours)*	°F/°C
700 & 700FD	90/32 70/21 50/10
	1½ 4 6½

4. If needed for workability, thin** with Amercoat 911 up to 1 pint per gallon PSX 700.
5. Apply a wet coat in even, parallel passes, overlap each pass 50 percent to avoid holidays, bare areas and pinholes. If required, follow with a cross spray at right angles to first pass.

Drying time (ASTM D1640) (hours) @ 40% R.H. or above

	°F/°C
touch (700)	90/32 70/21 50/10 32/0
touch (700FD)	1 3 6 12
through (700)	1 2 4½ 9
through (700FD)	4 6 11 38
	3 4½ 8½ 24

Recoat/topcoat time (hours) @ 40% R.H. or above

	°F/°C
minimum (700 over 700)	90/32 70/21 50/10 32/0
minimum (700FD over 700FD)	3 4½ 9 32
maximum***	2 3 7 18
	None

6. Brush and/or roll applications will require 2 coats to achieve a 7 mil DFT. There will be some surface texture, which is typical for brush and roll applications.
7. When applying PSX 700 directly over Dimetecote[®] or Amercoat 68HS see special thinning instructions.
8. Clean all equipment with thinner or Amercoat 12 cleaner immediately after use.

*Thinning material with ½ pt/gal after 3 hours will extend pot life to 5 hours at 70°F.

**See special thinning for application over Dimetecote and Amercoat 68HS primers.

***See surface preparation for aged coatings.

Thinning for Application over Dimetcote

Thin PSX 700 or 700FD with Amercoat 900 up to 1 pint per gallon to assist in film thickness control and to minimize bubbling. This will depend on the age of the coating, surface roughness and conditions during curing. Based on conditions an interval between the mist-coat and full-coat may assist in the application.

Safety Precautions

Read each component's material safety data sheet before use. Mixed material has hazards of each component. Safety precautions must be strictly followed during storing, handling and use.

CAUTION - Improper use and handling of this product can be hazardous to health and cause fire or explosion.

Do not use this product without first taking all appropriate safety measures to prevent property damage and injuries. These measures may include, without limitation: implementation of proper ventilation, use of proper lamps, wearing of proper protective clothing and masks, tenting and proper separation of application areas. Consult your supervisor. Proper ventilation and protective measures must be provided during application and drying to keep spray mists and vapor concentrations within safe limits and to protect against toxic hazards. Necessary safety equipment must be used and ventilation requirements carefully observed, especially in confined or enclosed spaces, such as tank interiors and buildings.

This product is to be used by those knowledgeable about proper application methods. Ameron makes no recommendation about the types of safety measures that may need to be adopted because these depend on application environment and space, of which Ameron is unaware and over which it has no control.

If you do not fully understand these warnings and instructions or if you cannot strictly comply with them, do not use the product.

Note: Consult Code of Federal Regulations Title 29, Labor, parts 1910 and 1915 concerning occupational safety and health standards and regulations, as well as any other applicable federal, state and local regulations on safe practices in coating operations.

This product is for industrial use only. Not for residential use.

Warranty

Ameron warrants its products to be free from defects in material and workmanship. Ameron's sole obligation and Buyer's exclusive remedy in connection with the products shall be limited, at Ameron's option, to either replacement of products not conforming to this Warranty or credit to Buyer's account in the invoiced amount of the nonconforming products. Any claim under this Warranty must be made by Buyer to Ameron in writing within five (5) days of Buyer's discovery of the claimed defect, but in no event later than the expiration of the applicable shelf life, or one year from the delivery date, whichever is earlier. Buyer's failure to notify Ameron of such nonconformance as required herein shall bar Buyer from recovery under this Warranty.

Ameron makes no other warranties concerning the product. No other warranties, whether express, implied, or statutory, such as warranties of merchantability or fitness for a particular purpose, shall apply. In no event shall Ameron be liable for consequential or incidental damages.

Any recommendation or suggestion relating to the use of the products made by Ameron, whether in its technical literature, or in response to specific inquiry, or otherwise, is based on data believed to be reliable; however, the products and information are intended for use by Buyers having requisite skill and know-how in the industry, and therefore it is for Buyer to satisfy itself of the suitability of the products for its own particular use and it shall be deemed that Buyer has done so, at its sole discretion and risk. Variation in environment, changes in procedures of use, or extrapolation of data may cause unsatisfactory results.

Limitation of Liability

Ameron's liability on any claim of any kind, including claims based upon Ameron's negligence or strict liability, for any loss or damage arising out of, connected with, or resulting from the use of the products, shall in no case exceed the purchase price allocable to the products or part thereof which give rise to the claim. In no event shall Ameron be liable for consequential or incidental damages.



Ameron Coatings • 201 North Berry Street, Brea, California 92821 • (714) 529-1951
Ameron PCG/Europe • J. F. Kennedylaan 7, 4191 MZ Geldermalsen, The Netherlands • (31) 345-587-587

APPENDIX C: DROPLET SUPERCOOLING ESTIMATE

Estimating the temperature of the liquid droplets is simplified if a lumped heat capacitance method can be used. To see if this is applicable, the following calculation was performed.

For very low Reynolds' numbers as is the case with micrometer sized droplets, an average Nusselt number of 2 can be assumed (Incorpera and DeWitt, 1996).

$$\therefore \overline{Nu}_D = 2 = \frac{\bar{h}D}{k_{air}} \quad (C.1)$$

$$\therefore \bar{h} = \frac{2k_{air}}{D} \quad (C.2)$$

where: \bar{h} = External Flow Convective Heat Transfer Coefficient (W/m²K),

k_{air} = Heat Transfer Coefficient (W/mK),

D = Droplet Diameter (m).

If $k_{air} = 0.0223$ W/mK and the average diameter of the spray is 50 μm Equation C.2 gives an average heat transfer coefficient of 900 W/m²K. The Biot number for the droplets is therefore:

$$Bi = \frac{\bar{h}D}{k_{air}} = 0.0075 \quad (C.3)$$

The lumped heat capacity method for calculation of transient systems, is applicable when the Biot number is below 0.1, and is described by Equation C.4 (Incorpera and DeWitt, 1996):

$$\frac{T - T_{\infty}}{T_i - T_{\infty}} = \exp \left[- \frac{\bar{h} A_s t}{\rho V c_p} \right] \quad (\text{C.4})$$

where: T = Temperature at time t ($^{\circ}\text{C}$),

T_i = Initial Uniform Temperature ($^{\circ}\text{C}$),

T_{∞} = Ambient Temperature ($^{\circ}\text{C}$),

A_s = Surface Area of Droplet (m^2),

V = Volume of Droplet (m^3),

ρ = Density of Droplet (kg/m^3),

c_p = Specific Heat Capacity ($\text{J}/\text{kg}^{\circ}\text{C}$),

t = time (sec).

For a water droplet with a diameter of $50 \mu\text{m}$, a density of $1000 \text{ kg}/\text{m}^3$, a specific heat capacity of $4167 \text{ J}/\text{kg}^{\circ}\text{C}$, Equation C.4 can be used to determine that it would take 0.01 seconds for the droplet to reach 75% of its surrounding temperature. It can therefore be assumed that the droplets from the supercooled fog system are close to the ambient temperatures when they impacted the plates.

APPENDIX D: DATA COLLECTION AND SYSTEM CONTROL CODE

D.1 Quick Basic Code for Temperature Control and Data Acquisition

```

'           wind_ice.txt
'           WIND1
'           June 2001
'           Tim Weis
'   Control and Data Collection code for ice creation on
'   Aluminum Sample plates using Datataker 500

DECLARE SUB filenamer ()
DECLARE SUB collect ()
DECLARE SUB display ()
DECLARE SUB Headers ()
DECLARE SUB adhere ()
DECLARE SUB ice ()
DECLARE SUB checktemp ()
DECLARE SUB datataker ()
DECLARE SUB shutdown ()
DECLARE SUB montr ()

COMMON SHARED cmd$(), dat(), ax(), un(), mon(), title$()
COMMON SHARED a$, b$, filename$, process$, number$, type$
COMMON SHARED heater%, watercntrl%, sprayer%
COMMON SHARED outp, post, negt, pressc, coilfon, coilfoff
COMMON SHARED heaton!, heatoff!
DIM SHARED cmd$(10), dat(10), ax(5), un(5), mon(10), title$(10)

'constants
title$(1) = "rpm"
title$(2) = "lead T"
title$(3) = "trail T"
title$(4) = "ice bed T"
title$(5) = "heater V"
title$(6) = "shaft hub T"
title$(7) = "sol #1 T"
title$(8) = "water T"
title$(9) = "air T"
title$(10) = "in shaft T"

post = 25.64      'C/mV thermocouple cal non-critical temps below 0C
negt = 25.96      'C/mV thermocouple calibration
pressc = .04      'mV -> psi callibration

heater% = 8        'integer heater off (high signal)
sprayer% = 0       'integer sprayer off (low signal)
watercntrl% = heater% '+ sprayer%

heaton! = .75

```



```

heatoff! = 1.25

OUT &H378, watercntrl%

'open com port and setup datataker
1 :
OPEN "COM1:4800,N,8,1,cs0,rs,ds0" FOR RANDOM AS 1 'opens com port
ON COM(1) GOSUB comhandler 'when a signal from com received goto
comhandler
COM(1) ON

CALL datataker

PRINT #1, "1DSO=0" 'turns off water circulation pump
PRINT #1, "2DSO=0" 'turns off centrifuge oil pump
PRINT #1, "3DSO=0" 'turns off coil fan
PRINT #1, "4DSO=0" 'turn spray vent and radiation heaters off

'program body
CLS

KEY 1, "stop" 'watch for F1 key in order to
ON KEY(1) GOSUB quit 'manually stop program
KEY(1) ON
KEY ON

KEY 2, "pump"
ON KEY(2) GOSUB pump
KEY(2) ON
KEY ON

KEY 3, "monitor"
ON KEY(3) GOSUB monitor
KEY(3) ON
KEY ON

KEY 4, "mkill" 'watch for F4 key to
ON KEY(4) GOSUB mkill 'emergency motor stop
KEY(4) ON
KEY ON

KEY 5, "ice" 'watch for F5 key to
ON KEY(5) GOSUB icing 'start icing data collection
KEY(5) ON
KEY ON

KEY 8, "restrt" 'watch for F8 key to
ON KEY(8) GOSUB restrt 'reset and restart program
KEY(8) ON
KEY ON

KEY 9, "cntrfg" 'watch for F9 key to
ON KEY(9) GOSUB adhesion 'start adhesion data collection
KEY(9) ON
KEY ON

CALL Headers

```

```

CALL display
END
'SUBROUTINES

comhandler:
WHILE NOT EOF(1)
a$ = INPUT$(1, #1)
b$ = b$ + a$
WEND
RETURN

'F1
quit:
CLS
LOCATE 16, 20
PRINT "Program terminated by user"
CALL shutdown
END
RETURN

'F2
pump:
PRINT #1, "1DSO=1"
CLOSE #1
END
RETURN

'F3
monitor:
CALL montr
END
RETURN

' F4
mkill:
CALL shutdown
END
RETURN

' F5
icing:
CLS
COLOR 7, 1
CALL Headers
LOCATE 16, 20
PRINT "Ice data collection"
CALL ice
END
RETURN

'F8
restrt:
CALL shutdown
start = TIMER
time = 0
  WHILE time < 2
    time = TIMER - start

```

```

WEND
GOTO 1
END
RETURN

```

```

' F9
adhesion:
CLS
COLOR 4, 7
CALL Headers
LOCATE 16, 20
PRINT "adhesion data collection"
CALL adhere
END
RETURN

```

SUB adhere

```
process$ = "a"
```

```

LOCATE 12, 5
INPUT "Specimen Number (##)"; number$
LOCATE 13, 5
INPUT "Heater resistance (ohms)"; resist
LOCATE 12, 40
INPUT "Heater type (a/f)"; type$
LOCATE 13, 40
INPUT "Mass of specimen (g)"; mass
mass = mass / 1000
LOCATE 16, 46
PRINT "ok to go..."

```

```

coilfon = -50!
coilfoff = -55!

```

```

CALL filenamer
LOCATE 14, 5
file$ = MID$(filename$, 17)
PRINT "FILE: ", file$

```

```
' *****headers for output *****
```

```

OPEN filename$ FOR APPEND AS #2
PRINT #2, "Mass of Specimen:,"; mass; ",kg,Heater Resistance:,";
resist; ",Ohms"
PRINT #2, "Time,RPM,Leading Edge T,Trailing Edge T,Ice Bed T, Heater
V,In-Shaft T,Pillow Block T,Ambient T,filename: ", file$
CLOSE #2

```

```
' ***** wait for motor to turn on *****
```

```

motoron% = 0
waiting$ = ""
count% = 0
OUT &H378, 0
PRINT #1, "1DSO=1"      'keep water circulating
PRINT #1, "2DSO=1"      'turn oil pump on

```

```

PRINT #1, "3DSO=1"      'keep cooling coil fan on
PRINT #1, "4DSO=1"      'radiation heaters on
OUT &H378, 0

CLS

' ***** Data collection and display *****

start = TIMER
fail% = 0
count% = 0
accel5! = 0!
col% = 1
mon(1) = 1
mon(2) = 2
mon(3) = 3
mon(4) = 6
mon(5) = 9
mon(6) = 10
outp$ = ""
CALL Headers

WHILE fail% < 8

    count% = count% + 1

    '***** Communicate with Datataker *****

501 :

    FOR i% = 1 TO 6

        b$ = ""
        T = TIMER
        errr% = 0
        PRINT #1, cmd$(mon(i%))

        DO
            IF (TIMER - T) > 5 THEN
                errr% = errr% + 1
                IF errr% = 2 THEN
                    OUT &H378, 0
                    GOTO 501: 'avoids endless loop
                END IF
                LOCATE 16, 25
                PRINT errr%
            END IF
        LOOP UNTIL INSTR(b$, CHR$(13) + CHR$(10) + CHR$(13) + CHR$(10))

        a = INSTR(b$, CHR$(32))
        a$ = MID$(b$, a, 6)
        dat(mon(i%)) = VAL(a$)

    NEXT i%

'signal conversions

```

```

' ***** Calibrations *****
dat(1) = dat(1) * 3.21
dat(4) = dat(4) * .1
dat(9) = dat(9) * negt ' (ABS(dat(5) - 122.5)) / 34.5
dat(6) = dat(6) * negt
dat(10) = dat(10) * negt

correct = dat(6) - dat(10)
dat(2) = (dat(2) * negt) + correct
dat(3) = (dat(3) * negt) + correct
' *****

' Display & Output Data

atime = TIMER - start
outp$ = outp$ + STR$(atime) + ", "

FOR i% = 1 TO 6
  IF i% < 4 THEN
    LOCATE 5 + mon(i%), 21
    PRINT USING "+####.###"; dat(mon(i%))
    outp$ = outp$ + STR$(dat(mon(i%))) + ", "

    ELSEIF i% >= 4 THEN
      LOCATE mon(i%), 61
      PRINT USING "+####.###"; dat(mon(i%))
      outp$ = outp$ + STR$(dat(mon(i%))) + ", "
    END IF
  NEXT i%

IF INKEY$ = CHR$(112) THEN 'manual detection of failure (hit "p")
  fail% = 1
END IF

IF fail% = 1 THEN
  rpm = dat(1)
  leadt = dat(2)
  trailt = dat(3)
  fail% = fail% + 1
  outp$ = outp$ + ", failure detected"
  ELSEIF fail% > 1 THEN
    fail% = fail% + 1
    outp$ = outp$ + ", failure detected"
  END IF

OPEN filename$ FOR APPEND AS #2
PRINT #2, outp$
CLOSE #2

outp$ = ""

WEND

' *** Ambient Air Temp ***
b$ = ""
PRINT #1, cmd$(9)
DO

```

```

LOOP UNTIL INSTR(b$, CHR$(13) + CHR$(10) + CHR$(13) + CHR$(10))
  a = INSTR(b$, CHR$(32))
  a$ = MID$(b$, a, 6)
  dat(9) = VAL(a$)
  dat(9) = dat(9) * negt

  w = rpm * 2 * 3.14159 / 60
  centrip = w * w * .19385
  centrip = rpm^2 * (2pi)^2 / ((60sec)^2 * radius)
  force = centrip * mass
  stress = force / .0025806
  stress = stress / 1000

LOCATE 23, 25
PRINT "Failure detected!"
PRINT "RPM: "; rpm; " Centrip accel: "; centrip; " m/s/s"
PRINT "FORCE: "; force; " N "; " STRESS: "; stress; "Pa"
PRINT "Ambient T: "; dat(9)
PRINT "Surface T, Leading Edge: "; leadt; "Trailing Edge: "; trailt

OPEN filename$ FOR APPEND AS #2
PRINT #2, ""
PRINT #2, "Release details:"
PRINT #2, "Heater Voltage: , ", dat(4)
PRINT #2, "RPM at Failure: , ", rpm, ",RPM"
PRINT #2, "Centrepital Accl: , ", centrip, ",m/s/s"
PRINT #2, "Mass of Specimen: , ", mass, ",kg"
PRINT #2, "Force: , ", force, ",N"
PRINT #2, "Stress: , ", stress, ",kPa"
PRINT #2, "Leading Edge T: , ", leadt
PRINT #2, "Trailing Edge: , ", trailt
CLOSE #2

OUT &H378, 4 'kill CF motor
PRINT #1, "2DSO=0" 'shut off oil pump

END SUB

SUB checktemp

IF dat(9) <= 3! THEN
  PRINT #1, "1DSO=1" 'turn water circulation pump on.

  IF dat(8) <= coilfoff THEN
    PRINT #1, "3DSO=0" 'turn fan off
  ELSEIF dat(8) > coilfon THEN
    PRINT #1, "3DSO=1" 'turn fan on
  END IF

ELSEIF dat(9) > 0! THEN
  PRINT #1, "1DSO=0" 'pump off
  PRINT #1, "3DSO=0" 'fan off
END IF

IF dat(8) <= heaton! THEN
  heater% = 0 'heater control is based on coil water temp
ELSEIF dat(8) >= heatoff! THEN 'because water is coldest here by fan

```

```

heater% = 8
END IF

```

```

watercntrl% = heater% + sprayer%
OUT &H378, watercntrl%

```

```
END SUB
```

SUB datataker

```

PRINT #1, "/e"          'disable echo
PRINT #1, "/m"          'disable error message

```

```
'initialize commands for datataker
```

```

cmd$(1) = "1V"          'tachometer signal
cmd$(2) = "2V"          'leading edge thermocouple Differential T
cmd$(3) = "3V"          'trailing edge thermocouple differential T
cmd$(4) = "4V"          'Heater Input Voltage (Accelerometer output
(50g))
cmd$(5) = "5V"          'Ice maker bed T
cmd$(6) = "6V"          'Centrifuge Box Temperature T
cmd$(7) = "7V"          'Nozzle #3 Water solenoid Differential T
cmd$(8) = "8V"          'Circulating Water Differential T
cmd$(9) = "9V"          'Ambient Air Differential T
cmd$(10) = "10V"        'Plate Temperature while icing T

```

```
END SUB
```

SUB display

```

LOCATE 18, 20
PRINT "Press 'F5' for data collection for icing"
LOCATE 20, 20
PRINT "Press 'F9' for data collection for adhesion"

```

```

coilfon = 5.25
coilfoff = 5!
heaton! = 1.5
heatoff! = 1.85

```

```

past% = 2
errr% = 0
pumpt = 0

```

```
99 :
```

```
FOR i% = 1 TO 10
```

```

LOCATE 2, 75
PRINT USING "##"; i%

```

```

b$ = ""
T = TIMER
PRINT #1, cmd$(i%)

```

```
DO
```

```
IF errr% >= 2 THEN
```

```

CLOSE #1
OPEN "COM1:4800,N,8,1,cs0,rs,ds0" FOR RANDOM AS 1 'opens com port
ON COM(1) GOSUB comhandler 'when a signal from com received goto
comhandler
COM(1) ON
CALL datataker
errrr% = 0
GOTO 99:
END IF

IF (TIMER - T) > 2 THEN
  errrr% = errrr% + 1
  LOCATE 16, 25
  PRINT errrr%
  OUT &H378, 0
  GOTO 99: 'avoids endless loop
END IF

LOOP UNTIL INSTR(b$, CHR$(13) + CHR$(10) + CHR$(13) + CHR$(10))

a = INSTR(b$, CHR$(32))
a$ = MID$(b$, a, 6)
dat(i%) = VAL(a$)

NEXT i%

'signal conversions

Heater Voltage Signal Conversion (10:1 reduction)
dat(5) = dat(5) * .1

'Ice Bed Temp T Type
dat(4) = dat(4) * negt

'RPM signal conversion (30:1 signal reduction)

dat(1) = dat(1) * 3.21

IF dat(1) > 10 THEN
PRINT #1, "2DSO=1" 'turn oil on
ELSEIF dat(1) < 50 THEN
PRINT #1, "2DSO=0" 'turn oil off
END IF

' Shaft Temperature Calibration

dat(10) = dat(10) * negt
dat(6) = dat(6) * negt

slipcor = dat(6) - dat(10) 'corrects for slip ring problems

' Thermocouple Calibration

IF dat(9) > 0! THEN
dat(9) = dat(9) * post
ELSEIF dat(9) < 0! THEN
dat(9) = dat(9) * negt

```



```

END IF

IF dat(8) > 0! THEN
dat(8) = dat(8) * post
ELSEIF dat(8) < 0! THEN
dat(8) = dat(8) * negt
END IF

IF dat(7) > 0! THEN
dat(7) = dat(7) * post
ELSEIF dat(7) < 0! THEN
dat(7) = dat(7) * negt
END IF

IF dat(2) > 0! THEN
dat(2) = dat(2) * post
ELSEIF dat(2) < 0! THEN
dat(2) = dat(2) * negt
END IF

IF dat(3) > 0! THEN
dat(3) = dat(3) * post
ELSEIF dat(3) < 0! THEN
dat(3) = dat(3) * negt
END IF

dat(3) = dat(3) + slipcor
dat(2) = dat(2) + slipcor

' Display location

FOR i% = 1 TO 5
LOCATE 5 + i%, 21
PRINT USING "+####.###"; dat(i%)
NEXT i%

FOR i% = 6 TO 10
LOCATE i%, 61
PRINT USING "+####.###"; dat(i%)
NEXT i%

errr% = 0

CALL checktemp

IF dat(9) < 0 THEN
PRINT #1, "4DSO=1"
ELSEIF dat(9) > 0 THEN
PRINT #1, "4DSO=0"
END IF

GOTO 99:

END SUB

SUB filenamer
'creates a filename for data based on date, process & sample #

```

```
' MMDDp##.dat
```

```
filename$ = "c:\qb45\tim\data\" + MID$(DATE$, 1, 2) + MID$(DATE$, 4, 2) + process$ + type$ + number$ + ".dat"
```

```
END SUB
```

SUB Headers

```
LOCATE 2, 1
PRINT "CENTRIFUGE SIGNALS"
LOCATE 2, 41
PRINT "ICING SIGNALS"
LOCATE 4, 1
PRINT "CH"
LOCATE 4, 4
PRINT "SIGNAL"
LOCATE 4, 21
PRINT "OUTPUT"
LOCATE 4, 41
PRINT "CH"
LOCATE 4, 44
PRINT "SIGNAL"
LOCATE 4, 61
PRINT "OUTPUT"
LOCATE 6, 1
PRINT "1"
LOCATE 6, 4
PRINT "Tachometer"
LOCATE 6, 35
PRINT "rpm"
LOCATE 6, 41
PRINT "6"
LOCATE 6, 44
PRINT "Shaft Air Temp"
LOCATE 6, 75
PRINT "DegC"
LOCATE 7, 1
PRINT "2"
LOCATE 7, 4
PRINT "Leading Edge T"
LOCATE 7, 35
PRINT "DegC"
LOCATE 7, 41
PRINT "7"
LOCATE 7, 44
PRINT "Sol #1 Temp"
LOCATE 7, 75
PRINT "DegC"
LOCATE 8, 1
PRINT "3"
LOCATE 8, 4
PRINT "Trailing Edge T"
LOCATE 8, 35
PRINT "DegC"
LOCATE 8, 41
PRINT "8"
```

```

LOCATE 8, 44
PRINT "Water Temp"
LOCATE 8, 75
PRINT "DegC"
LOCATE 9, 1
PRINT "4"
LOCATE 9, 4
PRINT "Ice Bed Temp"      'Heater Voltage
LOCATE 9, 35
PRINT "DegC"
LOCATE 9, 41
PRINT "9"
LOCATE 9, 44
PRINT "Nzl Ambient Air T"
LOCATE 9, 75
PRINT "DegC"
LOCATE 10, 1
PRINT "5"
LOCATE 10, 4
PRINT "no signal"
LOCATE 10, 35
PRINT ""
LOCATE 10, 41
PRINT "10"
LOCATE 10, 44
PRINT "Inside Shaft T"
LOCATE 10, 75
PRINT "DegC"

```

```

LOCATE 22, 20
PRINT "Press 'F1' to exit program"

```

END SUB

SUB ice

```

PRINT #1, "3DSO=1"      'turn cooling fan on

```

```

mon(6) = 4
mon(7) = 6
mon(8) = 7
mon(9) = 8
mon(10) = 10

```

```

process$ = "i"
type$ = "i"

```

```

LOCATE 12, 5
INPUT "Specimen number (##)"; number$
LOCATE 13, 5
INPUT "Spray duration (sec)"; duration
LOCATE 12, 40
INPUT "Spray interval (sec)"; interval
LOCATE 13, 40
INPUT "Number of spray cycles"; cycles%

```

```

LOCATE 16, 44
PRINT "hit SPACE BAR to start"

```

```

WHILE INKEY$ <> CHR$(32) 'space bar starts icing
WEND

coilfon = 1!
coilfoff = 0!

heaton! = -.5
heatoff! = .5

LOCATE 16, 44
PRINT "COLLECTING DATA....."

CALL filenamer
OPEN filename$ FOR APPEND AS #2
PRINT #2, "Specimen #, ", number$, " Spray Duration, ", duration
PRINT #2, "Spray Interval, ", interval, " # Spray Cycles, ", cycles%
PRINT #2, "Surface Temp(C), Ambient Air Temp (C), Bearing Temp(C),
Nozzle Temp (C), Water Temp (C), Inside Shaft T (C)"
CLOSE #2

LOCATE 15, 5
file$ = MID$(filename$, 17)
PRINT "FILE: ", file$

start! = TIMER 'start clock
delay = TIMER
count% = 0
event$ = " interval"

WHILE count% < cycles%

101 :
outp$ = ""

' Data collection and display

FOR i% = 6 TO 10

    b$ = ""
    T = TIMER
    PRINT #1, cmd$(mon(i%))
    DO
        IF (TIMER - T) > 10 THEN
            i% = 4
            GOTO 101:
        END IF
    LOOP UNTIL INSTR(b$, CHR$(13) + CHR$(10) + CHR$(13) + CHR$(10))

    a = INSTR(b$, CHR$(32))
    a$ = MID$(b$, a, 6)
    dat(mon(i%)) = VAL(a$)

    dat(4) = dat(4) * negt

    IF dat(7) > 0! THEN
        dat(7) = dat(7) * post
    ELSEIF dat(7) < 0! THEN

```

```

dat(7) = dat(7) * negt
END IF

IF dat(8) > 0! THEN
dat(8) = dat(8) * post
ELSEIF dat(8) < 0! THEN
dat(8) = dat(8) * negt
END IF

IF dat(6) > 0! THEN
dat(6) = dat(6) * post
ELSEIF dat(6) < 0! THEN
dat(6) = dat(6) * negt
END IF

dat(10) = dat(10) * negt

IF i% <= 6 THEN
LOCATE mon(i%) + 5, 21
PRINT USING "###.###"; dat(mon(i%))
ELSE
LOCATE mon(i%), 65
PRINT USING "###.###"; dat(mon(i%))
END IF

outp$ = outp$ + STR$(dat(mon(i%))) + ", "

time! = TIMER - start!

IF time! >= (interval + duration) THEN
sprayer% = 0
watercntrl% = sprayer% + heater%
OUT &H378, watercntrl%
start! = TIMER
count% = count% + 1
event$ = " interval"
PRINT #1, "2DSO=0"      ' pressure reapply

ELSEIF time! >= interval THEN
sprayer% = 1
watercntrl% = sprayer% + heater%
OUT &H378, watercntrl%
event$ = " spray"

ELSEIF time! >= (interval - .5) THEN
PRINT #1, "2DSO=1"      ' pressure release
PRINT #1, "4DSO=0"

ELSEIF time! >= 1! THEN
PRINT #1, "4DSO=1"      ' turn vent fan and radiation heaters off

ELSE
OUT &H378, watercntrl%
END IF

LOCATE 20, 10
PRINT "Count: ", count%, " time: ", time!

```

```

NEXT i%

IF (TIMER - delay) > 2 THEN

    outp$ = outp$ + event$

    OPEN filename$ FOR APPEND AS #2
    PRINT #2, outp$
    CLOSE #2

    delay = TIMER

END IF

CALL checktemp

WEND

PRINT #1, "2DSO=0" 'purge nozzle air on
PRINT #1, "3DSO=0" 'coil fan off
PRINT #1, "4DSO=1" 'radiation heaters & vent on

LOCATE 16, 44
PRINT "      all done!      "
LOCATE 22, 20
PRINT "ESC to EXIT, F8 to RESTART, F9 for SPIN"

coilon = 10!
coiloff = 9!

heaton! = 2.25
heatoff! = 2.75

WHILE INKEY$ <> CHR$(27) ' check ambient temp to keep pump/heater on

coilfon = 5.75
coilfoff = 8.1
OUT &H378, 0 'heaters on
PRINT #1, "3DSO=0" 'turn cooling fan off

102 :
FOR i% = 6 TO 9
    b$ = ""
    T = TIMER
    PRINT #1, cmd$(i%)
    DO
        IF (TIMER - T) > 10 THEN
            i% = 6
            GOTO 101:
        END IF
    LOOP UNTIL INSTR(b$, CHR$(13) + CHR$(10) + CHR$(13) + CHR$(10))

    a = INSTR(b$, CHR$(32))
    a$ = MID$(b$, a, 6)
    dat(i%) = VAL(a$)

```

' Signal Calibration

```

IF i% = 6 THEN
    dat(6) = dat(6) * pressc

ELSEIF i% = 7 THEN
    IF dat(7) > 0! THEN
        dat(7) = dat(7) * post
    ELSEIF dat(7) < 0! THEN
        dat(7) = dat(7) * negt
    END IF

ELSEIF i% = 8 THEN
    IF dat(8) > 0! THEN
        dat(8) = dat(8) * post
    ELSEIF dat(8) < 0! THEN
        dat(8) = dat(8) * negt
    END IF

ELSEIF i% = 9 THEN
    IF dat(9) > 0! THEN
        dat(9) = dat(9) * post
    ELSEIF dat(9) < 0! THEN
        dat(9) = dat(9) * negt
    END IF

END IF

LOCATE i%, 65
PRINT USING "###.###"; dat(i%)

```

NEXT i%

WEND

END SUB

SUB montr

```

LOCATE 18, 20
PRINT "Please enter the filename for this check....."
LOCATE 20, 20
PRINT "
LOCATE 20, 20
INPUT monitr$
monitr$ = "c:\qb45\tim\data\" + monitr$ + ".txt"
LOCATE 22, 20
PRINT "Enter signals to record, input '0' when finished."

```

```

x% = 1
j% = 0
pumpt = 0

```

WHILE x% <> 0

```

j% = j% + 1
INPUT mon(j%)

```

```

x% = mon(j%)

WEND

j% = j% - 1
CLS
CALL Headers
LOCATE 20, 20
PRINT , "type 'A' to quit"

head$ = ""
outp$ = ""
FOR i% = 1 TO j%
head$ = head$ + title$(mon(i%)) + ", "
NEXT i%

head$ = head$ + "time"

OPEN monitr$ FOR APPEND AS #2
PRINT #2, head$
CLOSE #2

coilfon = 5.25
coilfoff = 5!
heaton! = 1.5
heatoff! = 1.85
btime = TIMER

WHILE INKEY$ <> CHR$(65)
699 :

FOR i% = 1 TO j%

    b$ = ""
    T = TIMER
    errr% = 0
    PRINT #1, cmd$(mon(i%))

    DO
        IF (TIMER - T) > 10 THEN
            errr% = errr% + 1

            IF errr% = 2 THEN
                OUT &H378, 0
                GOTO 699: 'avoids endless loop
            END IF

            LOCATE 16, 25
            PRINT errr%
            END IF
        LOOP UNTIL INSTR(b$, CHR$(13) + CHR$(10) + CHR$(13) + CHR$(10))

        a = INSTR(b$, CHR$(32))
        a$ = MID$(b$, a, 6)
        dat(mon(i%)) = VAL(a$)

'signal conversions

```


'Centrifuge Box Temperature

```
IF mon(i%) = 6 THEN
  dat(6) = dat(6) * negt
```

' Accelerometer Calibration (20:1 reduction, calibrated 34.5mV = 1
'g)

```
ELSEIF mon(i%) = 5 THEN
  dat(5) = dat(5) * negt ' (ABS(dat(5) - 129)) / (34.5)
```

'Heater Voltage Signal Conversion (10:1 reduction)

```
ELSEIF mon(i%) = 4 THEN
  dat(5) = dat(5) * .01
```

' Ice Bed Temperature

```
ELSEIF mon(i%) = 4 THEN
  dat(4) = dat(4) * negt
```

'RPM signal conversion (2:1 signal reduction, calibrated to 3.66
'rpm = 1 mV)

```
ELSEIF mon(i%) = 1 THEN
  dat(1) = dat(1) * 3.21
```

```
IF dat(1) > 10 THEN
```

```
IF pump = 1 THEN
```

```
IF (TIMER - pumpt) < 3 THEN
```

```
  PRINT #1, "2DSO=1" 'turn oil on
```

```
ELSEIF (TIMER - pumpt) > 3 THEN
```

```
  PRINT #1, "2DSO=0" 'turn oil off
```

```
  IF (TIMER - pumpt) > 5 THEN pumpt = TIMER
```

```
END IF
```

```
ELSEIF pump = 0 THEN
```

```
  PRINT #1, "2DSO=1" 'turn oil on
```

```
  oldpumpt = pumpt
```

```
  pumpt = TIMER
```

```
  IF (pumpt - oldpumpt) > 5 THEN pump = 1
```

```
END IF
```

```
ELSEIF dat(1) < 50 THEN
```

```
PRINT #1, "2DSO=0" 'turn oil off
```

```
END IF
```

' Shaft Thermocouple calibration

```
ELSEIF mon(i%) = 10 THEN
  dat(10) = dat(10) * negt
```

' Thermocouple Calibration

```
ELSEIF mon(i%) = 9 THEN
```

```
IF dat(9) > 0! THEN
```

```
  dat(9) = dat(9) * post
```

```
ELSEIF dat(9) < 0! THEN
```

```

    dat(9) = dat(9) * negt
  END IF

  ELSEIF mon(i%) = 8 THEN
    IF dat(8) > 0! THEN
      dat(8) = dat(8) * post
    ELSEIF dat(8) < 0! THEN
      dat(8) = dat(8) * negt
    END IF

  ELSEIF mon(i%) = 7 THEN
    IF dat(7) > 0! THEN
      dat(7) = dat(7) * post
    ELSEIF dat(7) < 0! THEN
      dat(7) = dat(7) * negt
    END IF

  ELSEIF mon(i%) = 2 THEN
    IF dat(2) > 0! THEN
      dat(2) = dat(2) * post
    ELSEIF dat(2) < 0! THEN
      dat(2) = dat(2) * negt
    END IF

  ELSEIF mon(i%) = 3 THEN
    IF dat(3) > 0! THEN
      dat(3) = dat(3) * post
    ELSEIF dat(3) < 0! THEN
      dat(3) = dat(3) * negt
    END IF

  END IF

  ' Display location

  IF mon(i%) <= 5 THEN
    LOCATE 5 + mon(i%), 21
    PRINT USING "+####.###"; dat(mon(i%))
  ELSEIF mon(i%) >= 6 THEN
    LOCATE mon(i%), 61
    PRINT USING "+####.###"; dat(mon(i%))
  END IF

  LOCATE 2, 75
  PRINT USING "##"; mon(i%)

  outp$ = outp$ + STR$(dat(mon(i%))) + ", "
NEXT i%

rtime = TIMER - btime
outp$ = outp$ + STR$(rtime)

OPEN monitr$ FOR APPEND AS #2
PRINT #2, outp$
CLOSE #2

```

```

outp$ = ""

CALL checktemp

WEND

LOCATE 22, 20
INPUT "Restart (r) or quit (q): ", where$

IF where$ = "r" THEN
CALL Headers
CALL display
ELSE
CALL shutdown
END IF

END SUB

SUB shutdown
OUT &H378, 12      '0 : close solenoids
                   '4 : disable centrifuge motor
                   '8 : heaters off
                   '12 = total

PRINT #1, "1DSO=0"  'shut down water circulation
                   'digital output goes to 5V
                   'difference between Digital1 and 5V = zero

PRINT #1, "2DSO=0"  'shut down centrifuge oil pump
                   'digital output goes to 5V (same as above)

PRINT #1, "3DSO=0"  'shut down coil fan (same method as above)

PRINT #1, "4DSO=0"  'shut down nozzle radiation heaters
                   'shut down vent fan from spray chamber

CLOSE #1           'close output to datataker
END SUB

```

APPENDIX E: ERROR ESTIMATES

There are two key measured values for the current research, namely the surface temperature (T_s) when the adhesive failure occurred and the stress (ν_b) on the specimen at that point. Experimental errors are estimated for these two values in this appendix.

E.1 Surface Temperature Measurement Error Estimates

The surface temperature was measured indirectly, as was discussed in Section 4.1.1. Equation 4.6 was used to predict the surface temperature, T_s :

$$T_s = T_{TC} - \frac{q_c'' \cdot \Delta x_c}{k_c} \quad (4.6)$$

where T_s = predicted surface temperature at adhesive failure ($^{\circ}\text{C}$),

T_{TC} = embedded thermocouple reading ($^{\circ}\text{C}$),

q_c'' = heat transfer across the surface coating (W/m^2),

Δx_c = thickness of surface coating (m),

k_c = thermal conductivity of surface coating ($\text{W}/\text{m}^2\text{K}$).

The surface temperature error (εT_s) can therefore be estimated to be a combination of the error in the embedded thermocouple's temperature reading (T_{TC}) and the correction term $\left(\frac{q_c'' \cdot \Delta x_c}{k_c} \right)$, which will be referred to as CT for simplicity. The error in T_s can be written as:

$$\varepsilon T_s = \left[(\varepsilon T_{TC})^2 + (\varepsilon CT)^2 \right]^{1/2} \quad (E.1)$$

The error in the thermocouple reading came from two sources, the error inherent in the thermocouple circuit and the sampling frequency of the system to accurately

record a transient temperature. Although the manufacturer states a $\pm 1^\circ\text{C}$ error for K-type thermocouples, a Fluke 2180 RTD digital thermometer which has an accuracy of 0.05°C at -20°C was used to calibrate the thermocouples with to be within 0.18°C . Therefore an error of 0.23°C can be assumed in the signal itself. The sampling rate for the data was 1 sample per second, during which time temperature rise was typically 0.2°C . Because the failure detection was manual, it is possible that the failure could be recorded one sample late, leading to a sampling error of $+0.2^\circ\text{C}$. The error associated with the thermocouple reading (εT_{TC}) can therefore be estimated to be $\pm 0.43^\circ\text{C}$.

The error associated with the correction term can be estimated from equation E.3:

$$\therefore CT = \frac{q_c'' \cdot \Delta x_c}{k_c} \quad (\text{E.2})$$

$$\therefore \varepsilon CT = CT \left[\left(\frac{\varepsilon q_c''}{q_c''} \right)^2 + \left(\frac{\varepsilon \Delta x_c}{\Delta x_c} \right)^2 + \left(\frac{\varepsilon k_c}{k_c} \right)^2 \right]^{1/2} \quad (\text{E.3})$$

The thickness of the surface coating was supplied by the manufacturer to be within $1 \mu\text{m}$ and the minimum coating thickness was $70 \mu\text{m}$. The thermal conductivity was obtained from manufacturers' databases and is estimated to be accurate within $0.02 \text{ W/m}^2\text{K}$, with the lowest thermal conductivity of the specimens being $0.2 \text{ W/m}^2\text{K}$. The rate of heat transfer through the surface coating (q_c'') was predicted from equation E.4:

$$q_c'' = \frac{k_{Al} \cdot \Delta T_{x(10)-x(11)}}{\Delta x_{Al}} \quad (\text{E.4})$$

where k_{Al} = thermal conductivity of Aluminum (W/mK),

$\Delta T_{x(10)-x(11)}$ = temperature difference across last grid cell before the
surface coating ($^\circ\text{C}$),

Δx_{Al} = thickness of one grid cell (10% of plate thickness) (m).

$$\therefore \varepsilon q_c'' = q_c'' \left[\left(\frac{\varepsilon k_{Al}}{k_{Al}} \right)^2 + \left(\frac{\varepsilon \Delta T_{x(10)-x(11)}}{\Delta T_{x(10)-x(11)}} \right)^2 + \left(\frac{\varepsilon \Delta x_{Al}}{\Delta x_{Al}} \right)^2 \right]^{1/2} \quad (E.5)$$

The thermal conductivity of aluminum is 167 W/mK and the accuracy is estimated to be within ± 5 W/mK. The aluminum plates were made to an accuracy of 0.5 mm for 7 mm thicknesses. The temperature gradient ($\Delta T_{x(10)-x(11)}$) is predicted from the numerical code discussed in section 4.1.1. Because of the low thickness to height ratio of the plate a 1-dimensional model of the system is a good approximation, therefore $\Delta T_{x(10)-x(11)}$ can be estimated to be accurate within 5%. A typical value for the heat transfer rate (q_c'') is 18 W. Equation E.5 can therefore be solved to find an error estimate for q_c'' to be 9%.

A typical value for the correction term is 2.5°C . Therefore, if $CT = 2.5^\circ\text{C}$, and $\varepsilon q_c''/q_c'' = 9\%$, equation E.3 can be solved to find an estimated error of $\varepsilon CT = 0.25^\circ\text{C}$.

Finally, equation E.1 can now be solved:

$$\varepsilon T_s = \left[(\varepsilon T_{TC})^2 + (\varepsilon CT)^2 \right]^{1/2} = \left[(0.43^\circ\text{C})^2 + (0.25^\circ\text{C})^2 \right]^{1/2} = 0.497^\circ\text{C} \quad (E.6)$$

Therefore there is an estimated 0.5°C error in the surface temperature data.

E.2 Interface Stress Measurement Errors Estimates

As discussed in Section 3.4.2, Equation 3.5 is used to predict the stress on the rime ice sample:

$$v_b = \frac{m_{ice} \omega_r^2 \bar{r}}{A_p} \quad (3.5)$$

where m_{ice} = mass of rime ice (kg),

ω_r = rotor rotational speed (radians/sec),

\bar{r} = average radial distance from sample plate to axis of rotation (m),

A_p = surface area of test surface (m²).

Therefore the error in the interface stress can be estimated with equation E.7:

$$\frac{\epsilon U_b}{v_b} = \left[\left(\frac{\epsilon m_{ice}}{m_{ice}} \right)^2 + 2 \left(\frac{\epsilon \omega_r}{\omega_r} \right)^2 + \left(\frac{\epsilon \bar{r}}{\bar{r}} \right)^2 + \left(\frac{\epsilon A_p}{A_p} \right)^2 \right]^{1/2} \quad (E.7)$$

A scale was used to measure the mass of the rime ice to within 0.1 g, and the average sample had a mass of 6 g. A strobe tachometer was used to verify the calibration on the centrifuge tachometer, such that an error of 20 rpm can be assumed at a speed of 2000 rpm. The average radial distance was measured after the system was assembled and was found to be 0.194 m for the normal strength tests, and 0.172 m for the shear strength tests to an accuracy of 0.0001 m. The samples were created with a tolerance of 1 mm, therefore, the surface area of 2580 mm² is correct within 1 mm². Substituting these values into equation E.7 it can be found that the recorded interface stress is accurate within 1.5 %.